Norwegian University of Life Sciences

Aerodynamically Induced Yaw Behaviour for Floating Wind Turbines

Aerodynamisk induserte gir bevegelser for flytende vindturbiner

Eigil Andreas Solvang

Civil engineering and architecture

Acknowledgements

Abstract

The demand for more renewable energy grows stronger by the day. The world is experiencing more pollution and environmental damages from human activity than ever before. One of the possible solutions to produce more sustainable energy is offshore wind energy, more specifically floating wind energy. When transferring wind turbines to the sea, far from shore, they will be less intrusive on society as well as the wind is stronger and more constant.

This thesis dives deeper into the aerodynamically induced yaw motion of a wind turbine floater. It also attempts to explain the underlying physics based on wind direction, wind speed and yaw stiffness provided by the mooring lines.

To describe the fundamental mechanics, a static yaw system based on wind directions and rotor plane-angle for a wind turbine floater is presented. To find the combination of wind directions and -speed that causes large yaw rotations, numerical time-domain simulations are conducted in SIMA. A model of the INO WINDMOOR 12 MW turbine, using a semi-submersible floater is used in the study. This floating wind turbine is subjected to constant wind intensity with varying wind speeds and wind directions. This numerical study consists of two approaches: one analysis with a rotating floater, where platform yaw has been the output parameter, and one analysis fixing the floater and calculating the platform yaw moment based on internal forces. The internal forces are generated by the thrustforce acting on the turbine. Platform rotation and platform yaw moment is then matched and compared by using a non-linear mooring stiffness curve.

From the simulations it was observed a quite good correlation for the platform yaw between the two analysis for wind speeds in the operational domain (0-25 m/s). For wind speeds above 25 m/s, in the idling phase, a larger deviance was observed. The rotating floater experienced large rotations for some wind directions when subjected to an extreme case of 45 m/s. The fixed floater on the other hand, was unable to capture this self-reinforcing unstable yaw effect, which was observed for the rotating floater.

Sammendrag

Etterspørselen etter fornybar energi er høy og øker for hver dag som går. Verden opplever høyere gjennomsnittstemperatur, mer ekstremvær og høyere menneskeskapt forurensing enn aldri før. En av de mulige måtene å skape fornybar energi på er havvindkraft, da spesielt flytende havvind. Vindturbinene plassert til havs vil være mindre påtrengende på samfunnet, samtidig som de vil oppleve en mer konstant og sterkere vind.

Denne oppaven går dypere inn på den aerodynamisk induserte gir bevegelsen til en vindturbin flyter. Den forsøker også å forklare den grunnleggende fysikken basert på vindretning, vindhastighet og gir stivhet fra forankringslinene.

For å beskrive den grunnleggende mekanikken bak bevegelsen blir et statisk system for gir bevegelsen, basert på vindretning og rotor-plan orientering, presentert. For å kartlegge de mest kritiske kombinasjonene av vindretning og -hastighet med tanke på gir bevegelse, har det blitt gjort numeriske tids-plan simuleringer med programvaren SIMA. Her har en modell av INO WINDMOOR 12 MW turbinen blitt brukt. Denne turbinen bruker en halvt-nedsenkbar plattform som flytende fundament. Denne vindturbinen har blitt utsatt for konstant vindintensitet med varierende vindhastighet og vindretning. Det numeriske studiet inneholder to fremgangsmåter: En analyse hvor plattformen kan rotere, og en analyse hvor plattformen holdes fast. For den roterende plattformen er gir rotasjon output parameteren. For den fastholdte plattformen brukes de indre kreftene, som oppstår fra den aerodynamiske thrustkraften, til å regne ut et gir moment ved platform sentrum. Plattform rotasjon og gir moment regnes så om, og sammenliknes ved bruk av en ikke-lineær gir stivhetskurve.

Fra analysene ble det funnet god korrelasjon mellom de to fremgangsmåtene for vindhastigheter innenfor operasjonsområde (0-25 m/s). For vindhastigheter over 25 m/s, hvor turbinen er parkert, ble det observert et større avvik. Da ble det sett at den roterende turbinen fikk veldig store plattform rotasjoner for enkelte vindretninger ved et ekstremt vindtilfelle på 45 m/s. Ved høye vindhastigheter ble det observert en ustabil selv-forsterkende gir bevegelse for den roterende plattformen, som den fastholdte flyteren ikke klarte å gjenskape.

Table of Contents

List of Figures

List of Tables

List of Abbreviations

AOA	Angle of attack
BEM	Blade element momentum
CFD	Computational fluid dynamics
DEL	Design equivalent load
DNV	Det norske veritas
DTU	Danish university of technology
FE	Finite element
FLS	Fatigue limit state
FOWT	Floating offshore wind turbine
FPSO	Floating production, storage and offloading
FWT	Floating wind turbine
GE	General electric
IEC	International electrotechnical committee
MC	Mooring center
ML1	Mooring line 1
ML2	Mooring line 2
ML3	Mooring line 3
MW	Megawatt
OO	Olav Olsen
RNA	Rotor-nacelle-assembly
ROSCO	Reference open source controller
ROV	Remote operated vehicle
SDOF	Single degree of freedom system
TLP	Tension leg platform
UTS	Ultimate tensile strength

List of Symbols

η_1 Surge

η_2 Sway

η_3 Heave

η_4 Roll

η_5 Pitch

η_6 Yaw

x position

E Modulus of elasticity

F_x Force applied in x-direction

K_e Elastic stiffness

A Cross-sectional area

L Length

g Gravitational constant

ω_l Unit weight per length submerged line

ρ Density

T_l Line tension

C_{11} Restoring in surge

C_{22} Restoring in sway

C_{66} Restoring in yaw

Ψ Angle between anchor lines

F_i External force

t Time

V_{wind} Wind velocity

A_{swept} Swept area

P Power

$(T_H)_M$ Average horizontal force from mooring line

z_r Reference height

z Height above sea level

f frequency

S_k Single sided velocity component spectrum

σ_k Wind velocity standard deviation

U Mean wind speed

V_f Fluid velocity

ζ Wave elevation

ω Angular frequency

α Incoming Wind direction

m Mass

c Damping

u Displacement

$\dot{u}$ Velocity

$\ddot{u}$ Acceleration

U Mean wind speed

V_f Fluid velocity

1. Introduction

The most debated topic in the world these days is most likely sustainable energy production. We need energy for everything, from heating up our house, cooking dinner or driving to work. The world is experiencing more pollution and more environmental damages from human activity than ever before. Finding a sustainable manor to produce energy, and eventually replace fossil fuel consumption, is urgent. One of the possible ways to produce more sustainable energy is offshore wind. Land based wind is already in place in several countries world wide, but has in some instances met a lot of resistance from local residents regarding wildlife and more. A large wind turbine on land can be quite intrusive on the surroundings. Transferring these turbines to the sea, where the wind is stronger and there are less conflict of interest, is a more plausible way to largely expand the use of wind to generate sustainable energy. Bottom fixed offshore wind is already present in countries like Denmark, UK, Germany and Belgium in water depths below 60-70m. As of 2021 the installed offshore wind capacity only makes up 7% of the total onshore and offshore capacity worldwide. According to (Taylor et al., 2021) the UK was the country with most installed offshore wind capacity with 12.7 GW at the end of 2021.

In Norway there is significant potential to not only use the vast coastline for wind farms, but also for the Norwegian suppliers and contractors to use their experience from the oil & gas industry, and apply it to the offshore wind industry. The main reason offshore floating wind is not yet competitive is that the manufacturing process is too expensive. This leads effectively to that the kilowatt per hour price is higher than other sources of energy. This means that floating offshore wind projects today are dependent on subsidies, until the cost reduces and the floating industry gets more competitive. For it to be more competitive, the manufacturing and assembly needs to be industrialized on a larger scale.

My contribution to the research on floating wind turbines is a numerical and analytical study on the yaw behaviour of the INO WINDMOOR 12MW turbine. Hopefully the results and ideas of this thesis can be applied in the development of tomorrows floating wind turbines.

1.1   Previous research

The existing literature on yaw behaviour of floating wind turbines is slightly different from my objectives in this thesis. A large part of the the previous research focuses on the dynamic and/or coupled motion, such as roll-yaw or pitch-yaw. My take on the yaw motion is more static and more simplified. Below I have selected four recent research articles that have conducted research related to the coupled or uncoupled yaw motion for floating wind turbines. Following is a short description and summary of the articles.

(Haslum et al., 2022) discusses the roll-yaw lock phenomenon which was observed for the Hywind spar floater. This phenomenon is a dynamic effect caused by aerodynamic load and can be mitigated by ensuring the sufficient separation between the uncoupled period in roll and yaw. This paper will be discussed more in detail in Section 2.6.3.

A study on the yaw misalignment on the OO-star platform, developed by Norwegian Olav Olsen, is the topic in (Özinan et al., 2020). Here the DTU 10 MW turbine has been combined with the OO-star wind floater. This study highlights the difference between floating and bottom fixed turbines, focusing on where the floating turbines are free to translate and rotate. The freedom of movement will result in the susceptibility to the presence of yaw misalignment and following asymmetric tension load on the mooring lines. The tension transference during asymmetric loading will increase the fatigue on the mooring lines. From the simulations it was observed that for slightly above rated wind speeds, the yaw misalignment could increase the DEL or damage equivalent load up to 70% at the fairlead. The damage equivalent load in this study has been calculated using the rainflow algorithm.

In (Chen et al., 2021) the topic of the research was to investigate pitch, yaw and pitch-yaw effect on unstable aerodynamic performance. Several CFD simulations were conducted to investigate how the platform motion effected the rotor blades. From the simulations it was discovered that the angle of attack (AOA) of the airfoiles was quite sensitive to the yaw motions of platform. Furthermore, yawing of the platform was the explanation of fluctuations in the power output at rated wind speed. The fluctuations was related to the dynamic deflection process of the yaw motion.

(Li et al., 2020) investigated how the dynamic response to the yaw error is related to the wind-wave misalignment. In this analysis the OC4-5MW turbine was combined with the Deepcwind semi submersible platform. From the study it was discovered that the stability and efficiency of the power output was significantly effected by the yaw error. The yaw error had little effect on the motion and structural load, however, the wind-wave misalignment had little effect on power generation, but significantly affected the motion and following structural load on the floating wind turbine.

1.2   Recent developments

This section will briefly introduce some of the advancements made in floating wind technology in the recent years. It will mainly focus on the developments done in Norway, but also mention some floating wind projects worldwide.

The first large scale floating turbine in Norway was the Hywind demo, built in 2009 and located outside Karmøy, with a capacity of 2.3 MW. This turbine is to this day producing clean energy, and producing valuable data. It consists of a spar buoy floater, designed by Statoil (now Equinor), combined with a Siemens wind turbine. This pilot project was an important step in the upscaling from a single turbine to a wind farm configuration.

The worlds first floating wind farm, located at Buchan deep of the coast from Peterhead, Scotland, was named Hywind Scotland and started producing power the 8th of September 2017. This wind farm uses the further developed and upscaled Hywind spar concept from the Hywind demo. The floating substructure for this project was built in steel and towed horizontally and then upended before turbine assembly. This park consists of five 6 MW turbines with a total installed capacity of 30 MW. The power produced from these five turbines, is brought ashore in Scotland, powering 20 000 homes in the UK (Equinor, 2022).

Another wind farm located off the coast of Scotland is the Kincardine offshore wind farm. This floating wind farm is located 15km off the coast of Aberdeen and consists of five 9.5 MW turbine, and a total of 50 MW total installed system capacity. This park uses a semi-submersible floater design called Windfloat, designed by Principle power. The floating structure supports the 9.5 MW turbine from Vestas. Currently, this is the largest floating offshore wind farm in the world, set to be surpassed by Hywind Tampen upon completion(PrinciplePower, 2022).

What will be the worlds largest floating wind farm is now under construction outside the west coast of Norway, and is called Hywind Tampen. Sunday 13. of November 2022 the first turbine was in place and started producing energy. The construction of Hywind Tampen was halted due to the corona virus, and therefore is still under construction. In this project the Hywind floater is built in concrete instead of steel. The floating foundation is casted vertically using slip-forming, resulting in no need for upending of the substructure (Haslum, 2022). The total capacity of the farm will be 88 MW, consisting of 11 turbines with just over 8 MW capacity each. The intention for this offshore wind park is to electrify Troll and Snorre offshore oil and gas platforms, which will significantly reduce the CO_2 emissions from these fields. Figure 1.1 shows an illustration of the wind farm done by Equinor. (Equinor, 2021)

Figure 1.1: Hywind Tampen wind farm. (Equinor, 2021)

1.3   Objectives

The purpose of this of thesis will be to investigate the yaw motion of a wind turbine using a semi-submersible floater.The wind turbine I will use in this thesis is the INO WINDMOOR 12 MW turbine. The turbine is placed eccentrically relative to the mooring center, which has been observed as a factor contributing to a driving yaw moment and unstable yaw behaviour, caused by the aerodynamic thrustforce. Unstable yaw behaviour is considered to be mostly a static driven effect, where dynamic loads cause the platform to alternate between two static points of equilibrium.. The thesis is limited to investigating the static component of the yaw behaviour.

- Investigate what wind directions and wind speed, cause large static yaw rotations using a numerical model in SIMA.

- Study the effect of non-linear yaw behaviour by separating linear and non-linear effects.

- Discuss the acquired results and recommend future work to further understand and handle large yaw motions.

1.4   Scope

The scope of this thesis will be to describe platform yaw behaviour theoretically and numerically. Since there a very little previous research on this topic, I will work on the fundamentals. All the numerical analysis has been done by myself, but the SIMA model has been developed by the staff at SINTEF Ocean. The numerical analysis will mainly be aerodynamic loading. Waves are included in the model, but set to a negligible wave

height. A description of the yaw stiffness provided by the mooring lines will also be included in this thesis. Current is not included in the model and is outside the scope of this thesis.

1.5 Limitations

In this thesis I will not consider impact loading or any other accidental limit state (ALS) analysis. Fatigue or FLS will not be considered in this thesis. I will not investigate material models, other numerical models, or use any different software than SIMA. There will not be any work done related to the financial aspects of offshore wind, this thesis will focus solely on the structural part of a FOWT. I will not consider current, mainly because it is not included in the simulation model. It is still an important factor to consider in the analysis and design of a FWT. As mentioned wave loading and hydrodynamic forces on the floater will not be investigated although being an important environmental load to include. I will not look at coupled yaw behaviour like yaw-roll or pitch-yaw. This effect introduces dynamic properties, and my focus is mainly on the quasi-static behaviour.

1.6   Chapter overview

In this section, a brief summary of the content in the following chapters.

Chapter 2 Background theory
A chapter introducing the relevant theory to understand, scope, objective and the results from static - and numerical analysis. This chapter contains insight into; the parts of a wind turbine, different floater concepts, mooring systems, environmental loads and more.

Chapter 3 Method
This chapter is meant to explain the approach to answer the objectives set in chapter one. It introduces the software used for this thesis, and attempts to maintain healthy awareness using numerical methods.

Chapter 4 Numerical model
An introduction of the INO WINDMOOR turbine and the corresponding numerical model is done in this chapter. This chapter attempts to give the reader some insight in the some information about the turbine itself, as well as the modelling process done in SIMA.

Chapter 5 Static yaw model
In this chapter some further theory about yaw and mooring stiffness is discussed. This chapter proposes some fundamental ideas and assumptions to establish a theoretical model to derive the yaw moment as a function of wind-direction and RNA-angle. Furthermore a description of the non-linear yaw stiffness of the case study model and linear yaw stiffness is done

Chapter 6 Simulation results
This chapter consists of some calibration simulations done to verify that the model produces results in line with the base case model from (Silva de Souza et al., 2021). Furthermore simulations with constant wind from several wind directions and wind speeds has been conducted for a rotating and fixed floater. The output from both these analysis has been the yaw of the platform.

Chapter 7 Discussion
One of the last chapters of this thesis is the discussion of the results from the simulations in chapter 6 but also the theory concerning mooring stiffness and in chapter 5. This chapter aims to present some foundations and explanation for the results based on the theory.

Chapter 8 Conclusion

This chapter is a relatively short chapter meant to summarize the most important findings from chapter 5, 6 and 7.

Chapter 9 Future work

The final chapter in this thesis, contains my recommendations for future work regarding the results and ideas I have found in this thesis.

2. Background theory

Floating offshore wind has a enormous potential to be a leading source of energy in the future, being that the vast majority of the earths surface is water. The advantage floating wind has over bottom-fixed turbines is that the wind speed is higher further out at sea. Almost 80% of offshore wind resources is at water depth over 60m, which is roughly the limit for bottom-fixed turbines (Equinor, n.d.). An even more important factor is freedom in terms of operating location. Floating wind turbines can be placed further away from land and be less intrusive on existing marine life and shipping lanes. This chapter aims to introduce the basic knowledge that is required to understand the results of this thesis. The objectives of this thesis has been guiding for the theory required, and the following numerical study.

2.1 Floating offshore wind

Today the offshore wind industry is dominated by bottom-fixed structures. The limit of bottom fixed- wind turbines is approximately 60-70m, above this depth, floating turbines is a more preferable solution. As the water depth increases, The cost of mooring lines follows. It is therefore one of the most important design parameter. The floating structure will also require alterations following an increased sea depth, but a lot less than the mooring system (Ferrão, 2021).

2.1.1 Wind turbines

In this section I will give a description of some of the parts that makes up a wind turbine, and some definitions. A floating windturbine consists of several parts, and I will further describe some of the most fundamentals and largest. A floating wind turbine is based on a floating structure which acts as a foundation for the turbine. Connecting the turbine to the floater is the tower. The turbine itself is placed on the top of the tower, and comprises of the blades, hub and nacelle. These parts are the largest and most conspicuous which can be seen from the outside the turbine. Inside the turbine are parts like gears, drive train, dampers, shaft and so on (Manwell et al., 2010). The

following paragraphs until Section 2.1.2 are based on the theory presented in ((Manwell et al., 2010) and (Efficiency and Energy, 2022). Figure 2.1 describes the key components for a wind turbine. This turbine is not floating, but highlights the other components quite well.

Floater

The floating substructure essentially supports the entire wind turbine and keeps the turbine above the water. There are three main concepts that are used for floating structures. One of the concept is a buoyancy and ballast-stabilizing structure. This means that the structure uses water plane stability to keep structure upright. Another concept is ballast stabilizing structure. For this case the floater that has a very low centre of gravity and stays upright from inertia forces. Lastly there is a floating concept that uses the tensile strength of the mooring to keep stationary. All these floater designs will be further explained in the next section. The floater is an important structure being the part where the mooring lines are connected, ultimately fixing the entire floating wind turbine to the seabed.

Tower

The tower is the component elevating the blades over the water level. It is generally favourable for the power production that the blades are high above sea level, due to lower wind speeds and more turbulence closer to the water surface. In the design of the turbine it is paramount to avoid coupled vibrations between tower and rotor. Therefore the stiffness of the tower is an important design aspect. The tower height is usually 1-1.5 of the rotor radius.

Rotor

The most vital part of the wind turbine is the blades. These allows the kinetic energy of the wind to drive a generator producing electricity. Nowadays It is common for most turbines to have three blades, but some downwind turbines have only two.

Nacelle

The nacelle is the part of the turbine which houses the components related to the generation of electricity. Such as the generator, drive-train, braking system and so on. The nacelle sometimes require maintenance, and is therefore required to be accessible by offshore wind technicians.

Yaw system

A situation that can occur is the misalignment between wind direction and rotor plane. This would be a problem if the yaw system hadn't been invented. The primary objective of the yaw orientation system is to keep the blades or rotor plane into the wind, and producing power. Between the tower and turbine sits a yaw bearing that lets the turbine rotate about the z-axis towards the wind direction. The brain of the yaw system is the yaw controller which is located in the nacelle. This is a system which has sensors and technology to pinpoint the wind direction, and produce a signal to the yaw bearing which then rotates the rotor into the wind direction.
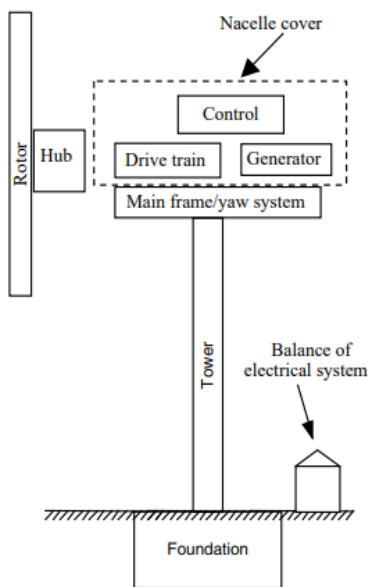
Figure 2.1: Key components of a wind turbine (Manwell et al., 2010)

2.1.2   Degrees of freedom

In Figure 2.2 there are some arrows and axis indicating the translation and rotation of the turbine. It is common to define the xy-plane parallel to the water surface and to let positive z-axis rise above the water level.

For the x-direction we call translation, *surge*, (η_1), and rotation, *roll* (η_4). In y-direction we call translation, *sway*, (η_2), and rotation *pitch* (η_5) . Lastly for the z-direction translation is called *heave,* (η_3), and rotation *yaw* (η_6) (Bashetty and Ozcelik, 2021). The yaw motion will be investigated further in this thesis.
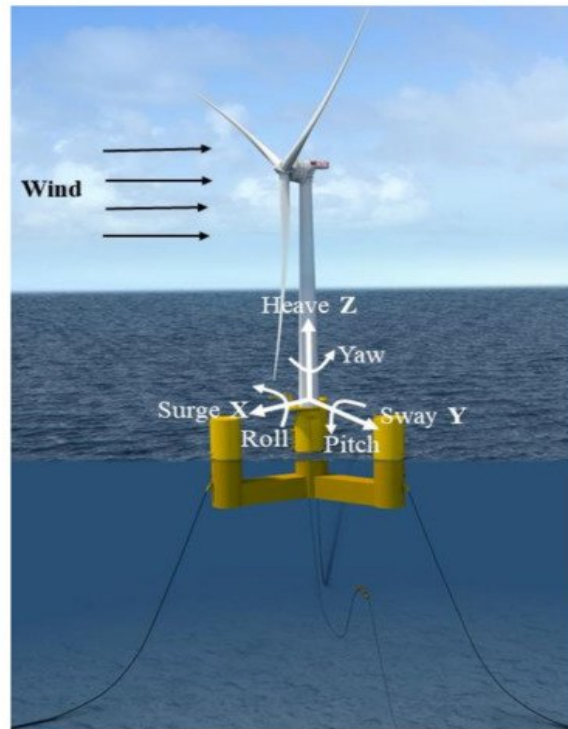
Figure 2.2: Degrees of freedom for a floating wind turbine (Bashetty and Ozcelik, 2021)

2.2 Offshore wind floater concepts

In this section I will introduce the most common floater concepts used to provide a stabilizing foundation for a floating wind turbine. We have three main types of floating concepts. Semi submersible platform, spar and tension leg platform. Some manufactures combine some properties of these floater concepts, but these three are the most adopted designs by the floating wind industry. In Figure 2.3, the semi-submersible platform (1) is on the left of the picture, and the spar (2) in the middle. To the right (3) is the TLP or tension-leg platform. For this thesis the semi-sub will be the most relevant design, because the WINDMOOR turbine uses a semi-sub floater.

2.2.1 Semi submersible platform

The semi-submersible platform is a water plane stabilizing structure. This floating structure remains stable with the combination of buoyancy and ballast. The columns provide ballast and flotation stability. The stabilizing forces acting on the structure is dependent on the volume submerged in water. For instance if the front part platform is is more submerged in the water, there will be a higher buoyancy acting on this part, and the rear will move upwards from the water surface. To maintain a stabilizing moment, this design often demands a fairly large and heavy structure. Possibly one of

the most important reason to choose a semi submersible platform is related to transport. The turbine can be mounted on the platform onshore before the transportation The platform produces little drag, when being towed to the production location. The spar buoy requires significantly higher water depth to be transported to the operating site (Castro-Santos and Diaz-Casas, 2016).

Another buoyancy stabilizing floating concept is called barge. The main difference between a barge foundation and semi-submersible platform is the difference in distributed buoyancy. A barge floater is typically a flat floating structure, while the semi-submersible is made up of columns, pontoons and secondary elements to connect the columns.

2.2.2   Spar floater

The spar buoy is a ballast stabilized offshore structure. Meaning the floater uses a center of gravity that is below the center of buoyancy. By having a centre of gravity so low in the structure, a large lever arm combined with the heavy ballast creates recovering forces to counteract destabilizing moments. The spar buoy has good resistance against pitch and roll movement. When it comes to fabrication the spar buoy has an advantage being easy to fabricate. For transportation it can be a bit more challenging, because it creates substantial drag and require substantial water depth. (Leimeister et al., 2018).

2.2.3   Tension leg platform

Finally, the tension leg platform is a structure which relies more on the mooring system than buoyancy or ballast as the semi submersible and spar. The water plane stiffness of the TLP platform is low compared to other floaters, but the stiffness relies mostly on the tensile strength of the mooring lines. The floating platform can be lighter and smaller than the semi-submersible, but can require a stronger mooring system. The turbine installation can similar to the semi submersible platform, be conducted onshore before the transportation to the operating location (Castro-Santos and Diaz-Casas, 2016).
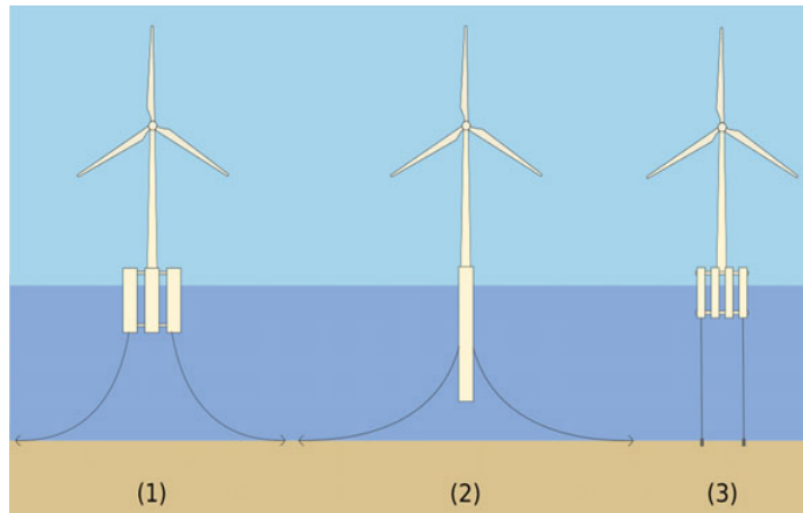
Figure 2.3: Floating foundation concepts from (Castro-Santos and Diaz-Casas, 2016). (1) Semi submersible (2) Spar floater (3) TLP

2.3   Mooring systems

For an offshore floating structure to maintain a fixed position, whether that be a platform, wind turbine or a FPSO, some anchorage system is required.A mooring system is a configuration of slender members which are meant to ensure stability and fixation of a floating structure. In recent time the most common mooring members are wires, fibre ropes and chains, or a combination (Faltinsen, 1990). Single point mooring means that only one mooring line is used to fix the floating structure to the sea bead. Spread mooring on the other hand, is a mooring system where several mooring lines are connected to the structure. Single point mooring systems are not so common offshore wind turbines but more common for ships. One of the reasons is the lack of redundancy. (Castro-Santos and Diaz-Casas, 2016) the most common spread mooring systems for offshore wind are catenary mooring, taut mooring and semi-taut mooring

2.3.1   Catenary mooring

Catenary mooring is a mooring type where the weight of the mooring lines is a significant part to the station keeping of the floating object. Catenary mooring lines are typically longer than the actual water depth, so that there is a part of the mooring line resting on the seabed. This leads to only horizontal forces at the anchor. The usage of catenary mooring is most common for shallower water depths, due to the large amount of mooring material needed to both reach the seabed, and have sufficient mooring length resting on the seabed itself (Faltinsen, 1990). This can get quite costly for large water depths. In Figure 2.4 there is a figure of a spar wind turbine with catenary mooring (a) to the left.

2.3.2   Taut mooring

For this mooring configuration the mooring lines are subjected to a higher pretension force, resulting in an angled positioned with the seabed at about 30-40 degrees. This system is stiffer compared to the catenary system, because there is little or no room for horizontal movements of the floater. In a taut mooring system the stiffness against motion is based on the elastic properties of the mooring line. Meaning the ability to withstand the tensile elongation. This mooring system is the most cost effective for deeper waters, but the anchors are required to withstand both horizontal and vertical forces. Another advantage for the taut-mooring system over the cateneray mooring system is the smaller foot print on the seabed. It is possible to use less mooring line length, which makes a cheaper and lighter mooring system (Wang, 2022). In Figure 2.4 b) there is an image of a spar floater using taut mooring.
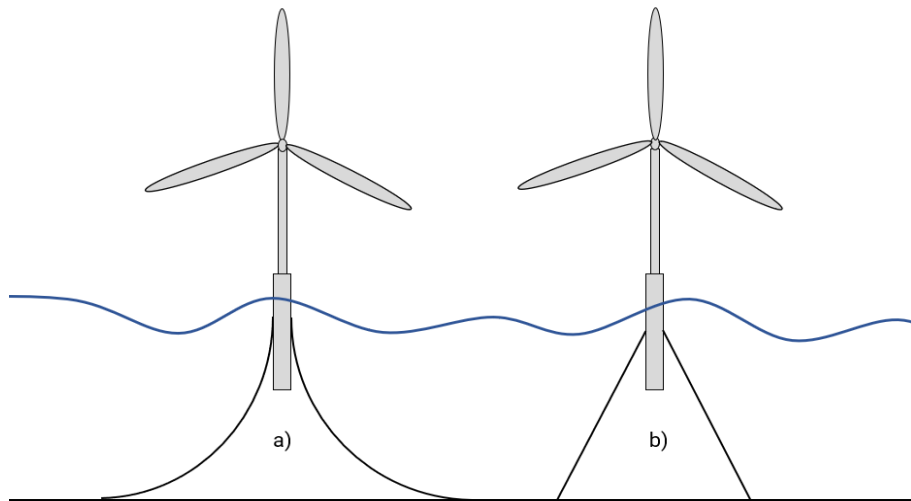
Figure 2.4: A spar floater with two types of mooring. a) Catenary mooring b) Taut mooring. Inspired by Figure 2.3

2.3.3   Semi-taut mooring

A semi-taut mooring configuration is a system that combines the advantages of catenary mooring and taut mooring. The elastic stiffness of taut-mooring and the gravitational forces on the mooring line on the seabed. It is a system that is more suited for deep water than catenary mooring.

2.3.4   Mooring stiffness

There are two main properties with the mooring systems, which provides stiffness to keep the floating object in a fixed position. That is geometric stiffness and elastic stiffness

Geometric stiffness

When a floater is subjected to external loads, the platform will change position or displace. To counteract this displacement of the floater the mooring lines changes geometry to provide restoring forces to keep the floater in place. The change in geometry or angular change of the mooring line, depends on the external force on the floater and the weight of the mooring line. This is a non-linear phenomenon and can be difficult to model explicitly. This principle is used in catenary mooring.

Elastic stiffness

The elastic stiffness of a mooring member is a linear property. The elastic stiffness is largely based on the axial stiffness of the mooring line, similar effect to axial stiffness of a truss member. When a mooring line is under tensile loading it will attempt to contract to withstand the loading. The elastic properties are determined from the material stiffness or Young's modulus, E, cross-sectional area, A, and the length of the line, L. The elastic axial stiffness, k_e, can be estimated as following (Bell, 2018):

$$k_e = \frac{EA}{L} \tag{2.1}$$

When considering elastic stiffness, the relationship between stress and strain is linear.If the load is sufficiently high the relationship will eventually be non-linear. if the load keeps increasing, the material will yield and ultimately fail (Callister and Rethwisch, 2020).

2.3.5   Restoring forces

The static forces, both from elasticity and geometrical changes can be described can be together by assuming a flat seabed, and neglecting the dynamic effects. The weight of the mooring line is naturally submerged in water, which adds a hydrostatic contribution. The mooring line is assumed to have no bending stiffness for the following case. In the equations below A is the cross-sectional area, E is the modulus of elasticity, w_l is the the unit weight per length submerged line, ρ is the water density and g is the gravitational constant (Faltinsen, 1990).

The tangential static forces in the mooring lines can be found with the following equa-

tion:

$$dT - \rho g A dz = [wsin\phi - F(\frac{1+T}{EA}]ds \tag{2.2}$$

For the radial static forces:

$$Td\phi - \rho g A z d\phi = [wcos\phi + D(\frac{1+T}{EA}]ds \tag{2.3}$$
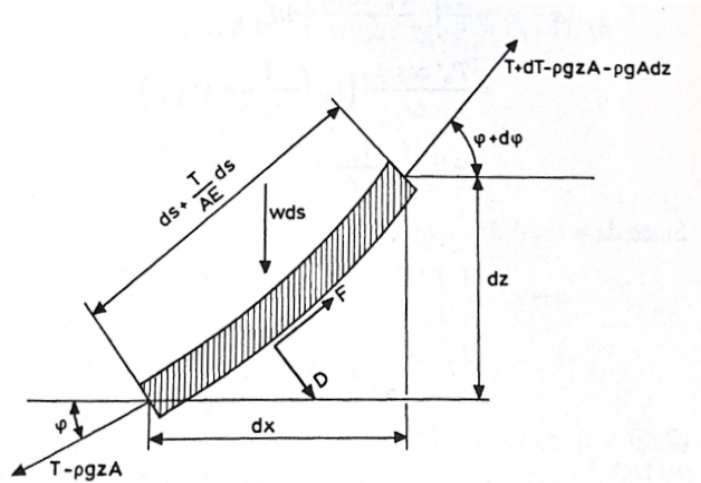
Figure 2.5: Forces acting on a section of a catenary anchor line (Faltinsen, 1990)

From the equations above, it is possible to find the position, X for a floating structure subjected to environmental loads. For this instance it is assumed that the structure uses catenary mooring, and knowing the environmental forces on the structure, as well as the point where the mooring line is connected to the floater. The horizontal component of the tension at water level in the mooring line, T_H, can be described by the line tension, T and the mooring line angle at fairlead ϕ_w.

$$T_H = Tcos\phi_w \tag{2.4}$$

If the horizontal motions are not too significant in magnitude, the horizontal forces acting on the floating structure, can be expressed by; the average horizontal force from the mooring line $(T_H)_M$, stiffness in x-direction (surge), C_{11} and the horizontal translation η_1

$$T_H = (T_H)_M + C_{11}\eta_1 \tag{2.5}$$

It is possible to find the stiffness against surge, C_{11} by differentiating of T_H with respect to X at the average horizontal force $(T_H)_M$. The relationship between X and T_H for a catenary line can be describe as

$$X = l - h(1 + 2\frac{a}{h})^{\frac{1}{2}} + a cosh^{-1}(1 + \frac{h}{a}) \tag{2.6}$$

By differentiating equation 2.5, it is possible to find C_{11} as expressed in eq. 2.4.

$$C_{11} = \frac{dT_H}{dX} = w\left[\frac{-2}{(1 + 2\frac{a}{h})^{\frac{1}{2}}} + cosh^{-1}(1 + \frac{h}{a})\right]^{-1} \tag{2.7}$$

Where a is the ratio of average horizontal force $(T_H)_M$ and w is the weight per unit submerged line length To find additional restoring coefficients in the equation of motion provided by the mooring system, the same procedure shown in eq. (2.4)- eq.(2.6) can be applied. The mooring system is assumed to be spread, meaning more than one mooring line. In the equations below k_i is the restoring coefficients for mooring line number i.

For surge:

$$C_{11} = \sum_{i=1}^{n} k_i cos^2 \psi_i \tag{2.8}$$

For sway:

$$C_{22} = \sum_{i=1}^{n} k_i sin^2 \psi_i \tag{2.9}$$

For yaw:

$$C_{66} = \sum_{i=1}^{n} k_i (x_i sin\psi_i - y_i cos\psi_i)^2 \tag{2.10}$$

2.4 Mooring materials

There are different mooring materials used to achieve geometric stiffness, elastic stiffness or a combination of the two properties. Those are mainly wires, fibre ropes and chains. Chains provide geometric stiffness, and fibre ropes and wires have more elastic properties.

2.4.1 Synthetic fibre ropes

Fibre ropes are very suitable for deep-water mooring, which will reduce the cost and weight of the mooring system. It is common to use polyester or polyethylene (Dyneema) to manufacture the fibre ropes. The benefits of using fibre ropes is a lightweight elastic behaviour. According to (Falkenberg et al., 2018), synthetic fibre ropes has a higher strength to weight ratio than steel wires. Polyester ropes have a visco-elastic behaviour. The tension to stretch relationship has a non-linear characteristic, and current stiffness is a function of the previous peak loading. Offshore fibre ropes are not suitable for contact with the seabed, although which the appropriate protection can be placed on the seabed. Furthermore the fibre ropes should not be subjected to direct sunlight.

2.4.2 Chains

Chains are made of rolled steel bars linked together. Steel chains are mostly used for it's weight and durability. Stud-link chains are used in shallow waters and studless chains are more common in deeper waters. The studless design is lighter and more resistant to fatigue. In Figure 2.6 both chains with stud-links (a) and studless chains (b) are shown. According (DNV, 2018) the steel grade used for chains is classified according to the minimum ultimate tensile strength. These grades are: R3, R3S, R4, R4S, R5 and R6. Where R3 has the lowest strength of 690 MPa and R6 the highest with 1100 MPa. In addition to higher UTS , the higher material grades have better fatigue resistance. A disadvantage of using higher steel grade is lower ductility compared to lower steel grades, the increased strength comes somewhat at the expense of the ability to deform. For further information about chains, the reader is referred to DNV GLs OS-E302. (DNV, 2018)

(a) Stud-Link   (b) Studless Chain
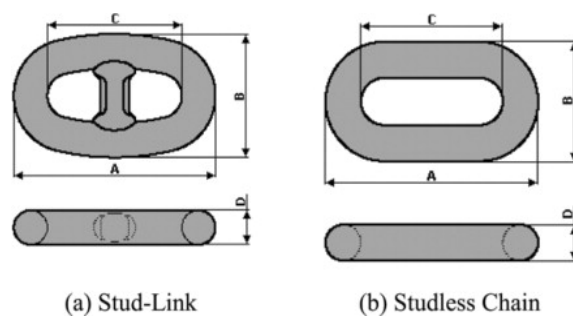
Figure 2.6: Two variants of steel chains from (Chakrabarti, 2015). a) Stud-link chain b) Studless chain.

2.4.3 Wires

Steel wires is a common lightweight alternative for mooring lines. Steel wires are slightly more fragile in terms of damage and fatigue compared to chains. However steel wires have more elastic behaviour than steel chains. In Figure 2.7 a cross-sectional view of the build-up of some wire variants is shown. For further information about manufacturing, design of steel wires the reader is referred to DNVGL-OS-E304 (DNV, 2020)

a) Six strand   b) Spiral strand

c) Half locked coil   d) Full locked coil
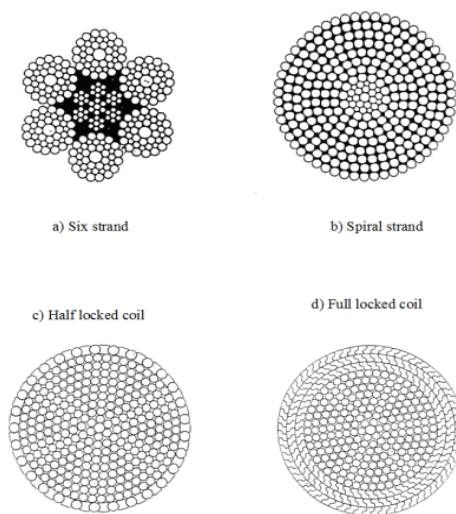
Figure 2.7: Cross-sectional view of of mooring wires from (DNV, 2020)

2.4.4   Mooring line attachments

Sometimes it is favourable to accompany the mooring lines with some components that can change the mooring line geometry, referring mainly to catenary mooring lines. As mentioned the geometric shape of the line is providing the stiffness of the FWT. For these purposes there are two components which are used, those are clump weights and buoyancy elements.

Clump weights

Clump weights are heavy objects imposed to the mooring line to restrict movement and contribute in providing restoring forces for the floating structure. Adding more weight to the mooring requires a larger force to lift the mooring lines of the seabed. The mooring lines are passed through inside the of the clump weights, confining the part of the mooring line close to the touchdown point (Ma et al., 2019).

Figure 2.8: Clump weight from (Ma et al., 2019)

Buoyancy elements

Buoyancy elements are applied to the mooring lines to create buoyancy at certain locations of the line. They are often used to avoid touchdown of the mooring lines on the seabed. This is not desirable for mooring materials that would be destroyed after contact with the seabed like polyester rope (Kvittem, 2022b).

2.5   Anchoring systems

The role of the anchors is to keep the mooring lines fixed to the seabed, and ultimately the offshore turbine or other floating structure in place. The type of anchor used depends on the soil conditions at the seabed, what type of mooring used, and the sea depth. Having a catenary mooring requires capacity to withstand large horizontal forces, while a taut or semi taut mooring requires anchorage that can resist both horizontal and vertical forces. Some anchor types used are: drag anchor, driven pile, suction anchors and lastly gravity anchors. Catenary mooring is often combined with drag-embedded anchors that can withstand large horizontal forces. Although piled- and gravity anchors are applicable. Taut mooring typically uses drive piles, suction anchors, or gravity anchors (Vryhof, 2015).

2.5.1   Suction Anchors

Suction anchors are a widely used in cases where the anchor need to withstand both horizontal and vertical forces. Such cases are common for taut and semi-taut mooring. Suction anchors are normally shaped like a cylinder, with an open bottom end, being the part that is lowered down into the seabed. Once the suction anchor is placed into the seabed, the water is extracted from the anchors, by a pump often using an ROV. This creates a pressure difference between the inside and outside, Suction anchors are not suitable in loose sandy soil or stiff soil where penetration is difficult. A significant part of the suction anchor is below the seabed (Design, n.d.),(Owen, 2020).

Figure 2.9: Suction anchor from (Design, n.d.)

2.5.2   Drag anchors

A very frequently used anchor is the drag embedment anchor. This anchor type is best suited for soft sediments such as gravel, sand, or silt. It is designed to withstand large horizontal forces, such as the case for a catenary mooring system. The capacity of the anchor is generated by the soil resistance in the embedded part of the anchor. A large vertical load will pull the anchor out of the seabed (Aubeny, 2016).

Figure 2.10: Drag anchor (Moorings, 2022)

2.5.3   Pile anchor

Driven pile or pile anchor is a versatile anchor type, applicable for a variety of seabed conditions. Pile anchors are a hollow steel pipe, embedded in the seabed by the means of a hammer or vibrator. It is an anchor type resisting both horizontal and vertical forces. The steel pipe need to be installed quite deep below the ocean floor. The holding capacity for the anchor is generated from surface friction between sand and the anchor, and the lateral resistance of the soil (Aubeny, 2016).

Figure 2.11: Driven pile anchor (NGI, 2022)

2.5.4 Gravity Anchors

For the gravity anchor, the holding capacity of the anchor is dependent on the weight. It requires medium to hard soil conditions. Designed mainly for vertical forces but will withstand horizontal forces as well. The direction of the force is not so governing for the demand on the anchor. For the gravity anchor to be sufficiently strong it is required to be quite large, and heavy which can lead to high installation cost. Removing gravity anchors upon decommissioning can be quite challenging (Vryhof, 2015).

Figure 2.12: Gravity anchors (Group, n.d.)

2.6   Yaw for FWT

The wind turbines of today are a complex piece of technology. Offshore wind turbines are equipped with technology and control systems that can optimize power production in all conditions. This is important in an environment where environmental loads are ever changing. For this section I will further describe the yaw-motion and corresponding yaw controller used to counteract the rotation.

2.6.1   Introduction

In Figure 2.2 a description of a floating wind turbines degrees of freedom was defined. To repeat, yaw, is rotation about the z-axis. Yaw or yawing will occur for some wind and sea states where mainly the wind will create a driving moment which will rotate the platform and, shift the rotor plane out of the wind direction. This will lead to a loss of power production which is undesirable. This yaw motion is essentially a static action, which is caused from the aerodynamic horizontal force acting on the turbine. The horizontal force acting on the hub has an eccentricity which is the distance from the mooring center to the hub point. Hence, the yaw moment that is being generated, is mainly dependent on the aerodynamic load from the wind. The imaginary mooring center is the where the axis's of the mooring lines would meet, at the center of the platform. On the other hand some environmental conditions that will counteract the yaw, due to a decreasing eccentricity. Then the operating environment will contribute to keeping the rotor plane in the wind and generating power. To quantify these environmental conditions is very desirable for which locations are favourable to place the turbine in, to generate maximum power without down-time.

The system that provides stiffness against yaw, is the mooring lines. The stiffness from this system is non-linear, where up to some angle of rotation, the relationship between force and yaw rotation is linear. For a large enough yaw rotation the stiffness from the mooring lines becomes higher, because the floater can only rotate so much before the lines are stretched out, and prevents further rotation of the floater (Kvittem, 2022a).

2.6.2   Static nature

The principle for static equilibrium is that the restoring forces must act in the direction of the opposing external force, so that the sum of forces equal zero.

As mentioned previously in the introduction, yaw is essentially a static phenomenon, but can be observed in a roll-yaw motion, which will be discussed in the following section. The static yaw motion can essentially be modelled using three parameters. A rotational spring, with stiffness k, an applied moment M_{yaw} and a corresponding rotation η_6. According to the theory of elasticity, one of the fundamental assumptions for material behaviour is linear relationship between stress and strain. For our case, where the mooring lines are providing the rotational stiffness for the FWT, the stiffness is linear for small rotations but non-linear as the applied moment increases.

2.6.3   Dynamic instability

The dynamic stability of a system is related to it's capacity to undergo harmonic oscillations from an exciting force and then eventually reach equilibrium as the oscillations become smaller and smaller in amplitude. If the oscillations grow in amplitude on the other hand, the system is unstable. To express the stability it is reasonable to include the inertia - and restoring forces. Further assuming linearity, the dynamic part of the yaw motion can be described as (Nielsen, 2007):

$$\eta_6 = \eta_{\;6a}e^{\sigma t} \tag{2.11}$$

Where η_{ia} is the amplitude of the motion, σ is a complex number, and finally t is time. Considering the exponent of 2.11, the oscillations will increase as time increases if the real part of σ is > 0. For the other case when the real part of σ <0 the oscillations will decrease over time

In (Haslum et al., 2022) the roll-yaw lock phenomenon discovered on the Hywind spar turbine has been described. A simplified 2DOF roll-yaw subsystem was adopted to explain the physical understanding of the phenomenon. For this system the eigenfrequencies and eigenvectors were found analytically. From this analysis it was concluded that the the stability of the system depends on the frequency separation between roll and yaw, and the relationship between the thrustforce and inertia of the system.

It was also observed that semi submersibles tend to have a higher natural yaw-period than roll-period, to mitigate the roll-yaw lock, the solution was to reduce the yaw stiffness from the mooring system. As the water depth increased the yaw period increased as well.

The roll period hardly changed with increasing water depth. Larger turbine and thrust-force capacity also contributed to a more susceptible roll-yaw lock behaviour.

The main difference from (Haslum et al., 2022) and the yaw-motion I am investigating in this thesis, is the coupling and the properties. I am focusing on the quasi-static yaw behaviour, and no coupling with pitch or roll.

If we have alternating rotations about the z-axis it is normally called fishtailing. Fishtailing is a dynamic phenomenon where a floating body performs an oscillatory motion in the the horizontal plane, with similar magnitude in alternating directions between two points of equilibrium (Tannuri et al., 2001). Fishtailing does not have to be related to floating bodies but can also to cars and planes. Fishtailing can typically occur for single point moored ships but also for FWT. In (Nielsen, 2007) a further explanation of directional stability and the conditions for a stable vs. unstable system is given for a single-point moored ship subjected to current and wind loads.

2.7 Environmental loads on offshore structures

The operating environment for an offshore windturbine can be harsh, and a challenging task for the design engineering team. For a FWT placed further out at sea than a bottom-fixed, or land based turbine, will generally experience higher wind speeds. Resulting in a larger aerodynamic load on the turbine. The environmental loads acting on a FWT has a stochastic nature, resulting in an ever changing operating environment. In this section I will consider the description of *wind* and *waves*. Current is also an important environmental load effecting the behaviour of a FWT, but will not be covered in this thesis, mainly due to the lack of current in the SIMA-model. The main environmental load I will investigate later in this thesis are varying wind direction and wind speed for constant wind conditions.

2.7.1 Wind

The fundamental force of nature that makes a wind turbine into a tool that produces renewable energy is the wind. The kinetic energy in the wind makes the blades turn and ultimately produces electrical energy. One of the most convincing arguments for developing offshore wind is that the wind speed is higher out at sea, and the wind intensity is more constant, than on land. There are several factors that influence the wind speed: Pressure gradients in the atmosphere, local weather and topography. Large pressure differences in the atmosphere will result in a high wind speeds. Local weather climate and topography will also influence the wind speed. The wind varies with height above sea level, increasing from sea level and upwards from the water surface. The wind direction has a joint probability with the formation of waves (Faltinsen, 1990). The power output of a turbine can be estimated with the following equation (Manwell et al., 2010).

$$P = \frac{1}{2} \rho A_{swept} V^3 \tag{2.12}$$

Where P is the power in Watts, ρ is the air density, which is approximately $1.225 Kg/m^3$. The air density can vary with location. A_{swept} is the swept area of the blades in m^2 and V is the wind velocity in m/s.

The aerodynamic load that the FWT experiences from the wind is complex, and random at nature. The wind direction, wind speed, turbulence are all factors that influences the aerodynamic loading on the structure. Wind direction is affected by the orientation of air pressure differences. To estimate the mean wind loading on the a FWT, IEC 61400-1 suggest to use either a logarithmic profile equation (2.13) or a power law profile

equation (2.14), to describe the relationship between wind speed and height above a sea surface (IEC, 2005) .

$$V(z) = V(z_r) \frac{ln(\frac{z}{z_0})}{ln(\frac{z_r}{z_0})} \tag{2.13}$$

$$V(z) = V(z_r)(\frac{z}{z_r})^a \tag{2.14}$$

Reference height is denoted z_r and height above sea surface with z. The parameter $V(z_r)$ is the mean wind speed at reference height z_r. z_0 is the roughness length. a is the wind shear or power law exponent often set to 0.14

.

Turbulence

Wind turbulence is fluctuations around the mean wind speed, due to dissipation of kinetic energy to thermal energy. When this energy transition is taking place, the result will lead to gusts. If turbulent wind is investigated for a longer period of time, the mean wind speed will be the most prominent. For a shorter period of time the wind speed will be quite varying. One of the most common ways to measure or express turbulence is turbulence intensity, TI. The turbulence intensity is defined by the relationship between the mean wind speed, U and the standard deviation, σ_U [m/s] based on the mean wind speed (Manwell et al., 2010).

$$TI = \frac{\sigma_U}{U} \tag{2.15}$$

Figure 2.13 shows a typical fragment of wind data here sampled at 8 Hz. This data set has a mean wind speed of 10.4 m/s and a standard deviation of 1.63 m/s. Thus, the turbulence intensity over the ten-minute period, is 0.16. according to equation (2.15). Furthermore, it is clear to spot the fluctuating character of time-series and somewhat random nature of turbulent wind over the short time interval.
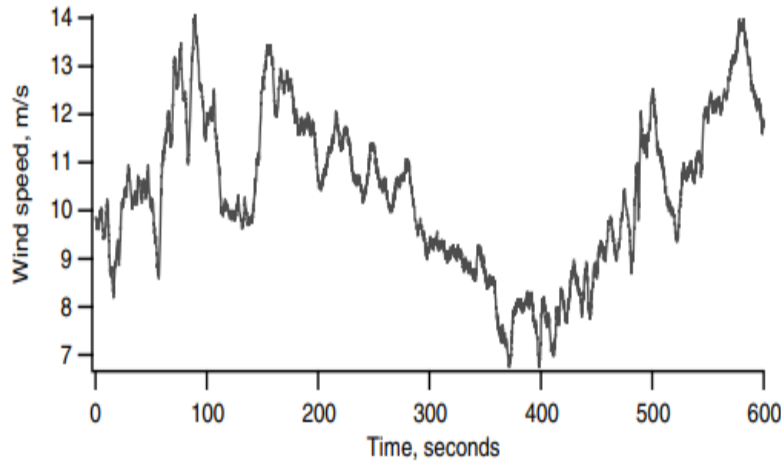
Figure 2.13: Turbulent wind speed time-series from (Manwell et al., 2010)

Wind spectrum

To describe the short-term stochastic nature of the wind, it is possible to describe the energy variations present in varying wind speed using the frequency. This is called a wind spectrum. According to the IEC 61400-1 there are several spectra available, but a widely used spectrum is the Kaimal spectrum. The component spectral density is given by equation (IEC, 2005)

$$\frac{f S_{k(f)}}{\sigma_k^2} = \frac{4 f L_k / v_{hub}}{(1 + 6 f L_k / v_{hub})^{5/3}} \tag{2.16}$$

Here f is the frequency in Hertz, k is an index describing the direction of the wind velocity, S_k is the single sided velocity component spectrum. Furthermore, σ_k is the standard deviation of the velocity and L_k is the velocity component integral scale parameter. According to DNV-RP-C205 section 2.3.2.12, the Frøya wind spectrum is recommended for offshore applications, unless data from relevant site suggest otherwise. The mean wind speed U, can be expressed by average period T, and height z (DNV, 2014).

$$U = (T, z) = U_0 \cdot \left\{ 1 + C \cdot ln \frac{z}{H} \right\} \cdot \left\{ 1 - 0.41 \cdot I_u(z) \cdot ln \frac{T}{T_0} \right\} \tag{2.17}$$

Where $H = 10$m, $T_0 = 1$ hour, $C = 5.73 \cdot 10^{-2} \sqrt{1 + 0.148 U_0}$ and $I_u = 0.06 \cdot (1 + 0.043 U_0)$ This wind profile is valid for averaging period $T < T_0$.

In Figure 2.14 the Kaimal and Frøya wind spectra are plotted together in 3D. The Kaimal spectrum is abbreviated as IEC and Frøya as API. The horizontal plane in the figure describes the correlation between height above sea surface and frequency, while the vertical axis describes the spectral power density .

The Kaimal spectrum mainly depends on the wind speed at hub-height while Frøya wind spectrum depends on wind speed and height. The Frøya wind spectrum typically has more energy in the low frequency range, that could cause excitation of low frequency structural modes (Guo et al., 2014) .
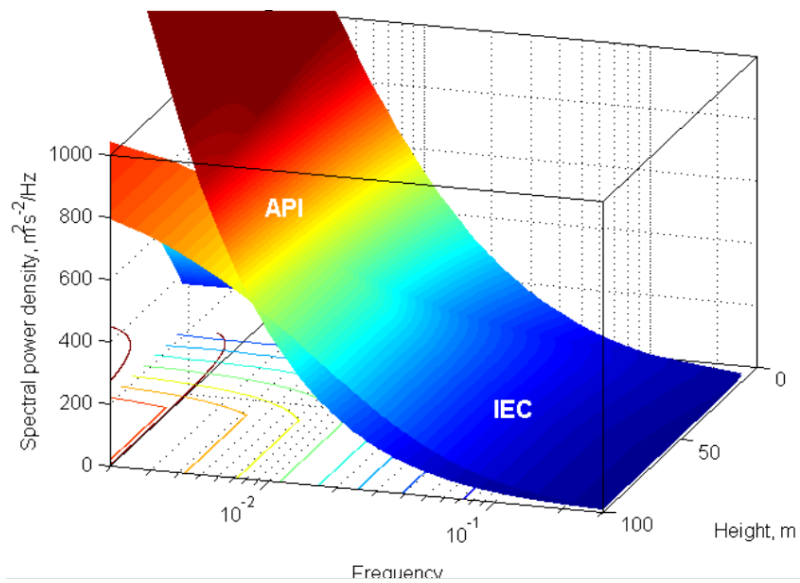
Figure 2.14: Frøya (API) and Kaimal (IEC) wind spectrum plotted together from (Guo et al., 2014)

2.7.2   Aerodynamic forces

In this section a brief summary of the fundamental theory, on how to describe the aerodynamic demand on the turbine is presented. To find the acting force on the blades generated from the wind, a common method to apply is the blade element momentum method. This method is based on conservation of momentum or momentum theory, which states that the force of the blades is the only contributor to the change in momentum across the rotor span. Blade element theory describes the analysis of forces at a defined section of the blade, as a function of blade geometry. Together these two theories make up the blade element momentum theory (Manwell et al., 2010).

To find the exerted forces on the blades of a wind turbine, it is convenient to discretize the blade geometry into smaller segments with a distance dr as shown in Figure 2.15a. Following the discretization, the aerodynamic forces are computed for the defined segment and finally added together to represent the blade(s). Figure 2.15b) shows the velocity at an airfoil. In the figure the drag force is acting parallel to the dashed line in and the lift force is acting perpendicular in the same plane. The variable V in Figure 2.15b) represents the relative blade wind speed, ϕ is the angle of incidence, α is the angle of attack (AOA), and β represents the twist of the airfoil relative to the rotor plane, c is the chord length, Ω is the rotational speed at a given blade section and lastly U_x is the wind speed at the operational site. For a turbine in operation the rotational speed Ω_r is higher than the wind speed (Olczak et al., 2016). Oppositely for an idling turbine the wind speed is higher than the rotational speed.

(a) Rotor discretization   (b) Airfoil velocity
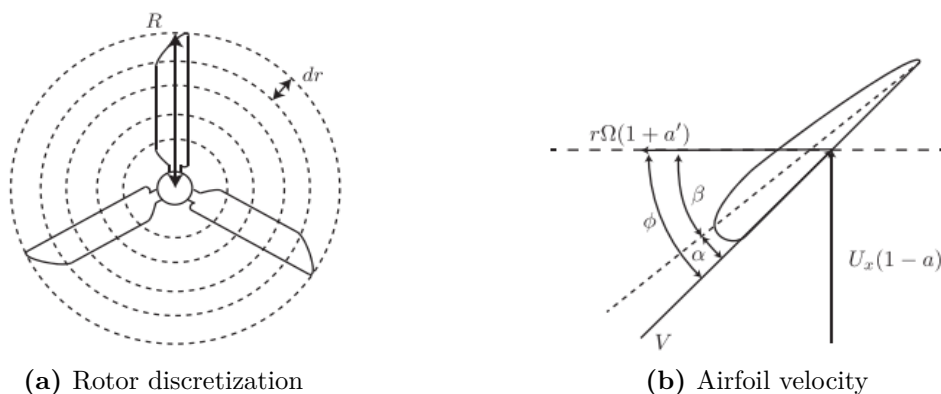
Figure 2.15: Blade element momentum method. (Olczak et al., 2016)

From the theory and methodology mentioned above, it is possible to describe the aerodynamic forces acting on a blade element. The three relevant force for this analysis are lift, drag and pitching moment, and can be expressed as following (Eliassen, 2015):

$$F_{Lift} = \frac{1}{2}\rho V^2 c C_L \tag{2.18}$$

$$F_{Drag} = \frac{1}{2}\rho V^2 c C_D \tag{2.19}$$

$$F_{Moment} = \frac{1}{2}\rho V^2 c^2 C_M \tag{2.20}$$

Where ρ is the air density, V is the relative blade wind speed, c is the chord length and C_L, C_D and C_M are lift, drag an pitching moment coefficients respectively.

2.7.3   Waves

The following section will contain theory on waves. The wave loading on a FWT is important to capture a realistic behaviour. The floating substructure is the part of the wind turbine that most frequently will experience wave loading. However the tower can also be subjected to large wave loads for high wind speeds. Generally for higher wind speeds, the response is more wave dominant than aerodynamic. Waves can be defined as a propagating disturbance in a medium. The medium the waves are propagating through, will give certain characteristics. The relevant waves that are acting on a FWT are ocean waves. Ocean waves so-called surface waves, and are typically transverse, where there is wave crest and wave trough. One wave cycle is from crest to crest (Helmholtz et al., 2022).

Regular waves

Regular waves are defined as a sinusoidal with constant wave amplitude, wave length and wave period. Hence a regular propagating wave can be described as

$$\zeta = \zeta_a sin(\omega t - kx) \tag{2.21}$$

The variable ζ is describing the wave elevation based on position x, and time t. Further, ω is describing the angular frequency for the wave oscillation, and ζ_a is the wave amplitude (Arntsen and Krogstad, 2000). Since sine varies from -1 to 1, and $\zeta < \zeta_a$, the absolute value of the wave elevation is never larger than the wave amplitude. The angular frequency ω can be found from:

$$\omega = \frac{2\pi}{T} \tag{2.22}$$

Irregular waves

A more realistic approach to model sea waves is considering them as irregular. For regular waves there is one single frequency throughout the wave motion. For an irregular wave, there is a combination of several frequencies. A convenient consequence of linear wave, or Airy theory is that irregular waves can be modelled by regular waves of unalike amplitudes, wavelength and direction (Faltinsen, 1990).

$$\zeta = \sum_{j=1}^{N} A_j \ sin(\omega_j t - k_j x + \varepsilon_j) \tag{2.23}$$

Where A_j, ω_j, k_j and ε_j is wave amplitude, circular frequency, wave number and arbitrary phase angle of wave j. To model long term sea behaviour, it is important to know

the joint frequency of the significant wave height and the mean wave period. For a short-term sea state, the significant wave height and the mean wave period are assumed constant throughout the time period. The significant wave height and mean wave period will vary in long term modelling of sea behaviour.

Wave spectrum

Wave spectrum is a statistical way to model the irregular nature of the sea. The wave spectrum can be estimated from wave measurements. The fundamentals of the wave spectrum modelling approach is that the sea can be described as a stationary random process. The consequence of this assumption is that the random process is limited in time, in the range from around 30min to close to 10 hours (Faltinsen, 1990). Several spectra exist, but two widely used wave spectra are JONSWAP-spectrum and Pierre-Moskowitz spectrum. These are plotted together in Figure (2.16). The JONSWAP-spectrum is based on the fundamentals of the Pierre-Moskowitz spectrum.
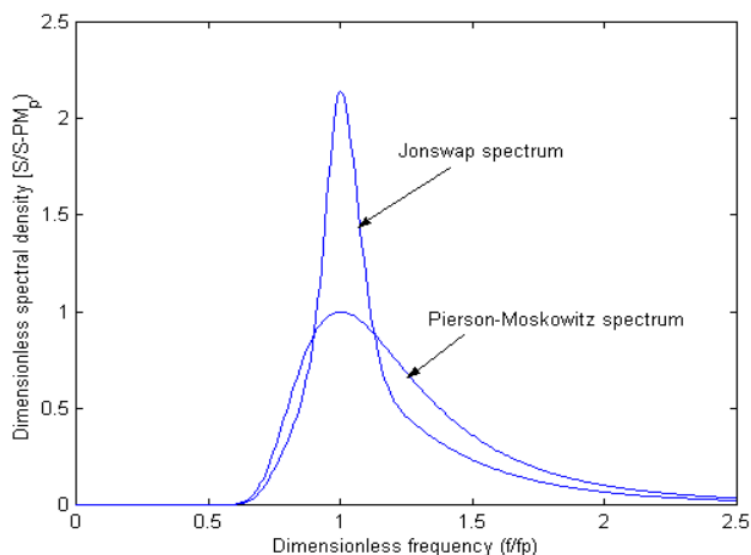
Figure 2.16: JONSWAP-spectrum and Pierre-Moskowitz spectrum (Arntsen, n.d.)

The case study model in SIMA uses a three parameter JONSWAP wave spectrum to model the waves in the simulation environment.

2.8   Structural dynamics

In this section I will give a brief introduction on the derivation of the equation of motion from a generic SDOF-system. Then I will briefly describe how the equation of motion is used to model the rigid body dynamics of a floating structure. Even though the majority of the simulations are dynamic in this thesis, the output and objectives are of static nature.

2.8.1   SDOF and the equation of motion

A single degree of freedom system is a system where there is only one permitted direction of rotation or translation. A generic SDOF-system comprises of a mass, m, stiffness k, and a damper, c. The mass will contribute to inertia forces, the stiffness is essentially the elastic resistance acting opposite to the applied loading. The damper is included in the system to account for energy-loss and overall conservation of energy. In Figure 2.17 a SDOF system is presented. In this system only horizontal translation of the mass is permitted. The spring represents the stiffness, the square placed on the rollers represents the mass, and the dashpot the damping in the system. When developing an idealized SDOF like this, it is common to lump the mass in one body, even though the real mass is distributed otherwise. The expression $u(t)$ represents a function describing the displacement of the mass with respect to time. $p(t)$ is a function describing the external loading acting on the system, also as a function of time (Tomasi, n.d.).
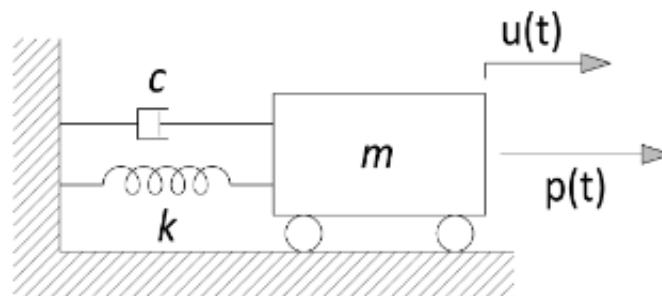
Figure 2.17: Generic SDOF system from (Tomasi, n.d.)

From these parameters introduced, some equations can be formulated to describe the relationship of the system.

The inertial forces in the system $f_i(t)$ can be derived using D'Alemberts principle and newtons second law.

$$f_i(t) = m\ddot{u}(t) \tag{2.24}$$

The damping force is the product of the damping constant c and the velocity.

$$f_d(t) = c\dot{u}(t) \tag{2.25}$$

Furthermore the spring force can derived similarly. The spring force, similar to Hooke's law is the product of stiffness and displacement(position).

$$f_k(t) = ku(t) \tag{2.26}$$

To find the full equation of motion, equilibrium is considered. To maintain equilibrium the sum of forces has to equal 0. Hence the internal forces in the system must equal the external forces applied to the system. p(t) represents the external excitation forces.

$$\Sigma_{forces} = 0 \tag{2.27}$$

$$f_i(t) + f_d(t) + f_k(t) = p(t) \tag{2.28}$$

inserting the previous expressions for the internal forces gives the equation of motion.

$$m\ddot{u}(t) + c\dot{u}(t) + ku(t) = p(t) \tag{2.29}$$

2.8.2   Floating Rigid body dynamics

Depending on the field of engineering, the notation for the parameters in the equation of motion can vary. From (Haslum et al., 2022) a simplified expression for the rigid-body dynamics of a FWT in still water can be described as:

$$(M_s + M_a)\ddot{\eta} + B\dot{\eta} + (K_h + K_m)\eta = F_t \tag{2.30}$$

Starting on the left hand side of the equation, the mass in system consists of M_s, being the structural mass matrix. M_a is the hydrodynamic added mass matrix. The added mass is the inertia added to the system to represent the inertia of the fluid, opposing the motion of a body moving through it (Lopresto et al., 2017). $\ddot{\eta}$ is the acceleration of the system. η is the displacement vector containing all 6 degrees of freedom, $\eta = [\eta_1\ \eta_2\ \eta_3\ \eta_4\ \eta_5\ \eta_6]$. Which respectively corresponds to surge, sway, heave, roll, pitch and yaw. These degrees of freedom was described in Figure 2.2. B is the damping matrix, consisting of aerodynamic and hydrodynamic viscous damping, and $\dot{\eta}$ is the acceleration vector. The stiffness of the system has two contributions, k_h and k_m. This is the hydrostatic stiffness matrix k_h describing how the load from the net weight and buoyancy varies with change from origin position.k_m is representing the mooring stiffness. Finally F_t is a vector including the aerodynamic turbine loads, $F_t = [F_1\ F_2\ F_3\ F_4\ F_5\ F_6]$. This equation is suitable for low frequency excitation forces and small movements about initial position.

3. Method

This chapter will consist of an introduction to the method used for investigating the objective presented earlier in this thesis. Furthermore I will explain the procedure regarding the simulation software, and lastly general considerations when using numerical methods as an engineering tool.

3.1 Case study

The method I will be using to answer the objective earlier introduced, is a case study using the INO WINDMOOR 12 MW turbine. The background for me using this model for my thesis, is the WINDMOOR research project. This is a 4-year research project funded by the research council of Norway, with the main goal of reducing cost and improve the design of offshore floating windfarmes. Furthermore the research group has formulated some key knowledge which is investigated in the research (SINTEF, n.d.).

1. *Create validated hydrodynamic models in the low-frequency domain*

2. *Better understand atmospheric conditions and aerodynamic interaction between turbines in a wind farm.*

3. *Optimize global analysis for wind farms*

My thesis will not directly contribute to this project, but through a case study consisting of numerical time-domain simulations of the INO WINDMOOR turbine, I will investigate a phenomenon that has been observed in the previous work on the floating wind turbine. If I were to connect the topic of this thesis to one of the key points, I would probably associate it with the goal regarding better understanding of atmospheric conditions and aerodynamic interaction. Given that my study will only consider one turbine and not a farm, it is still important to properly describe the aerodynamic behaviour for one turbine. If we have good models for one turbine by itself, then increasing the number of turbines, including wake effects and other mechanics will a natural next step in complexity.

The tools I will be using to conduct this study is mainly SIMA, which I will further describe in the next section. In addition to SIMA I will use Python for post-processing and plotting of simulation data from SIMA.

3.2 Simulation software

3.2.1 SIMA

SIMA is workbench for marine applications, tailored to analysing slender structures. It is developed by SINTEF Ocean, but distributed together with DNV-GL. Two of it's main components used in this thesis are SIMO, and RIFLEX (DNV, n.d.).

SIMO

SIMO is the module which simulates motion and fixation of a floating structures. This module consists of non-linear time-domain simulation, flexible modelling of multibody systems and environmental forces due to wind,waves and current, to mention some. SIMO can use frequency properties as input for the time-domain simulations, where the simulation is coupled with forces and displacements in common nodes using the RIFLEX solver. (SINTEF-Ocean, n.d.(b)).

RIFLEX

RIFLEX is the FE-solver, which is tailored to the analysis of slender structures. RIFLEX uses time-domain computations containing a step by step integration of the dynamic equilibrium equation. For every progressing time-step the mass, damping and stiffness matrix are updated. The updating of the matrices makes the analysis non-linear (SINTEF-Ocean, n.d.(a)). Examples of slender structures are: mooring lines, steel pipelines and tower, blades of a wind turbine.

3.2.2 Python

Python is a higher-order object oriented programming language with emphasis on user friendliness. It has a very wide user base and well documented syntax. I will use python to import .h5 files that are exported from SIMA. To import these files I will mainly use the QATS package which is part of the python library. QATS was made to handle import, processing and visualization of time-series from SIMA. Using the QATS library it is possible to do signal processing, statistical analysis, count cycles for fatigue analysis and plotting, to mention some features (DNV-GL, n.d.). I will use both the QATS GUI, and scripting to post process data. To find the intended result from a

dynamic simulation, the stable time series has been used, from 500s to 1000s in most cases. In the first part of the simulations the fluctuations in the results are too large.

Table 3.1: Software overview

Software	Task
SIMA	Time-domain simulations and FE-analysis
Python	Post-processing,visualization and plotting.

3.3   Simulations as an engineering tool

To solve an engineering problem we develop models. The great statistician George Box once said (Wasserstein, 2010) : "All models are wrong but some are useful." The essence of this quote is that a model does not depict reality, we make certain assumptions to develop models. When working on the design of a bridge, residential building or a floating wind turbine it is beneficial to create a model. This lets the engineer make calculations on a simplified structure. It is however very important to bear in mind that a model has limitations. Knowing the limitations of the model is crucial for sensible results of the analysis. In addition to model errors, using simulations can also cause rounding errors or numerical errors. Simulations are an approximation and can deviate slightly. Numerical errors could also be linked to the misinterpretation of unit systems.

When working with a model which is nowadays usually numerical, it is very useful and necessary to compare the results to some analytical method or experimental results. For example to analyze a floating wind turbine by hand, would be too complicated and time consuming. Therefore a numerical study with the use of a simulation software seems like most appropriate solution. For complex load situations like a floating structure out at sea, it is a great advantage to use numerical methods to apply loads and to subsequently find the stresses on the structure. To acquire these results otherwise, it would be an idea to use experimental methods. For offshore wind engineering it is common in the early stages, to use a down-scaled model in a test basin or similar to verify numerical results. If an offshore wind project has sufficient funding and resources, a full scale pilot can be built to collect valuable data for further design and operation (Nielsen, n.d.). Generally in engineering it is good practice to compare results between methods, not only rely on one method (Kvittem and Nygaard, 2021).

In this thesis the platform yaw and yaw moment has been found for both a rotating floater and a fixed floater, to compare the behaviour when subjected to aerodynamic loading. Using two different methods to ultimately find the same parameter, makes the work robust and also versatile. I think this holistic approach, has increased the learning outcome from the work in this thesis.

4. Numerical model

In this chapter, I will begin to introduce the INO WINDMOOR 12 MW turbine which is the turbine I will be using for the case study. Furthermore, I will proceed with the numerical model which is developed in SIMA, calibrated with experimental testing done in SINTEF Ocean's test basin in Trondheim. The purpose of this chapter is to understand the underlying physics of the model and modelling approach. The ability to understand the building blocks that makes up the model, is paramount to be able to interpret and evaluate the results from the analysis. The modelling of the 12MW turbine has been done by the staff at SINTEF Ocean, and has been provided to me by my supervisor, Marit Irene Kvittem.

4.1 INO WINDMOOR 12MW

4.1.1 Introduction

The wind turbine has a semi submersible floater jointly designed by Inocean and Equinor. This floater is made of steel and consists of three coloumns, connected by secondary beams and floating pontoons. Inocean also provided the design for the mooring system, with three hybrid catenary lines. The hybrid mooring lines are made up of steel chains and polyester rope.

The location for the turbine is thought to be gulf of Maine, which is a location with medium strength met-ocean conditions. Gulf of Maine is located on the east-coast in the United States of America, located just outside Maine and Massachusetts. Where reference sea depth is in the range of 60-200m and average wind speed at 100m is 9.8 m/s (Gómez et al., 2015)

4.1.2   Turbine characteristics

The design of this turbine is based on the 10 MW turbine developed by DTU. (Danish university of technology) This model has been accepted by several universities and research institutions. This model was then modified by IEA WIND TCP, to make it more similar to current offshore wind turbines. The same airfoiles from the IEA 10 MW are used in the 12MW turbine, while blade dimensions and structural properties have been up-scaled by using standard up-scaling laws. The turbine modified by IEA WIND TCP has been the basis for design of the INO WINDMOOR FWT. The nacelle/hub properties was derived from the Haliade X 12MW wind turbine from GE. These properties were found from published data from manufacturer. (Silva de Souza et al., 2021)

In Table 4.1, some key information about the INO WINDMOOR turbine has been assembled. Here the dimensions and mass of the turbine components are described, as well as properties related to the rated wind speed and power production.

Table 4.1: Key properties for the INO WINDMOOR 12MW turbine from (Silva de Souza et al., 2021)

Parameter	INO WINDMOOR 12MW	Unit
Rated electrical power	12.0	(MW)
Specific power	324.8	W/m^2)
Rotor orientation	Clockwise rotation	Upwind
Number of blades	3	
Rotor diameter	216.9	(m)
Hub diameter	5.0	(m)
Blade length	105.4	(m)
Blade prebend	6.8	(m)
Shaft tilt	6.0	degrees (°)
Rotor precone	-4.0	degrees (°)
Hub Height	131.7	(m)
Cut-in/rated/cut-out wind speed	4.0/10.6/25.0	(m/s)
Cut-in /rated rotor speed (rpm)	5.5/7.8	(rpm)
Generator efficiency	94.4	(%)
Maximum Tip Speed	94.4	(m/s)
Individual blade mass	63.024	(Kg)
Total blade mass	189.072	(Kg)
Hub mass	60 000	(Kg)
Nacelle mass	600 000	(Kg)

Figure 4.1 is depicting the entire floating wind turbine. With the floater, turbine and tower. Mooring lines are not included in this figure.

Figure 4.1: INO WINDMOOR 12MW turbine from (Silva de Souza et al., 2021)

Below in table 4.2 I have added a table including the rigid-body natural periods from decay simulations conducted in SIMA. Decay simulations are based on damped free-vibration mechanics. The system is excited from an external force, and the natural periods for the desired degree of freedom can be found respectively. The values in the tables are describing the time in seconds, it takes to complete one full cycle of oscillation in respective translations and rotations.

Table 4.2: Rigid body natural periods for the INO WINDMOOR. (Silva de Souza et al., 2021)

	Surge	Sway	Heave	Roll	Pitch	Yaw
Natural periods (s)	97.3	98.0	16.3	29.5	31.4	88.0

4.1.3   Mooring

At the bottom of this page and the next, there are two tables describing the mooring system, coordinates, and material properties. Table 4.3 describes the coordinates of the three mooring lines, and rotation with respect to each other. There is an angle of 120° between the mooring lines. The fairlead is the point of attachment at the platform and the anchor is naturally the point the below water level connecting the mooring line to the seabed. The water depth is considered to be 150m and the seabed is considered flat. From the mooring line geometry, sea depth and seabed topography, the pretension forces in the mooring lines are about 1050 kN.

In Table 4.4 I have added a table related to the mooring properties. The mooring lines consists of chains and polyester ropes, where the chains provide the weight necessary for the catenary effect, and the fibre ropes provide strength, and maintains a low weight of the mooring system. At the fairleads, the top of the mooring lines are made of steel chains. Joining the chain structure at the anchor and floater, is the polyester rope. The chains and fibre rope configuration below have approximately similar stiffness to mass/length ratio.

In the final Table, 4.5 on the next page, the linear restoring coefficients from the mooring system has been added. In the case study model these values has been incorporated using FEM, as cable/bar elements and will provide stiffness implicitly by forces at the fairlead.

Table 4.3: Mooring line coordinates from (Silva de Souza et al., 2021)

Mooring line	Fairlead			Anchor			
	x(m)	y(m)	z(m)	x(m)	y(m)	z(m)	Azimuth(deg)
ML1	42.7	0.0	0.0	700	0.0	-150.0	180
ML2	-21.4	37.0	0.0	-350.0	606.2	-150.0	300
ML2	-21.4	37.0	0.0	-350.0	606.2	-150.0	60

Table 4.4: Mooring line segment properties from (Silva de Souza et al., 2021)

Segment	Type	Length (m)	Equiv. diam (m)	Mass/length (kg/m)	Axial stiff (MN)
1	130 mm Stud.chain	25.0	0.234	377.7	1443.0
2	190 mm Polyester	85.0	0.190	60.7	228.0
3	190 mm Polyester	85.0	0.190	46.0	228.0
4	130 mm Stud.chain	499.8	0.234	353.6	1443.0

Table 4.5: Linear restoring coefficients from mooring system. (Silva de Souza et al., 2021)

Degree of freedom	Stiffness matrix component	Value
Surge	k_{11}	89800 N/m
Sway	k_{22}	89800 N/m
Yaw	k_{66}	1.2165×10^8 Nm/rad

4.2   SIMA-model

To analyze the behaviour of the INO WINDMOOR turbine, a numerical model was es-
tablished in SIMA. The coordinate system used for the model is a Cartesian coordinate
system (x,y,z) with the x-y plane coinciding with the water level, and positive z-direction
being upwards from the water surface. Waves and wind coming from 0° corresponds
to propagation along positive x-direction. Propagation along the positive y-axis cor-
responds to wind or waves from 90°. Following that, 180° will be negative x-direction
corresponding to the environmental load acting on the hub before the nacelle. Positive
rotation around z-axis will be counter-clockwise, from x-axis towards y-axis. Below in
Figure 4.2 there is an image illustrating the definition of the axis.
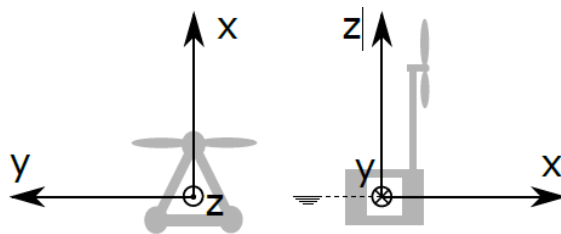
Figure 4.2: Coordinate system from (Silva de Souza et al., 2021)

4.2.1   Platform

The platform was modelled as a SIMO rigid body with applied loads from FE-elements
in RIFLEX. RIFLEX however, has not been used to compute response of the floater.
A rigid body is essentially a point in space with mass, stiffness and damping. In Table
4.6 below I have enclosed some key information for the floating substructure from (Silva
de Souza et al., 2021). These values are describing the dimension of the hull and inertia
properties. The mass and center of gravity can be used to estimate the inertia of the
platform which is given at the origin of the body in SIMA.

Table 4.6: Hull & inertia properties from (Silva de Souza et al., 2021)

Property	Value	Unit
Column diameter	15.0	meter (m)
Column height	31.0	meter (m)
Pontoon width	10.0	meter (m)
Pontoon height	4.0	meter (m)
Center-center distance	61.0	meter (m)
Deck beam width	3.5	meter (m)
Deck beam height	3.5	meter (m)
Total substructure mass	11974.0	metric tons (mt)
Total substructure CG_x	-5.91	meter (m)
Total substructure CG_z	-9.7	meter (m)
Total substructure R_{xx}	23.66	meter (m)
Total substructure R_{yy}	18.63	meter (m)
Total substructure R_{zz}	28.10	meter (m)

The hydrostatic stiffness matrix contains only the the water plane stiffness. The buoyancy of the platform is accounted for by including a separate force acting in the centre of buoyancy. Gravity is included in the definition of the semi body. The water plane stiffness in pitch or roll for the INO WINDMOOR platform can be estimated with the following expression (Eliassen and Verma, 2021).

$$C_{44/55,wp} = \rho g \Sigma_{i=1}^3 \left(\frac{\pi D^4}{64} + b^2 A \right)$$

(4.1)

The water density is denoted ρ, g is the gravitational acceleration, D is the diameter of the platform columns, b is the distance from the origin to center of the column in either pitch or roll direction. From Table 4.6 the column diameter is 15m.

In (Silva de Souza et al., 2021) equations (6.4) gives a more detailed description of the calculation of the linear restoring coefficients. For these calculations small displacement angles in pitch and roll are assumed.

4.2.2 Tower

The tower structure has been modelled by beam elements. The entire tower consist of 20 beam elements, with an axisymmetric cross-section (CRS1) and decreasing diameter with increasing height from the platform. The tower elements with corresponding cross-sectional properties, mass and stiffness are provided in Table 5.8 in (Silva de Souza et al., 2021). To model the tower there has been used two supernodes. One at the top by the turbine and one at the tower base. The bottom supernode at the platform origin is the slave node. The tower is modelled as a steel member with density, $\rho = 7500 kg/m^3$ and a modulus of elasticity, $E = 211$ GPa. The key parameters of the tower geometry and mass has been assembled in Table 4.7

Table 4.7: Tower properties properties from (Silva de Souza et al., 2021)

Parameter	Value	Unit
Diameter top	5.97	meter (m)
Diameter bottom	9.90	meter (m)
Thickness at top	30.1	millimeter (mm)
Thickness at bottom	90.0	millimeter (mm)
Length	110.20	meter (m)
Mass	1161.6	metric tons (mt)
CG_z from base	56.65	meter (m)

4.2.3   Wind turbine

To model the wind turbine a blade element momentum model (BEM) has been used (Manwell et al., 2010). To capture dynamic stall and -wake effects, Øye's model has been applied in this case. The wind turbine blades are modelled using beam elements, 18 elements in total. These beam elements are bi-symmetric (CRS2), and the elements for the tower were axi-symmetric (CRS1). To model the tower shadow effects on the turbine potential theory has been applied.

4.2.4   Control system

The controller used in the SIMA-model is based on a open source controller called RO-SCO or **R**eference **O**pen**S**ource **CO**ntroller for wind turbine applications. This control system was chosen due to the wide functionality and open source availability. The INO WINDMOOR turbine reaches rated power at 10.5 m/s, then the blade pitch is induced to reduce aerodynamic load on the turbine. (Silva de Souza et al., 2021). The controller's gains has been tuned for the INO WINDMOOR turbine, for above rated wind speed. The main purpose of the tuning the controllers gains to the INO WINDMOOR turbine, is to avoid using a great deal of energy in to the blade pitching, at constant rotor speed.

5. Static Yaw behaviour

In this chapter I will theoretically describe the yaw motion of the case study model. I will introduce a static system with one degree of freedom. This is not to be mistaken by a dynamic single-degree of freedom system. The purpose of this is to be able to compare analytical results with simulations. Furthermore a comparison between a linear, non-linear mooring and offset stiffness is discussed.

5.1 Static Yaw system

A driving factor for increasing yaw angle of the FWT is the eccentricity between the hub-point and the point of rotation, which is the platform center. The lever arm of this eccentricity is perpendicular to wind direction. When the wind direction shifts, it takes time for the yaw system to rotate the RNA into the new direction. The yaw mechanism tends to be quite slow-moving, rotating about $0.5°/sec$ (Kvittem, 2022b). The thrustforce acts perpendicular to the rotor plane, but eccentrically relative to the platform center. This contributes to a driving moment, resulting in increased yaw angle of the platform.

The theory on unstable behaviour is related to the lever arm or eccentricity. A positive yaw angle which reduces the lever arm, will be restoring. Oppositely, a positive yaw angle which increases the lever arm will be reinforcing the rotation, therefore unstable.

To describe the eccentric placement of the hub-point relative to the platform center, one have to consider the distance from platform center to the tower, and from the tower to the hub. This is because the platform will have a yaw angle, η_6 and the RNA will have a separate angle, α. The RNA will have the same angle as the wind direction. The yaw controller will rotate the RNA into the wind, with a relative angle to the orientation of the platform. The yaw controller of the platform will rotate the RNA before the platform rotates.

For the further description of the yaw system, a coordinate system where origo is in the middle of the platform is used. First the rotor plane is rotated towards the new wind direction, α, then the slow moving hub rotation leads to the yaw angle of the platform, η_6. Using polar coordinates, the position (x.y) of the hub relative to a RNA-angle α, and distance r from tower can be expressed as:

$$x_{hub} = x_{tower} + r_{hub}cos(\alpha) \tag{5.1}$$

$$y_{hub} = y_{tower} + r_{hub}sin(\alpha) \tag{5.2}$$

The next step in estimating the yaw rotation, is finding the position of the tower based on the hub position. The hub point is able to rotate independently of the platform, and have it's own rotation α, as mentioned. This is to keep the rotor plane into the wind and to produce power. By applying coordination transformation about origo, using the platform yaw angle, η_6, its possible to express the position of the tower using the hub coordinates (Davidsen, 2010) as following:

$$x_{tower} = r_{hub}cos(\alpha - \eta_6) \tag{5.3}$$

$$y_{tower} = r_{hub}sin(\alpha - \eta_6) \tag{5.4}$$

Using the relation:

$$cos(A - B) = cos(A)cos(B) + sin(A) + sin(B) \tag{5.5}$$

$$sin(A - B) = sin(A)cos(B) - cos(A) + sin(B) \tag{5.6}$$

I end up with the following expression for the tower position:

$$x_{tower} = r_{hub}[cos(\alpha)cos(\eta_6) + sin(\alpha)sin(\eta_6)] \tag{5.7}$$

$$y_{tower} = r_{hub}[sin(\alpha)cos(\eta_6) - cos(\alpha)sin(\eta_6)] \tag{5.8}$$

When multiplying the expressions in (5.9) and (5.10) and using (5.3) and (5.4) the expression becomes:

$$x_{tower} = x_{hub}cos(\eta_6) + y_{hub}sin(\eta_6) \tag{5.9}$$

$$y_{tower} = -x_{hub}sin(\eta_6) + y_{hub}cos(\eta_6) \tag{5.10}$$

The tower position can also be expressed in matrix form:

$$\begin{bmatrix} x_{tower} \\ y_{tower} \end{bmatrix} = \begin{bmatrix} cos(\eta_6) & sin(\eta_6) \\ -sin(\eta_6) & cos(\eta_6) \end{bmatrix} \begin{bmatrix} x_{hub} \\ y_{hub} \end{bmatrix} \tag{5.11}$$

In Figure 5.1 below there is an overhead view of the floating turbine where the platform has a yaw rotation η_6, and the RNA has a rotation α. In the figure, it is also visible that the rotation of the turbine up against the wind direction w is in progress. As mentioned this movement is typically quite slow and will contribute to the driving yaw moment. In the figure there is also added three key points which are; the platform center or origo (x_0, y_0), tower position (x_{tower}, y_{tower}) and hub position (x_{hub}, y_{hub}). The thrustforce is acting in the hub-point, shown with a blue arrow in the figure. The eccentricity e is denoted in blue, and shown with a blue line. The slope of the eccentricity matches the slope created by the hub rotation α.
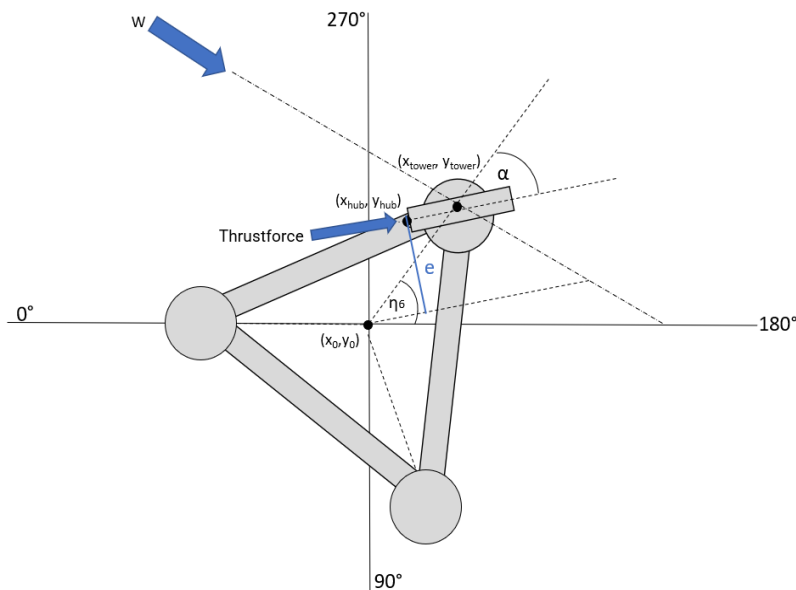

Figure 5.1: Static yaw system

In the following paragraph I have chosen to use a general notation to ease the expressions. The mooring center (x_0, y_0) will be referred to as P, the tower point (x_{tower}, y_{tower}) will be called R and finally the hub point (x_{hub}, y_{hub}) will be called Q. The line l will have the same directional vector as the wind direction w. x_{wind} is the point where the line l intersects the x-axis.

To find an expression for the eccentricity e, I want to find the distance between a line defined by a vector $\vec{V}$, and the mooring center P. From the vector $\vec{V}$, it is possible to define a line l, which has $\vec{V}$, as the directional vector. The point of interest that is lying on the line l, is the hub-point which I will denote Q. Then the distance from the mooring center P, to the line l, using the hub-point Q, will be eccentricity. Finding the distance from P, to l, is the same as finding the length of $\vec{PQ}$, where the point Q, is located on the line l, such that $\vec{PQ} \perp \vec{V}$. The perpendicular nature between the vectors can be used to express the relationship using the scalar product.

Instead of stating $\vec{PQ} \perp \vec{V}$, it is possible to state that $\vec{PQ} \cdot \vec{V} = 0$ (NDLA, 2022).

In Figure 5.2 there is a simplified figure describing the notation, with similar orientation as Figure 5.1. This figure assumes that the hub-point Q is positioned on the line l and not rotating like in Figure 5.1.
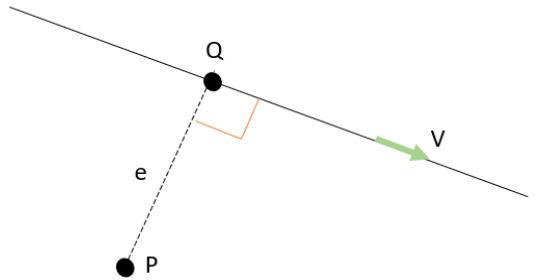
Figure 5.2: Simplified approach to find eccentricity, e, from the hub-point

It has to be stated that the mathematical framework needs to be tested further to be used. Especially the coordination transformation needs to be tested, and probably tuned to be sufficiently accurate. Due to lack of time in this thesis work, I have not had the time to test and verify the mathematics for the static system. Although I think the ideas and foundation could be very exciting and powerful after some further work.

5.2   Mooring stiffness

In this section I will investigate the yaw stiffness provided by the mooring lines. It is interesting to investigate the non-linear nature of the yaw stiffness for an increasing load. Theoretically the yaw stiffness provided by the mooring lines is non-linear above a certain limit. After this the stiffness increases more for larger rotations.

As mentioned the driving yaw moment is a static phenomenon, where the aerodynamic load and eccentricity of the hub is increasing rotation about the vertical axis. To investigate the yaw stiffness in the model I have used simulations in SIMA, in combination with Hooke's law for rotation, to estimate the relationship between applied moment and rotation (Bell, 2018).

$$F = k\theta \tag{5.12}$$

The yaw stiffness from the base case is reported in Table 4.5, corresponding to $1.26165 \cdot 10^8$ Nm/rad. This value has been used as k, in equation (5.12). This is a linear value, which is a simplification. The moment applied to the case study model in SIMA has been around z-axis at the center of the platform (0,0,0). The SIMA coordinates for the directional vector for the specified moment was (0,0,1). Further I increased the load incrementally with an estimated increase of about 2° of rotation up to 30°. Finding this non-linear force-displacement let's me more correctly estimate the yaw stiffness behaviour of the mooring lines.

In Figure 5.3 I have plotted the results based on output from simulations. The red curve is the non-linear yaw stiffness for the case study model, based on 13 dynamic simulations. From the simulations a static yaw angle has been found after 1000s simulation time.
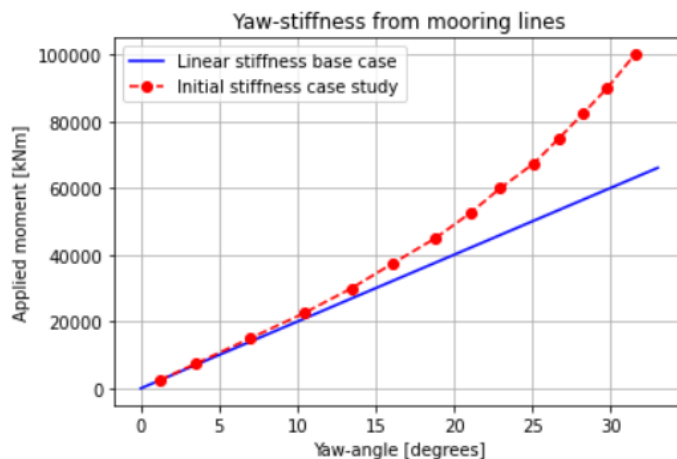

Figure 5.3: Yaw-stiffness of the mooring shown as a force-displacement plot

As we can see from the figure, the yaw stiffness provided by the mooring lines has in fact a non-linear shape as expected from discussions as well as explained in (Haslum et al., 2022). Together with the yaw stiffness derived from the simulations I have plotted the linear stiffness that has been provided in (Silva de Souza et al., 2021). From Figure 5.3 it is evident that the case study model follows the linear relationship between applied moment and rotation to about 11-12°. After discussing with my supervisor, we found it sensible to assume that the relationship between applied moment and yaw rotation is the same for opposite rotational direction or negative values. Later in this thesis this assumption has been used to convert between yaw moment and -rotation, especially in chapter 6.

5.3   Offset mooring stiffness

What could happen to a floating wind turbine is that the floater is given an offset by a horizontal force. This leads to a changed yaw stiffness due to a geometric change in the mooring line. In principle, considering catenary mooring and a floater subjected to wind, the windward side will have an increase in tension, because the floater is moving away from that anchor position, causing more chain to be lifted from the seabed and larger horizontal contribution from the mooring lines. The leeward side on the other hand will have more chain lying on the seabed, resulting in less tension as the floater moves towards the anchor.

To generate the same yaw stiffness curve as seen in Figure 5.3, with a horizontal offset, the platform is given a displacement in x-direction by 1700 kN, which corresponds to the maximum thrustforce at rated wind speed (10.5 m/s). In addition to this horizontal force, the exact same yaw moment or moment about z-axis as the previous analysis is also applied. This horizontal force in the x-axis is applied in (0,0,0) with a directional vector of (1,0,0),(-1,0,0). The moment is applied exactly the same as the previous analysis at (0,0,0). From the horizontal force $F_x = 1700kN$ the global horizontal offset from the simulations is about 20m towards ML1. For offset in the negative x-direction the global offset position of the platform was around 12m towards ML2 and ML3. In Figure 5.4, there is an image capturing the position of the offset force for positive offset and mooring line positions. As mentioned before, positive x-directions is from 0° towards 180°
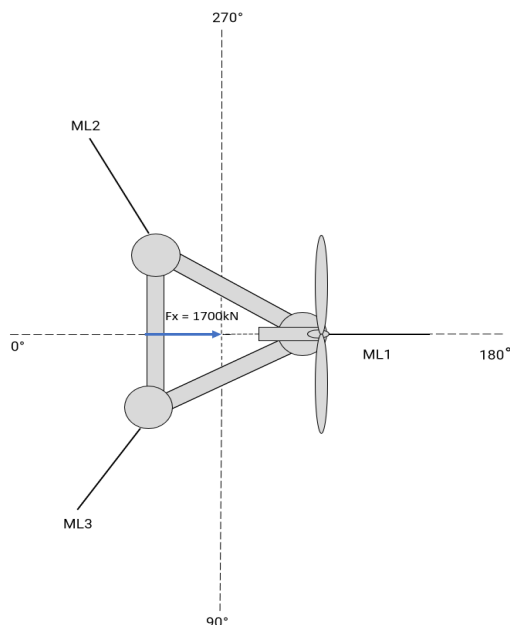
Figure 5.4: Overhead view of turbine and mooring line configuration with offset force

From the simulations I found the overall trend to be that applying a horizontal force in positive and negative x-direction, gave less rotation for the same moment as the initial stiffness. The offset stiffness, initial stiffness and base case stiffness are all plotted together in Figure 5.5 The shape of the offset curves are very similar to the initial stiffness, with a non-linear shape. An explanation for the stiffer response can be related to the catenary effect of mooring lines. For positive x-direction, when applying the offset, ML2 and ML3 are experiencing higher stretch due to the horizontal movement towards the anchor of ML1. This causes more chain on the seabed to be lifted and causing a larger horizontal contribution at the fairlead. For offset in negative x-direction the response is marginally softer than offset in positive x, but stiffer than the initial stiffness with no offset. The response in negative x-direction is slightly softer due to the catenary effect mentioned for positive x. In addition the mooring line resultant force is not in line with the x-axis as ML1, causing the resultant force in ML2 and ML3 to have two force components.
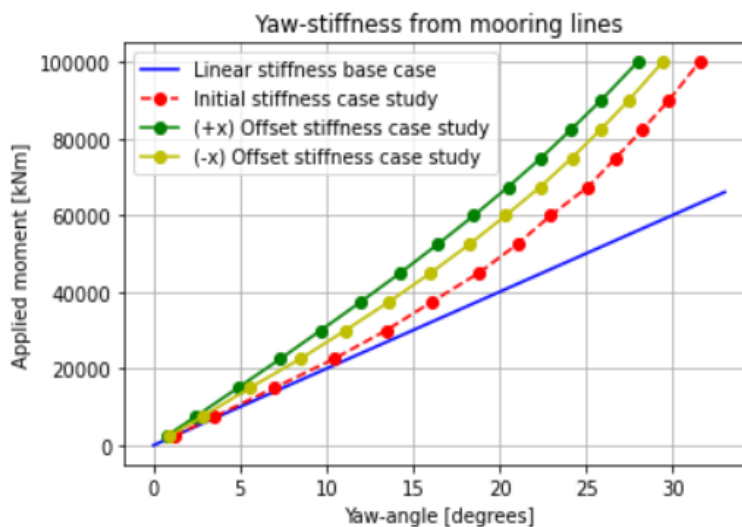
Figure 5.5: Offset - and initial Yaw stiffness of the mooring shown as a force-displacement plot

Using the offset stiffness curves in Figure 5.5 to convert from yaw moment to rotation, or vice versa, will most likely be somewhat inaccurate, except for wind at rated speed. The offset force of 1700 kN is the maximum thrustforce on turbine at 10.5 m/s. Therefore the offset force will be different in cases where the wind is higher or lower than the applied thrustforce. The main reason that no other offset forces has been applied is mainly due to limited working time on the thesis.

6. Simulations results

This chapter will include the results from the numerical analysis in SIMA. The numerical analysis consists of finding the yaw moment and yaw angle for a fixed and rotating floater, subjected to constant wind from varying wind directions and -speeds. Being in the situation that the model I have been using is not developed by me, I found it important for personal learning and for the sake of accurate results, to generate some reference data using the case study model and compare it to the results from (Silva de Souza et al., 2021).

6.1 Model verification

Firstly I have chosen to compare the static tensile forces in the mooring lines to the reported 1050 kN in the base case paper (Silva de Souza et al., 2021). In addition, I have recreated some curves regarding turbine performance, more specifically rotor speed and thrust force with varying wind speed. The turbine is not active for wind exceeding 25 m/s, as the blade pitch will set to 88 degrees and idling commences. One possible source of error in the calibration process is the simulation time. For some properties the simulation time could have been extended to further pinpoint the desired property. For cases with greater uncertainty the simulation time has been extended, but in general the simulation time has been 1000s for the analysis. Another factor to consider when comparing the results is the boundary conditions for the floater. The base case model is calibrated with the floating platform fixed, while the case study model is floating naturally, restricted by the mooring.

6.1.1 Mooring lines

In the preliminary simulations the pretension forces in the mooring lines were lower than the reported 1050 kN in (Silva de Souza et al., 2021). From SIMA, I found the average tensile forces in the mooring lines to be around 720 kN. The lower pretension forces was related to the connection point on the floating platform. When receiving the model, the mooring lines were connected at the bottom of the platform columns. The mooring

lines were supposed to be connected at the middle of the column height at the water level. Elevating the point of attachment on the columns resulted in more chain being lifted from the seabed, and the angle relative to the seabed was increased, increasing the forces in the mooring lines.

The forces in the mooring lines are not exactly the same due to the fact that the platform has a very small static angle relative to the water line. This small angle $(2 - 3°$ degrees.) is introduced to better balance the thrustforce acting on the rotor.

Mooring line 1 has the highest static force at the fairlead of 1125 kN, while the lowest static force at the anchor is 910 kN. The average tensile force across mooring line 1 was then 1018 kN. Mooring line 1 is the line which is attached at the column where the turbine is placed.

For mooring line 2 the tensile force was 1196 at the fairlead, and 969 kN at the anchor, averaging a static force of 1083 kN in the line.

Lastly for mooring line 3 the forces were identical to mooring line 2, with 1196 kN at the fairlead and 969 kN at the anchor. This results in an average tensile force of 1083 kN. In Table 6.1 I have added the average forces found from the case study model compared to the reported pre-tension force from Silva de Souza et al., 2021. From the table it is evident that the tensile forces in the mooring lines are very similar, an error of 3 % is found when comparing the average in the mooring line to the base case.

Table 6.1: Static mooring forces comparison

Mooring line	Case study (average) [kN]	Base case [kN]	Error [%]
ML1	1018	1050	3.1
ML2	1083	1050	3.0
ML3	1083	1050	3.0

In Figure 6.1, there is a plot describing the mooring line tension as a function of position along the x-axis. Position 0 m is at the fairlead and 696 m is at the anchor. From the figure it is possible to observe that the rate of change of the curves are close to identical. The tensile forces in ML1 and ML2 have an identical value, while ML1 being connected to the turbine column, has slightly lower forces.
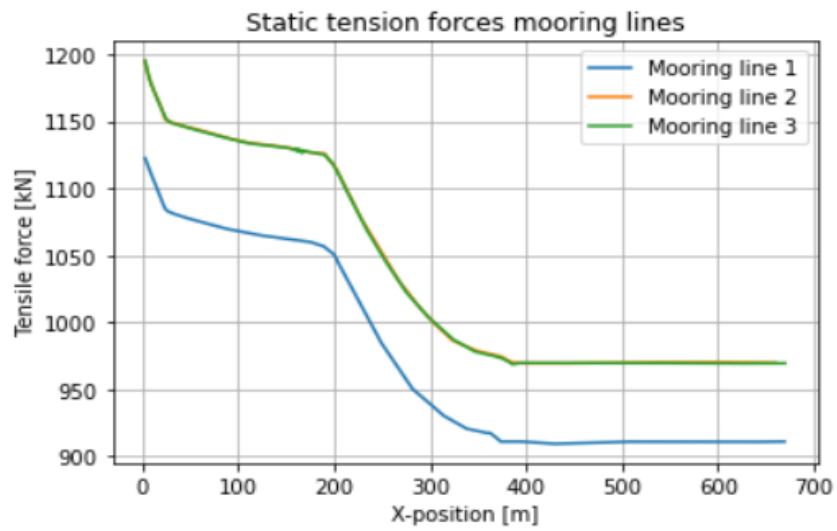
Figure 6.1: Mooring line tension from SIMA

6.1.2 Turbine

To verify that the the turbine is performing as intended, I have recreated some of the plots related to wind turbine performance from (Silva de Souza et al., 2021). The properties I have decided to compare are; rotor speed (rpm) and thrustforce with varying wind speed. I have denoted the x-axis with mean wind speed, due to the fluctuations in wind speed acting on the turbine throughout the time-domain simulations. This section is also important to verify that the controller is also working as intended.

In the Figure 6.2 below, a comparison of the thrustforce acting on the turbine relative to the mean wind speed can be found. From comparing the results from my simulations in SIMA with the results from (Silva de Souza et al., 2021), it is evident that the turbine performance is close to identical. Thrustforce without peak shaving has not been added in this plot, but can be found in (Silva de Souza et al., 2021).
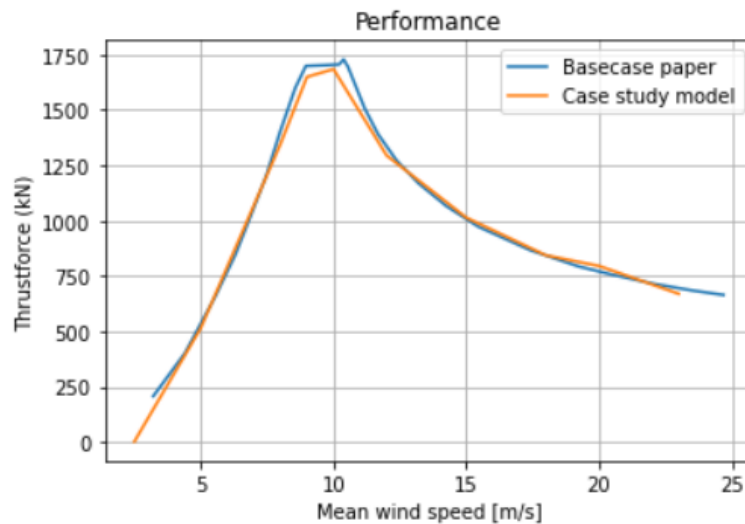
Figure 6.2: Thrustforce output comparison

In the case of the rotor speed, the case study model and base case model show very similar trends in figure 6.3. The y-axis is not showing the rotor speed in absolute terms, but showing the revolutions per minute for a given wind speed. Compared to (Silva de Souza et al., 2021) the case study model is showing marginally higher max rpm for wind speeds over 10 m/s. For wind speeds lower than 10 m/s there is quite a good match between the two curves.

Figure 6.3: Rotor speed output comparison

6.2   Constant wind

In this section the purpose is to quantify which combinations of wind speed and wind direction that causes large platform yaw,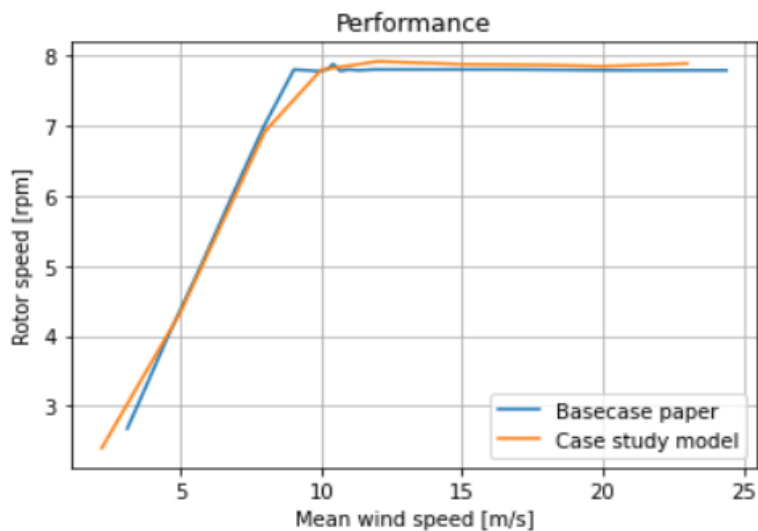 using the case study model. Two types of analysis using constant wind has been done. The first analysis has been done by subjecting the turbine to increasing wind speed with varying wind direction, and finding the steady state platform yaw angle in SIMA. The second analysis takes a different route to the same goal, finding the yaw angle by using the internal forces at the tower-base to calculate yaw moment at platform center, when the floater is fixed. The fixed floater is subjected to exactly the same wind speed and wind directions. Introducing the fixed floater analysis, comparable data to the rotating floater is created, and further motivates the search for different yaw effects in the respective analysis.

Only constant wind has been investigated in this section. The significant wave height is set to 0.001m and peak period to 10s, causing the contribution from waves to the platform response to be more or less negligible. The result of this is mainly aerodynamic loading. To quantify the wind states that are most crucial in terms of yaw rotation for the INO WINDMOOR turbine I have chosen 9 wind directions and 7 wind speeds. Wind directions from 0° up to and including 320°, with an incremental increase of 40°. For the wind speed I have started at 5m/s and then increased by 5m/s up to and including 30m/s and one extreme case of 45m/s.

The simulations has been done using two SIMA environments. The reason for using two environments is the high demand on the FWT in the first 100-300s of the simulations, which leads to numerical errors. The cure for this inconvenience was to use a separate wind file to ramp up to the desired wind speeds (>25 m/s), instead of setting the wind speed from the first simulation iteration. The script, generating these files are found in Appendix B.3.

In Figure 6.4 an overhead view of the turbine with incoming wind directions in the SIMA-model is shown. Positive rotation is counter clockwise, which will be from positive x-axis to positive y-axis. X-axis spans from 0° to 180° and y-axis from 90° to 270°. In example, rotating from 90° to 180° would be positive rotation.
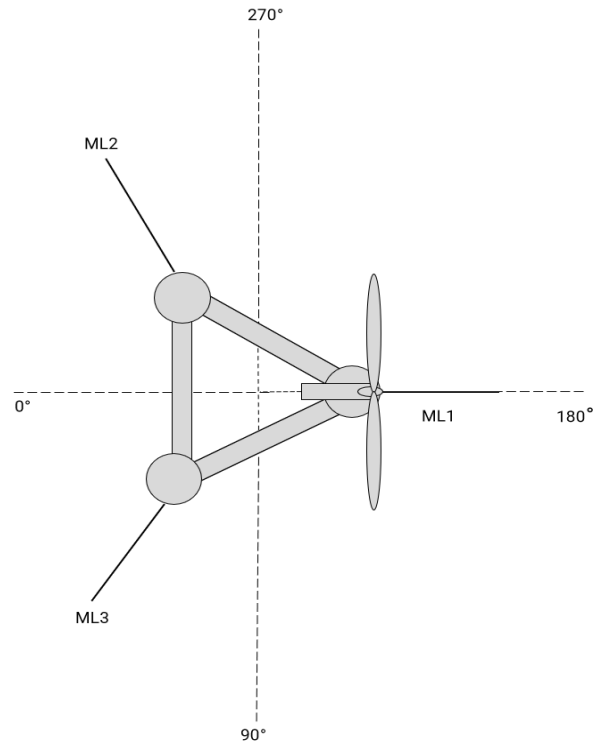
Figure 6.4: Definition of directions and mooring layout in SIMA

To make it easy to post process the results I have defined some criteria for colour coding the results. The yaw angle of the platform is denoted η_6. The η_6 values has been exported from SIMA at t = 1000s. For the criteria to handle both positive and negative rotation it was important to use the absolute values, because the aerodynamic load can cause both clockwise (-) and counterclockwise rotation (+).

$$|\eta_6| \leq 10 = Green \tag{6.1}$$

$$10 < |\eta_6| < 20 = Yellow \tag{6.2}$$

$$20 \leq |\eta_6| < 30 = Red \tag{6.3}$$

6.2.1   Rotating floater

This analysis consists of dynamic simulations where the output of the simulation has been the steady state yaw angle, which is meant to represent a static value. To compare the yaw rotation with the fixed analysis Figure 5.3 has been used.

The simulation results from SIMA are assembled in Table 6.2, Figure 6.5 and Appendix A.1.1

The varying horizontal parameter in Table 6.2 is the wind direction, (°) and wind speed (m/s) the vertical. After some 80 simulations, the general trend is that an increasing wind speed leads to an increasing yaw angle, until rated wind speed. The wind direction also plays an important role in affecting the eccentricity which drives rotation of the platform. From rated wind speed to 15 m/s the yaw angle drops slightly for all wind directions until idling at 25 m/s.

For wind coming at 0° the platform hardly experiences any rotation. For this wind direction, irregular loading and minor unbalances in the system and even some coincidences can decide whether the turbine rotates clockwise or counterclockwise. This theory also applies for wind coming at 180°.

For wind at 40° we start to see some rotation of the platform. The most extreme value is around rated wind speed, where the yaw angle is nearly 13°. From the rated wind speed, the yaw angle actually decreases after the turbine enters the idling phase to the 5° at 45m/s. This is the nearly the same angle as 5m/s produced. The most critical domain for wind coming from 40° is from 10 to 20 m/s.

The trend is quite similar for wind coming from 80°. This wind direction causes a higher magnitude of the platform rotation, but the same behaviour seen for wind at 40° is present here as well. The most extreme value is 18,07° for a wind speed of 10 m/s. In the extreme case of 45m/s the yaw angle is about slightly over two times the value for 40°.

The next wind direction is wind coming from 120°. Also here the most critical yaw angle is found at 10-20 m/s. The main observation that sets this direction apart from the previously mentioned, is the large increase in rotation from 30 to 45 m/s. The rotation doubles in this increase in wind speed, from 10.60° to 22.62°. This wind speed and wind direction most likely triggers some self-reinforcing effect, where the eccentricity of the turbine and mooring center increases.

Wind coming from 160° and 200° has a very similar trend as seen for 120°, except wind from 200° rotates the platform clockwise (-). Both have rotation of less than 10° up to 30 m/s. After 30 m/s the rotation increases by about 100% to 24.62° for wind from 160° and -22,95° for wind at 200°.

For wind coming from 240° the rotation behaviour is quite similar to 200° and 160° except the rotation is larger in the range of 10 to 20m/s. For wind coming from 120° to 240° the largest yaw rotation is the extreme case or 45 m/s.

Lastly wind from 280° and 320°, gives less rotation for the higher wind speeds than 120°-240°. However the rotation at 10 m/s for wind coming from 280° is the highest of any wind direction.

Table 6.2: Static yaw angle for varying wind direction and wind speed (Rotating floater)
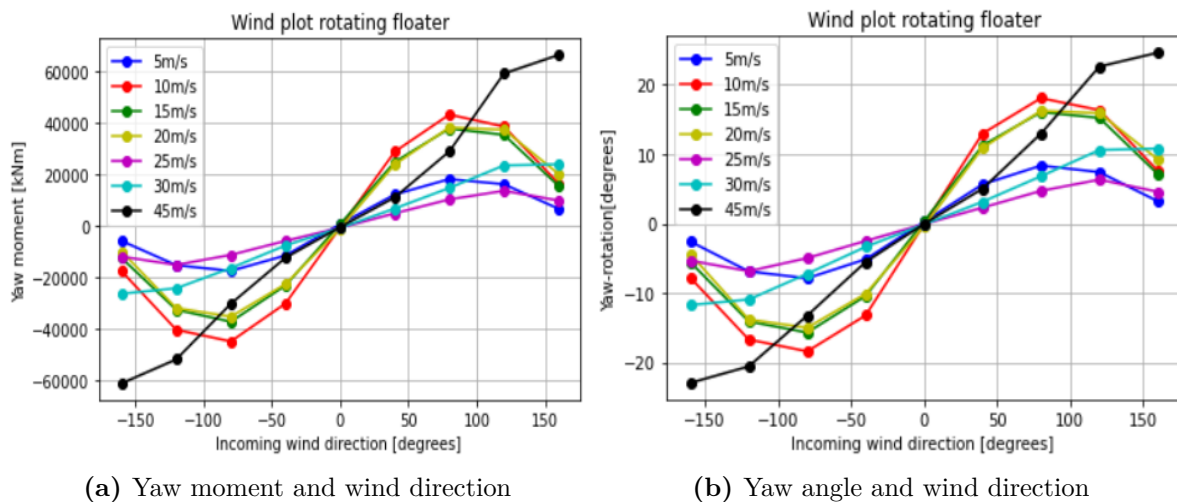
| | | **Wind direction** [°] | | | | | | | | |
		0	40	80	120	160	200	240	280	320
Wind speed [m/s]	5	0.27	5.65	8.35	7.41	3.21	-2.58	-6.89	-7.88	-5.14
	10	-0.1	12.97	18.07	16.34	7.61	-7.80	-16.70	-18.41	-13.22
	15	0.33	11.24	16.06	15.22	7.12	-5.56	-14.10	-15.70	-10.43
	20	-0.42	10.90	16.25	15.91	9.25	-4.39	-13.82	-15.00	-10.10
	25	-0.08	2.30	4.71	6.33	4.58	-5.33	-6.86	-4.97	-2.50
	30	-0.11	3.14	6.82	10.60	10.80	-11.73	-10.94	-7.23	-3.35
	45	-0.04	5.02	12.96	22.62	24.62	-22.95	-20.57	-13.25	-5.53

To sum up, the most critical domain in absolute terms for the wind turbine is wind coming from the range of 120°- 240°. Especially 160° and 200° are quite crucial in terms of producing a significant yaw angle. For all the other cases, excluding wind from 0°, the peak rotation is at around rated wind speed (10.5 m/s). The most critical case in-terms of operational state, meaning wind speed < 25m/s, are 40°-120° and 240°-320°. This wind speed domain is probably more governing than the extreme case, due to the level of level of frequency. The turbine will more likely experience wind speeds around rated wind speed more often than extreme wind speeds over 30m/s.

There is in fact some symmetry regarding the domain 10-20m/s for 40°, 80°, 120° and 240°, 280° and 320°. All these wind direction gives a rotation of the platform between 10° and 20° for wind speeds between 10 m/s and 20 m/s.

In the Figure 6.5 there are two plots intended to compare yaw moment at mooring center, and yaw rotation of the platform for an increasing wind speed. For this figure negative notations has been used for wind directions over 160°. Meaning -40° corresponds to 320°, -80° to 280° and so on. Using the results from Table 6.2 and Figure 5.3, the yaw angle has been matched with a yaw moment at mooring center. As expected the shape of the curves are more or less identical. One source of inaccuracy can originate from the yaw angle to yaw moment conversion from Figure 5.3, which is the force-displacement plot, visualising the non-linear yaw stiffness.

From the figures, the shape for 5m/s to 20m/s is quite similar. These curves have a parabolic shape which changes shape depending if incoming wind direction is positive or negative. For wind speeds above 25 m/s the curve looks more linear, with extreme values at 160° and -160° for 30 m/s and 45 m/s.

(a) Yaw moment and wind direction   **(b)** Yaw angle and wind direction

Figure 6.5: Comparison between yaw moment (a) and yaw angle (b) for increasing wind speeds

6.2.2   Fixed floater

In this section I will disclose the results from the fixed floater analysis. As mentioned earlier the internal forces at the tower base has been used to find yaw moment and platform yaw angle. To convert these results the mooring stiffness curve in Figure 5.3 in section 5.2 has been used. One key aspect to the driving yaw moment for this analysis is the eccentric location of the shear forces acting relative to the platform center. The hypothesis for this analysis after some discussion with my supervisor, was that fixing the floater would give some deviance compared to the rotating floater. This is mainly due to some non-linear effects that are present when the floater is allowed to rotate are removed when the floater is fixed.

The internal forces in this analysis were found at the tower base, which more specifically is segment 1 and element 1 of the tower in the SIMA model. The shear force arm is the distance from the center of the platform to the tower. The shear forces in the tower are generated from the thrustforce acting on the hub. The axisymmetric tower elements (CRS1) have two shear force directions. Shear force in local y-direction, Vy, and shear force in local z-direction, Vz. The local y-direction of the element coincides with y-axis the global coordinate system. Resulting in a tangential force on the platform causing a rotation. However the shear force in the local z-direction coincides with the global x-direction, resulting in a lever arm of 0, acting in the direction of the eccentricity. From the SIMA model I found the shear force lever arm to be 35. 218m from origo to the tower base supernode.

To sum up, a simplified general expression for the yaw moment at the platform center for the fixed floater can be written as:

$$M_{yaw} = V_i \cdot l + M_T \tag{6.4}$$

Where V_i is the shear force in the relevant direction, l being the lever arm (35.218m) and finally M_T is the torsional moment or torque at the tower base. As mentioned the shear forces V_z and V_y, are acting perpendicular in respect to each other. From Figure 6.6 and Figure 6.7, I have defined the relationship between wind directions and rotational direction. In these figures the global axis definition has been applied, causing V_z to be replaced by V_x. Denoting the wind direction as w_{dir}, then $0° < w_{dir} < 180°$ will give a counterclockwise (+) rotation of the platform based on the direction of V_y. Similarly if $180° < w_{dir} < 360°$ then the V_y will cause a clockwise (-) rotation of the platform, as shown in Figure 6.7
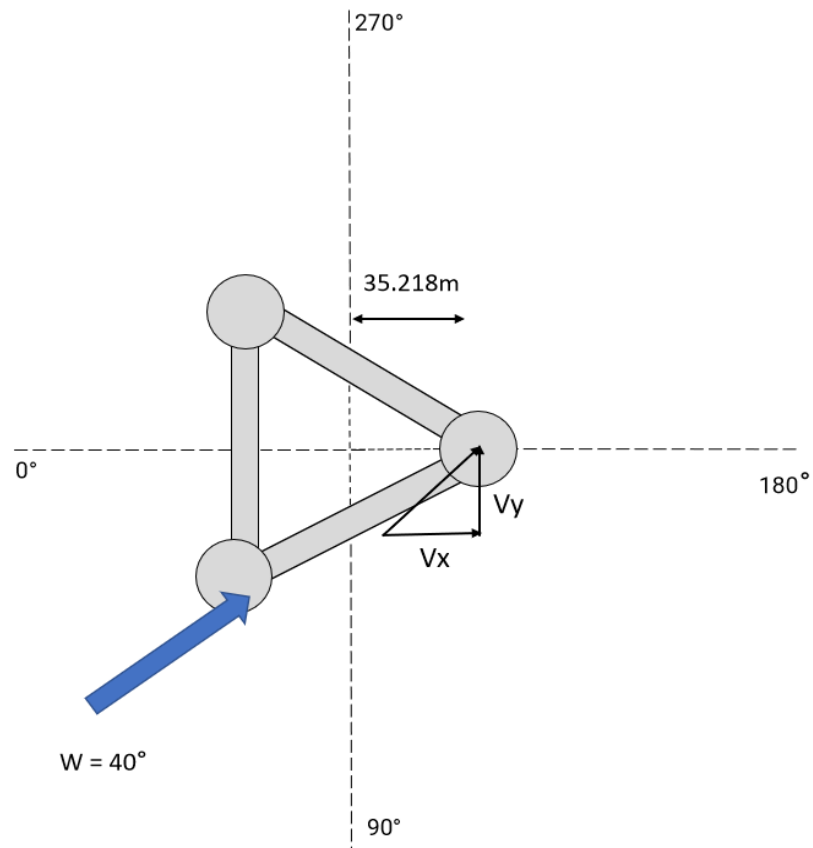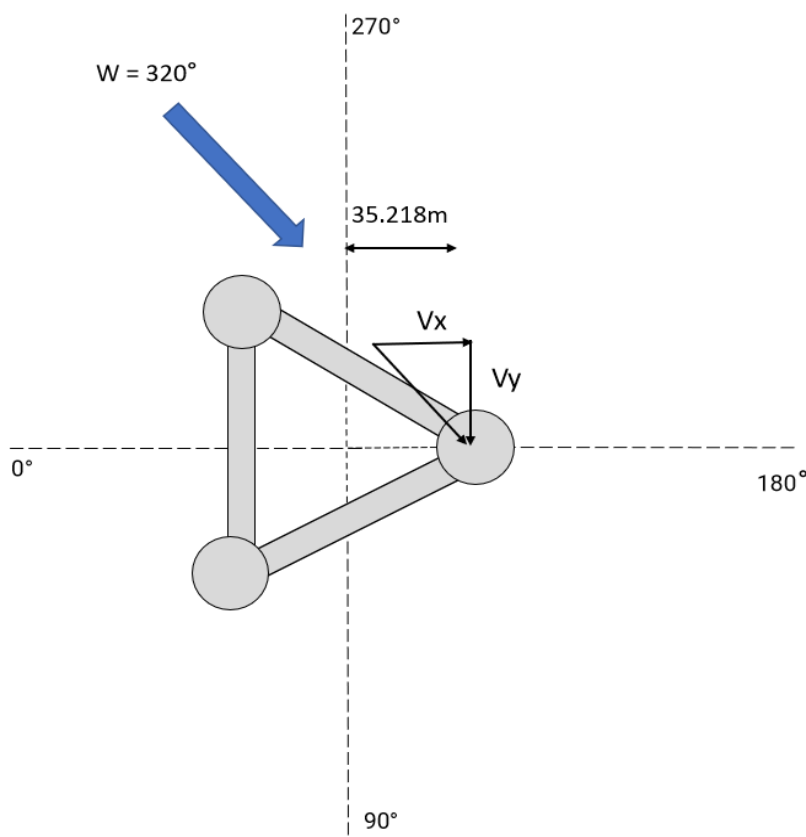
Figure 6.6: Tower base forces for $0° < w_{dir} < 180°$

Figure 6.7: Tower base forces for $180° < w_{dir} < 360°$

In Table 6.3, Figure 6.8 and Appendix A.1.2. the results from the analysis are assembled. Table 6.3 uses the same colour coding based on the same criteria as defined in Section 6.2. The tower forces from the SIMA simulations can be found in Appendix A.1.3.

For wind coming from 0° the results are quite similar as the rotating floater. The rotation is between 0 and 1 degree. The direction of rotation is a slightly different from the rotating floater. As mentioned earlier wind from 0° has a somewhat random nature, being that the rotational direction could be determined on coincidences or small imbalances.

Wind from 40° and 80° has quite good correlation between rotating and fixed floater, for the majority of wind speeds investigated here. There are some deviance, but the colour coding for all the cells are the same except for 20 m/s from 40° and 10m/s from 80°. For 10m/s the fixed floater has a yaw angle of 21.64°, and 18.07° for the rotating. For 15m/s and 20 m/s the results are quite similar with 1°-3° difference. For 25 m/s and 30 m/s, the results are even closer with 0.5° to 1.5° difference. For the extreme case of 45 m/s, wind from 80° gave an almost identical yaw angle, while for wind at 40° the difference is about 4°.

The next wind direction of 120° follows the same trend as seen for 40° and 80°. The fixed floater has slightly higher yaw angle at 10 m/s than for the rotating case. For 15 m/s and 20 m/s the fixed floater has a lower yaw angle than the rotating. For the extreme case of 45 m/s, The rotating floater showed some self-reinforcing yaw effect, which resulted in rotation of 22.62°, which is one of the highest in the analysis. This does not seem to be captured for wind from 120°, or any other wind direction for the fixed floater analysis.

For wind coming from 160° and 200° the results are similar up to 20-25 m/s. From there there is a slight increase of rotation and large self reinforcing effect for the rotating floater. From the fixed floater analysis on the other hand, the results are 5.05°, vs. 24.62° and -5.85 vs. -22.95° for 45 m/s. Wind from 160° and 200° seem to capture the self-reinforcing rotation effect even worse than wind from 160° and 200°

For the final three wind directions the yaw behaviour is quite similar to 40°, 80°, and 120° just opposite rotation direction.

Table 6.3: Static yaw angle for varying wind direction and wind speed. (Fixed floater)

Wind direction [°]

		0	40	80	120	160	200	240	280	320
Wind speed [m/s]	5	0.33	4.94	7.75	6.86	2.63	-2.99	-7.26	-8.26	-5.53
	10	-0.49	15.7	21.64	20.55	9.99	-9.09	-19.52	-21.69	-15.53
	15	0.7	10.83	15.05	13.61	5.88	-6.76	-13.96	-15.93	-11.88
	20	0.55	7.60	15.17	10.93	4.45	-5.59	-11.85	-13.88	-10.92
	25	0.15	3.26	5.11	4.59	1.64	-1.13	-4.86	-5.21	-3.57
	30	0.23	4.39	6.93	6.15	2.35	-2.76	-6.65	-7.47	-4.57
	45	0.61	9.02	13.09	11.64	5.05	-5.82	-12.88	-11.35	-10.30

From the results, it is clear that the peak rotation of the floater is at rated wind speed. This is understandable since the internal shear forces are driven by the thrustforce. When the thrustforce is at its largest, the shear forces are most significant and the rotation is largest.

In Figure 6.8 below I have added two plots comparing the wind direction and yaw moment in the mooring center. As for the rotating floater the trend between yaw moment and yaw angle is nearly identical. There are some small deviations between yaw moment and yaw angle, most likely due to the inaccurate matching yaw moment to corresponding yaw rotation and vice-versa using Figure 5.3.
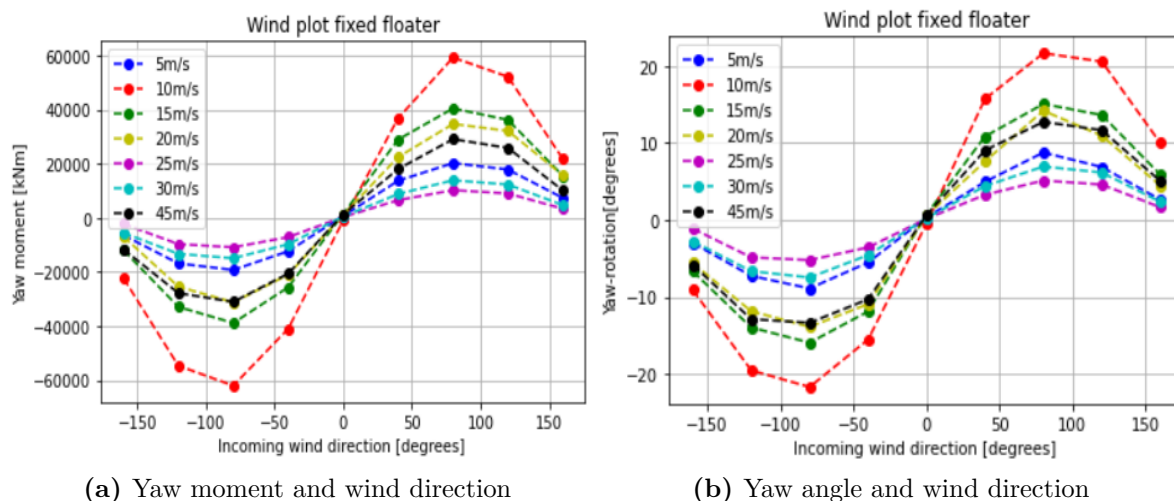

(a) Yaw moment and wind direction   **(b)** Yaw angle and wind direction

Figure 6.8: Comparison between yaw moment (a) and yaw angle (b) for increasing wind speeds

6.3   Comparison

6.3.1   Rotating & fixed

In Figure 6.9 there are two wind plots covering all investigated wind speeds for both rotating and fixed floater. In Figure 6.9a the wind speed in the operational area are presented, 5-20 m/s, and in Figure 6.9b 25-45 m/s are included. In both figures the rotating floater corresponds to the solid line, and the fixed floater as the dashed line. Even though the colours are shown with a solid line, the same colours also applies for the dashed lines. It is quite clear that the correspondence between rotating and fixed floater is quite similar, for the operational area as shown in figure 6.9a. After the turbines enters the idling phase, the yaw behaviour seems to change for the rotating floater. The fixed floater maintains the same curve shape as seen for lower wind speeds. For 25 m/s the rotation of the floater is quite similar for both the rotating and fixed case, but for 30 m/s and 45 m/s the shape of the curve seem to change quite drastically. It still holds the symmetric character about wind from 0°, but has a more linear shape than a the parabolic.

One of the reasons why the rotation is largest at about 80°-90° and then decreases, could be related to the eccentricity, or lever arm of the thrustforce. For this wind direction the lever arm, from the hub to the platform center, is at it's largest.
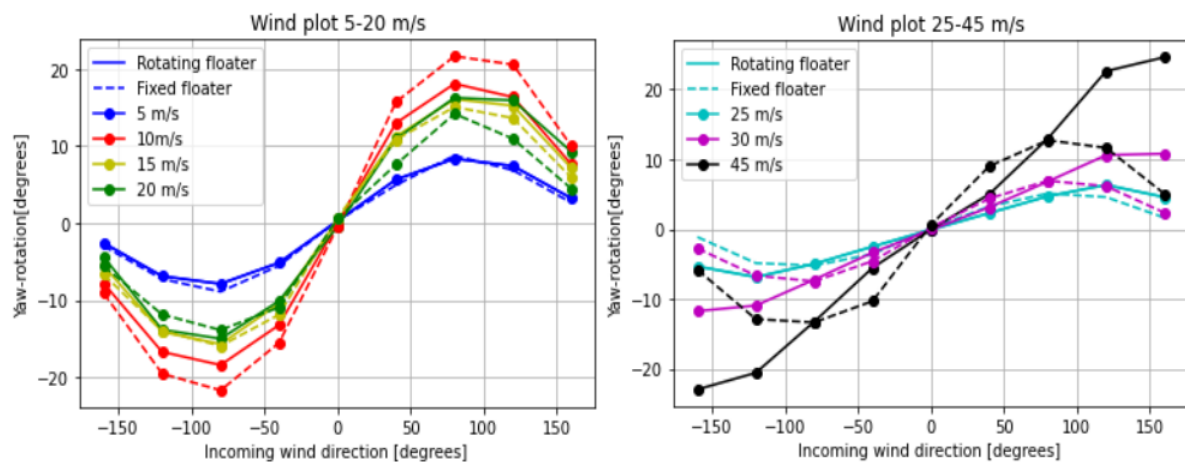
(a) Yaw rotation and wind direction for 5-20 m/s **(b)** Yaw rotation and wind direction for 25 -45 m/s

Figure 6.9: Comparison between yaw angle for increasing wind speeds for both rotating and fixed floater

6.3.2   Offset & initial stiffness for fixed floater

To investigate the non-linear effect from offset stiffness on the yaw behaviour, I have used Figure 5.4 to convert the yaw moment at platform center to rotation (°) for the fixed floater. I have used an offset of 1700 kN in positive x-direction, which corresponds to green curve in the figure. In Figure 6.10, I have added a plot describing the incoming wind direction and platform rotation for a wind speed of 10 m/s. This plot consists of three curves, the rotating floater and the two stiffness cases for the fixed floater. According to the figure, using the offset stiffness gave a better correlation between the fixed and rotating floater. Using the initial stiffness overestimated the platform yaw for the fixed analysis. From the figure it is quite clear that all the curves follows the same trend, but the magnitude of rotation is slightly larger for the fixed analysis using the initial mooring stiffness curve.
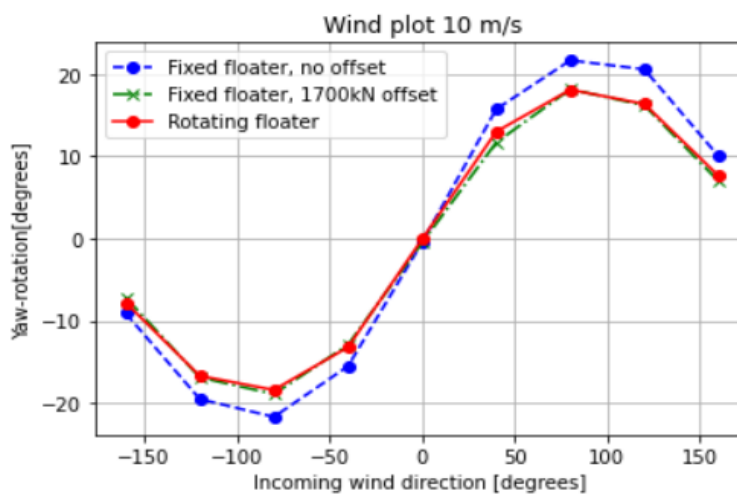

Figure 6.10: Wind plot for 10 m/s for fixed floater with initial- and offset stiffness, plotted together with rotating floater.

7. Discussion

The following chapter will discuss and interpret the results, ideas and suggestions presented in chapter 5 and 6. This chapter is related to the first part of the third objective presented in Section 1.3. I will briefly summarize the results in the corresponding sections and focus on the explanation and underlying mechanics behind the results. The discussion chapter is structured in the same order as the chapter 5 and 6, with the static yaw theory first followed by the numerical results. I have chosen not to further discuss the verification results in Section 6.1, mainly because this section does not contribute directly to the objectives set earlier in this thesis. It is however a very important foundation for assuring the results that do contribute to the objectives are both accurate and reasonable.

7.1 Static yaw behaviour

Chapter 5 consisted of some theoretical foundation which is used in chapter 6. The chapter has been an attempt to establish a theoretical one degree of freedom system for platform yaw, based on the wind direction and orientation of the rotor. Furthermore I have also investigated the relationship between linear and non-linear yaw stiffness and effect initial and offset yaw stiffness. The yaw stiffness from the mooring lines has been important in converting from yaw moment at platform center to yaw rotation.

7.1.1 Static yaw system

The goal of this section was to find an expression for the platform yaw η_6, as a function of wind direction and rotor angle. To find a model for this the idea was to define a 2D coordinate system with two orientations, The platform yaw rotation η_6, and RNA or hub angle α. The idea was that the wind direction would coincide with the hub angle, after the yaw controller would rotate the rotor-plane or RNA into the wind. While this is happening the platform would rotate and get a yaw rotation η_6. As mentioned this analytical method, needs some more verification and testing. I do believe that it could be a powerful tool, being a simple model to estimate yaw behaviour.

7.1.2   Mooring-stiffness

In this section, the purpose was to quantify the yaw stiffness of the case study model, and show that a non-linear yaw stiffness is more accurate than assuming a linear stiffness. The linear domain of the yaw stiffness is shown in Figure 5.3. The reported base case stiffness coincided with the case study stiffness up to 10°- 11° of rotation. The linear domain could also be verified by hand calculations using Hooke's law for rotation, which was quite accurate within the linear domain, but was more inaccurate for angles over 12°. As mentioned in Section 5.2, I found it reasonable to apply the same yaw stiffness curve for negative values of moment and yaw angle. After seeing the results from the constant wind analysis, especially Figure 6.5 and Figure 6.8, I clearly see some symmetric response whether the wind is coming from 0° to 160°, or 0° to -160° (200°). Even though there is not perfect symmetry, the yaw moment or rotation is quite similar in terms of magnitude for the opposite directions.

7.1.3   Offset mooring stiffness

As mentioned in chapter 5 the most likely reason for the stiffer response when given an offset in positive x-direction, is the shape of two of the three mooring lines are changed. The platform surge causes ML1 and ML2 to lift more chain of the seabed and causing a larger horizontal contribution at the fairlead. Applying the horizontal force in negative x-direction gave a softer response than positive offset but stiffer than initial stiffness with no offset. In this case mooring line 2 and 3 has two force components to due to the mooring line orientation with the coordinate system.

The reason why a platform offset will in most cases result in higher yaw stiffness can be supported with the catenary mooring line equations. The relevant equations that can be used to mathematically support this notion are especially equations (2.4), (2.5) and (2.7) in Section 2.3.5.

Equation 2.4 in 2.3.5 from (Faltinsen, 1990) states that the horizontal component at at the water level is the product of the line tension T, and the cosine to the mooring line angle at the fairlead ϕ_w . Introducing a platform offset will increase this mooring line angle and more chain is lifted of the seabed. Equation 2.7 in the same section from the same reference, expresses the stiffness in surge using catenary mooring. From this equation the a variable is effected by an offset. The variable a is the ratio of average horizontal force $(T_H)_M$ and the weight per unit submerged line length. When introducing an offset the horizontal force contribution to the mooring line is increased. From observing that a platform offset effects the yaw stiffness in the simulations, and the variables used in the catenary mooring line equations, it can be concluded that same horizontal force that contributes to stiffness in surge also effects the yaw stiffness.

Meaning that surge stiffness affects the yaw stiffness.

Based on this theory an offset in y-direction would also most likely result in a stiffer response than the initial stiffness. Although it would be interesting to investigate, to be sure.

7.2   Constant wind

The motivation behind the two different numerical approaches for the constant wind analysis has been to highlight the linear vs. non-linear effect. The main non-linear effects observed in this analysis has been the effect of offset stiffness and aerodynamic forces affected by platform rotation. For the rotating analysis the aerodynamic load is not applied perpendicular to the rotor plane, because of the platform rotation. For the fixed floater analysis on the other hand, the aerodynamic load is applied perpendicular to the rotor-plane. Overall the behaviour was quite similar for lower wind speeds, but showed a larger deviance for yaw behavior in the idling phase.

7.2.1   Rotating floater

The analysis for the rotating floater was the first analysis conducted to pinpoint the combination of wind direction and wind speed, would cause large yaw rotations for the case study model. The findings from the analysis was that for 40°- 80° and 280°- 320° the operational window (5- 25 m/s) gave the highest yaw rotation. To be precise, a wind speed of 10 m/s gave the largest yaw rotation. While for wind directions 120° - 240°, the extreme case of 45 m/s gave the highest yaw rotation of the analysis of between 20° to 25°.

The reason why the yaw rotation drops after rated wind speed (10.5 m/s) is most likely related to the thrustforce decreasing. This effect is observed for all investigated wind directions except for 0°, According to Figure B.5 in (Silva de Souza et al., 2021) a blade pitch angle is introduced after rated wind speed is reached. From figure 6.2 The thrustforce is largest at rated wind speed (10.5 m/s), and then decreases to about 25 m/s, when idling commences.

In the operational domain a possible explanation for the behaviour could be related to the offset mooring stiffness. From the results in the Section 6.3.2, I found that imposing an offset of 1700 kN in positive x-directions for the fixed floater, resulted in nearly identical values for yaw rotation at 10 m/s. Initially the difference between the two analysis was the largest for 10 m/s. In addition to those results, the difference between fixed and rotating floater was not so large for the operational domain before imposing the offset. After the turbine started idling the behaviour of the rotating floater is very different from the fixed floater.

One of the reasons that the yaw rotation is so large for when the turbine is idling, especially for for wind directions 120° to 240°, could be explained by aerodynamic forces acting with a relative angle on the rotor plane. When the turbine is given a certain rotation, a relative angle between rotor and wind directions for the aerodynamic

forces arises. The aerodynamic loads change as a function of floater position. This is a non-linear effect compared to behaviour for the fixed floater. Being in the idling domain the wind speeds are quite high, causing a significant aerodynamic load on the turbine. This effect increases the eccentricity, which ultimately increases the rotation of the platform. For the lower wind speeds this effect is most likely less present. For a turbine in operation the effective rotational speed at the blade tip, is higher than the wind speed.

7.2.2 Fixed floater

The results from the fixed floater analysis were quite similar to the rotating floater in some cases, but showed some deviance throughout the analysis. For lower wind speeds the correlation was generally good, but for 30m/s and 45 m/s the difference was quite significant. Especially wind directions 40°-120° and 240°- 320°, had quite good correlation from including 5 m/s to 25 m/s.

The shear force at the tower base generated from the aerodynamic load, was the driving factor for the yaw moment. This was mainly due to the eccentric position of the tower relative to the mooring center. In this analysis the aerodynamic load was applied in the rotor plane. In Appendix A.1.3 the internal tower forces exported from SIMA are assembled. To illustrate the difference in order of magnitude for shear force and torque I have made two comparisons from the data. In example, wind coming from 40° for 15m/s the shear force is causing a yaw moment of $759kN \cdot 35.218m = 26730.462kNm$. The torque at the tower base on the other hand has a value of 2200 kNm. In order of magnitude the shear force from the thrustforce is a lot larger, compared to the torque. The torque is mainly driven by the gyroscopic moment from the rotation of the rotor. For 20 m/s from the same wind direction, yields similar results: $535kN \cdot 35.218m = 18841.63kNm$ The torque at the tower base is 3605 kNm, which is slightly higher than the previous wind direction. The shear force generated at the tower base from the thrustforce acting on the turbine is clearly the driving factor here.

The torsional moment or torque at the tower base is dependent on the rotation of the blades. Therefore the torsional moment reaches maximum value at rated wind speed, and stays constant until 25m/s and decreases when the turbine starts idling (bladepitch = 88°). Figure 6.3 shows that the rotor speed in rpm, stays constant after rated wind speed to about 25 m/s. After the pitch angle of 88 is induced in the blades, the rotor speed is very low, because the pitch angle in the blades is not generating lift, making it harder for the blades to rotate. To sum up, the torsional moment is changing in correlation with blade pitch, because the rotor speed is very low, so the gyroscopic moment from the blade rotation is fairly low. The tower torque is theoretically not

really affected by the wind direction as long as the thrustforce acts normal to the rotor-plane. This is more or less what i have observed from the simulations. Although there was some small differences for the different wind directions.

8. Conclusion

The first objective of this thesis has been to investigate what wind-directions and wind speeds causes large static yaw rotations for the INO WINDMOOR 12 MW turbine. Large yaw rotations are driven by the increase of the lever arm of the thrustforce, and magnitude of the thrustforce itself. A positive yaw angle which reduces the lever arm, will be restoring. Oppositely, a positive yaw angle which increases the lever arm will be reinforcing the rotation, and will be unstable.

From the numerical study, the largest yaw rotations for the floater was found for the extreme case of 45 m/s with wind coming from 120° to 240°. The peak rotation for this domain was 24.62°. For the operational domain, the platform yaw was the largest at rated wind speed for all wind directions, except wind from 0°. The largest rotation at rated wind speed was 18.41°, for wind coming from 280°.

The second objective was related to the non-linear yaw behaviour by separating linear and non-linear effects. This was done by doing the same numerical study on a fixed floater, and using the internal forces at the tower base caused by the thrustforce, to calculate the yaw moment at the platform center.

From the simulations it was observed a quite good correlation for the platform yaw between the two analysis, for wind speeds in the operational domain (0-25 m/s). For wind speeds above 25 m/s in the idling phase a larger deviance was observed. As mentioned previously, the rotating floater experienced very large platform rotation for some wind directions when subjected to an extreme case of 45 m/s. The driving factor for this behaviour is most likely a non-linear effect, where the aerodynamic forces exerted on the turbine changes as the platform rotates. This causes a significant load to act across the rotor-plane, and contribute to a large rotation. This effect can most likely explain the different shape seen in Figure 6.9b for the rotating floater.

For the operational domain this non-linear wind effect is most likely much less present. For lower wind speeds the yaw rotation for the fixed and rotating platform are quite similar. Fixing the floater eliminates the relative angle dependent on wind direction and rotor orientation for the aerodynamic load. In the fixed analysis the aerodynamic load is acting perpendicular to the rotor plane. However, the non-linear effect of offset stiffness could be an explaining factor for the deviance observed in the operational domain. Introducing an offset of 1700 kN for the fixed floater, resulted in almost identical yaw rotation compared to the rotating floater for rated wind speed (Figure 6.10). The non-linear effect of wind occurring in the idling phase, seems to be most powerful non-linear effect contributing to large yaw rotations.

For the fixed floater, the driving factor to the platform yaw was the shear force. Due to the eccentric position of the turbine to the center of platform, the lever arm and shear force at the tower base produced a significantly yaw moment larger moment than torque at the tower base.

The final objective was related to the discussion of the acquired results and recommendations for future work. The discussions have been mainly about the magnitude of aerodynamic forces, the angle and eccentricity of the aerodynamic forces, and the global stiffness provided by the mooring lines. For both the aerodynamic forces and mooring stiffness there is non-linear behaviour. The force applied by the wind on the rotating floater, changes with the platform rotation. Similarly, for the mooring stiffness, the resistance against yaw motion, also changes with platform rotation and position (offset). The more the platform rotates the stiffer the system gets. Introducing an offset or surge motion also increases the yaw stiffness. The further recommendations for future work can be found in the next chapter.

9. Future work

From the findings in this thesis, I have concluded with some recommendations for future work, that will further understand the mechanism that trigger large yaw motions. More knowledge on the topic will make it easier to mitigate this behaviour, and design floating wind turbines which will be more robust against large yaw motions.

- Use the existing foundation for the analytical yaw model to find an expression for the eccentricity and ultimately get an expression for the yaw rotation.

- Test the validity of analytical formulas with simulations or the simulation results from this thesis

- Run further simulations with offset in both y-directions to quantify the mooring behaviour.

- Investigate the effect of yaw stiffness on the dynamic character of fishtailing, and suggest acceptable order of magnitude for displacements.

- Run further analysis for wind speeds in the idling phase to, get more simulation data for the non-linear effect on the rotating floater.

- Rerun the constant wind analysis with an active yaw controller, and compare the yaw rotation of the platform with and without controller.

- Do some simulations with turbulent wind and compare the yaw rotation or moment with constant wind analysis.

- Include regular waves into the model to see the effect of waves in the constant wind analysis.

- Compare yaw behaviour for the case study model with a centrically placed turbine like the OO-star. Compare the effect of eccentricity as a driving factor for the yaw moment.

- Rerun constant wind analysis with a different mooring configuration. In example 6 lines or 4 mooing lines.

References

Arntsen, Ø. A. and Krogstad, H. E. (2000). Linear wave theory part A: Regular waves. (Read 02.11.2022).

Arntsen, Ø. A. (n.d.). 3 Sea State Parameters And Engineering Wave Spectra (). (Read 03.11.2022). URL: https://folk.ntnu.no/oivarn/hercules_ntnu/LWTcourse/partB/3seastate/3%5C%20SEA%5C%20STATE%5C%20PARAMETERS%5C%20AND%5C%20ENGINEERING%5C%20WAVE%5C%20SPECTRA.htm.

Aubeny, C. (2016). Performance of Anchors for Floating Offshore Windfarms. *Geotechnical Engineering for US Offshore Wind Infrastructure. Boston 25.04.2016.* (Read 04.11.2022).

Bashetty, S. and Ozcelik, S. (2021). Review on Dynamics of Offshore Floating Wind Turbine Platform. *Energies.* (Read 02.09.2022). DOI: 10.3390/en14196026.

Bell, K. (2018). *Matrisestatikk: Statiske beregninger av fagverk, rammer og buer.* Vol. 4. (Read 15.10.2022). Fagbokforlaget. Chap. 4. Grunnlaget på matriseform.

Callister, W. D. and Rethwisch, D. G. (2020). *Callister's Material Science And Engineering.* Vol. 10. (Read 15.10.2022). Wiley & sons (Asia) Pte Ltd. Chap. 6, and 8.

Castro-Santos, L. and Diaz-Casas, V. (2016). *Floating Offshore Wind Farms.* (Read 10.09.2022). Springer international publishing.

Chakrabarti, S. (2015). *Handbook of offshore engineering.* Vol. 2. (Read 12.10.2022). Elsevier science.

Chen, Z., Wang, X. and Kang, S. a. (2021). Effect of the Coupled Pitch-Yaw motion on the Unsteady Aerodynamic Performance and Structural Response of a Floating Offshore Wind Turbine. *Processes.* (Read 10.09.2022). DOI: 10.3390/pr9020290.

Davidsen, B. (2010). Forelesningsnotater i matematikk: Matriser- en innføring. (Read 03.11.2022). URL: http://www.ingfag.no/matematikk/notater/Matriser/Transformasjoner.pdf.

Design, S. (n.d.). *Suction anchors.* (Accessed 05.11.2022). URL: https://subseadesign.com/products-services/suction-anchors/.

DNV (2014). Environmental Conditions and Environmental Loads DNV-RP-C205. Offshore standards, Det Norske Veritas, Høvik, NO. (Read 17.11.2022).

DNV (2018). Offshore mooring chain. DNVGL-OS-E302 . Offshore standards, Det Norske Veritas, Høvik, NO. (Read 22.10.2022).

DNV (2020). Offshore mooring steel wire ropes. DNVGL-OS-304 . Offshore standards, Det Norske Veritas, Høvik, NO. (Read 14.10.2022).

DNV (n.d.). *Marine operations and mooring analysis software - Sima.* (Accessed 07.12.2022). URL: https://www.dnv.com/services/marine-operations-and-mooring-analysis-software-sima-2324.

DNV-GL (n.d.). *Qats documentation.* (Read 03.09.2022). URL: https://qats.readthedocs.io/en/latest/#.

Efficiency, E. and Energy, R. (2022). *How a Wind Turbine Workds -Text Version.* (Accessed 29.11.2022). URL: https://www.energy.gov/eere/wind/how-wind-turbine-works-text-version.

Eliassen, L. (2015). *Aerodynamic loads on a wind turbinerotor in axial motion.* (Read 07.12.2022). Phd thesis. Norway. University of Stavanger. URL: https://uis.brage.unit.no/uis-xmlui/handle/11250/284344.

Eliassen, L. and Verma, A. (2021). Wind turbine modelling: How to model an offshore wind turbine in SIMA. (Read 23.11.2021).

Equinor (2021). *Equinor tildeler kontrakter for 3,3 milliarder for Hywind Tampen.* (Accessed 3.09.2022). URL: https://www.equinor.com/no/news/archive/2019-10-31-hywind-tampen.

Equinor (2022). *Hywind Scotland.* (Accessed 25.11.2022). URL: https://www.equinor.com/energy/hywind-scotland.

Equinor (n.d.). *Flytende havvind.* (Accessed 30.11.2022). URL: https://www.equinor.com/no/energi/flytende-havvind.

Falkenberg, E., Yang, L. and Åhjem, V. (2018). The Syrope Method For Stiffness Testing Of Polyester Ropes. *37th International Conference on Ocean, Offshore and Arctic Engineering.* (Read 02.09.2022). DOI: 10.1115/OMAE2018-77944.

Faltinsen, O. M. (1990). *Sea loads on ships and offshore structures.* (Read 04.09.2022). Cambridge University Press.

Ferrão, J. C. A. (2021). Teams meeting with senior structural engineer at Aker Offshore Wind. (10.12.2021).

Gómez, P., Sánchez, G., Llana, A. and Gonzalez, G. (2015). Qualification of innovative floating substructures for 10MW wind turbines and water depths greater than 50m. (Read 27.09.2022).

Group, F. (n.d.). *Marine Renewable Energy:Mooring and Anchoring.* (Accessed 05.11.2022). URL: https://www.farinia.com/fmgc/marine-renewable-energy/mooring-and-anchoring.

Guo, Y., Damiani, R. and Musial, W. (2014). Simulating Turbulent Wind Fields for Offshore Turbines in Hurricane-Prone Regions (Poster). (Accessed 29.11.2022). URL: https://www.osti.gov/biblio/1130129.

Haslum, H., Marley, M., Navalkar, S. T., Skaare, B., Maljaars, N. and Andersen, H. S. (2022). Roll–Yaw Lock: Aerodynamic Motion Instabilities of Floating Offshore Wind Turbines. *Journal of Offshore Mechanics and Arctic Engineering.* (Read 29.10.2022). DOI: 10.1115/1.4053697.

Haslum, H. (2022). Teams meeting with senior advisor for floating wind technology at Equinor. (02.12.2021).

Helmholtz, H. V., Thorne, K., Rayleigh, L. and Mach, E. (2022). Wave: physics. (Read 07.11.2022). URL: https://www.britannica.com/science/wave-physics.

IEC (2005). Wind turbines –Part 1: Design requirements, IEC 61400-1, International Eletrotechnical Comission, Genève, CH. (Read 11.11.2022).

Kvittem, M. I. and Nygaard, T. A. (2021). *Symmetri,feil og begrensninger.* Lecture notes from TBM250. (Accessed 12.10.2022).

Kvittem, M. I. (2022a). Supervision meeting with Marit Irene Kvittem. (Read 23.08.2021).

Kvittem, M. I. (2022b). Weekly Teams supervision meeting with Marit Irene Kvittem. (14.10.2021).

Leimeister, M., Kolios, A. and Collu, M. (2018). Critical review of floating support structures for offshore wind farm deployment. *Journal of Physics: Conference Series* 1104. Read: 24.10.2022. DOI: 10.1088/1742-6596/1104/1/012007.

Li, X., Zhu, C., Fan, Z., Chen, X. and Tan, J. (2020). Effects of the yaw error and the wind-wave misalignment on the dynamic characteristics of the floating offshore wind turbine. *Ocean engineering.* (Read 12.11.2022). DOI: https://doi.org/10.1016/j.oceaneng.2020.106960.

Lopresto, V., Langella, A. and Abrate, S. (2017). *Dynamic Response and Failure of Composite Materials and Structures.* (Read 19.09.2022). Woodhead Publishing. Chap. 2.2.6 Added mass effect. DOI: 10.1016/B978-0-08-100887-4.09987-X.

Ma, K.-T., Luo, Y., Kwan, T. and Wu, Y. (2019). *Mooring system Engineering for Offshore Structures.* (Read 27.09.2022). Gulf Professional Publishing. Chap. 9. Hardware – Off-vessel components. DOI: 10.1016/B978-0-12-818551-3.00009-0.

Manwell, J. F., McGowan, J. and Rogers, A. . (2010). *WIND ENERGY EXPLAINED:Theory, Design and application.* Vol. 2. (Read 03.09.2022). John Wiley & sons Ltd.

Moorings, A. (2022). *Mooring anchors.* (Accessed 04.10.2022). URL: http://abc-moorings.weebly.com/mooring-anchors.html.

NDLA (2022). *Koordinatene til et punkt. Avstand i planet.* (Accessed 08.12.2022). URL: https://ndla.no/nb/subject:1:734bd33b-da6d-49b0-bb34-c6df5b956f8e/topic:1:2737083d-8400-4a9f-b864-b05c42a470df/topic:1:e5fe1c9c-34a1-4651-b511-3deb3cdc98c8/resource:5bd8f20e-251b-4ef1-b282-2d2384513d50.

NGI (2022). *Offshore geoteknikk.* (Accessed 04.11.2022). URL: https://www.ngi.no/Tjenester/Fagekspertise/Offshore-geoteknikk.

Nielsen, F. G. (2007). Leture Notes in Marine Operations. (Read 20.10.2022).

Nielsen, F. G. (n.d.). *Hywind- From idea to world's first wind farm based upon floaters.* (Accessed 18.10.2022).

Olczak, A., Stallard, T., Feng, T. and Stansby, P. (2016). Comparison of a RANS blade element model for tidal turbine arrays with laboratory scale measurements of wake velocity and rotor thrust. *Journal of Fluids and Structures* 64. (Read 06.12.2022). DOI: 10.1016/j.jfluidstructs.2016.04.001.

Owen, A. (2020). *Future Energy.* Third Edition. (Read 05.11.2022). Elsevier. Chap. 17.4.2 Suction/drilled/driven pile anchors. DOI: https://doi.org/10.1016/B978-0-08-102886-5.00017-7.

PrinciplePower (2022). *Kincardine Offshore Wind Farm.* (Accessed 29.11.2022). URL: https://www.principlepower.com/projects/kincardine-offshore-wind-farm.

Silva de Souza, C. E., Berthelsen, P. A., Eliassen, L., Bachynski, E., Engebretsen, E. and Haslum, H. (2021). Definition of the INO WINDMOOR 12 MW base case floating wind turbine. (Read 04.09.2022).

SINTEF (n.d.). *Advanced Wave and Wind Load Models for Floating Wind Turbine Mooring System Design.* (Accessed 01.11.2022). URL: https://www.sintef.no/projectweb/windmoor/.

SINTEF-Ocean (n.d.[a]). *SIMA documentation: RIFLEX. Dynamic-time domain analysis.* (Accessed 07.12.2022). URL: https://sima.sintef.no/doc/4.4.0/riflex/theory/dynamic_time_domain_analysis.html.

SINTEF-Ocean (n.d.[b]). *SIMA documentation: SIMO.* (Accessed 07.12.2022). URL: https://sima.sintef.no/doc/4.4.0/simo/index.htm.

Tannuri, E. A., Simos, A. N., Leite, A. J. P. and Aranha, J. A. P. (2001). Experimental Validation of a Quasi-Explicit Hydrodynamic Model:Fishtailing Instability of a Single-point Moored Tanker in Rigid-Hawser Configuration. *Journal of Ship Reasearch.* (Read 20.11.2022). DOI: 10.5957/jsr.2001.45.4.302.

Taylor, M., Ralon, P., Al-Zoghoul, S. and Jochum, M. (2021). Renewable Power Generation Costs In 2021. *International Renewable Energy Agency.* (Read 21.11.2022).

Tomasi, R. (n.d.). Single degree of freedom system. Lecture notes in TBA320 structural dynamics (). (Read 15.10.2022).

Vryhof, A. (2015). *Vryhof Manual: The guide to anchoring.* Vol. 5. (Read 10.11.2022). Chap. 1 and 2.

Wang, H. (2022). *Encyclopedia of Ocean Engineering.* (Accessed 22.11.2022). Springer Nature Singapore: 1933–1937. DOI: 10.1007/978-981-10-6946-8_146.

Wasserstein, R. (2010). George Box:a model statistician. *Significance.* (Read 18.10.2022). URL: https://rss.onlinelibrary.wiley.com/doi/pdf/10.1111/j.1740-9713.2010.00442.x.

Özinan, U., Kretschmer, M., Lemmer, F. and Cheng, P. W. (2020). Effects of yaw misalignment on platform motions and fairlead tensions of the OO-Star Wind Floater Semi 10MW floating wind turbine. *Journal of Physics* 1618. (Read 10.09.2022). DOI: 10.1088/1742-6596/1618/5/052081.

Appendix A. Excel sheets

This appendix contains the results from the constant wind analysis in colour coded excel tables, and the internal forces at the tower base exported from SIMA.

A.1   Yaw angle

A.1.1   Rotating floater

Wind speed [m/s]	Wind Direction [°]								
	0	40	80	120	160	200	240	280	320
5	0,27	5,65	8,35	7,41	3,21	-2,58	-6,89	-7,88	-5,14
10	-0,1	12,97	18,07	16,34	7,61	-7,80	-16,70	-18,41	-13,22
15	0,33	11,24	16,06	15,22	7,12	-5,56	-14,10	-15,70	-10,43
20	-0,42	10,90	16,25	15,91	9,25	-4,39	-13,82	-15,00	-10,1
25	-0,08	2,3	4,71	6,33	4,58	-5,33	-6,86	-4,97	-2,50
30	-0,11	3,14	6,82	10,6	10,80	-11,73	-10,94	-7,2253	-3,35
45	-0,04	5,02	12,96	22,62	24,62	-22,95	-20,57	-13,25	-5,53

A.1.2 Fixed floater

Wind speed [m/s]	Wind Direction [°]								
	0	40	80	120	160	200	240	280	320
5	0,33	4,94	7,75	6,86	2,63	-2,99	-7,26	-8,26	-5,53
10	-0,49	15,7	21,64	20,55	9,99	-9,09	-19,52	-21,69	-15,53
15	0,7	10,83	15,05	13,61	5,88	-6,76	-13,96	-15,93	-11,88
20	0,55	7,60	15,17	10,93	4,45	-5,59	-11,85	-13,88	-10,92
25	0,15	3,26	5,11	4,59	1,64	-1,13	-4,86	-5,21	-3,57
30	0,23	4,39	6,93	6,15	2,35	-2,76	-6,65	-7,47	-4,57
45	0,61	9,02	13,09	11,64	5,05	-5,82	-12,88	-11,35	-10,3

A.1.3   Tower base forces

			W = 0 deg			s		
Ws	Vy (kN)	Vz (kN)	M_T(kNm)	Lever arm (m)	Yaw moment kNm	Yaw fixed floater		Yaw from free floater
5	0,76		639	35,218	665,766		0,33	0,27
10	0,59		-1007	35,218	-986,221		-0,49	-0,1
15	8,32		1110	35,218	1403,014		0,70	0,33
20	9,65		768	35,218	1107,854		0,55	-0,42
25	-2,0866		-375,19	35,218	301,704		0,15	-0,08
30	-1,4908		-516	35,218	463,367		0,23	-0,11
45	-4,864		-1 397	35,218	1226,100		0,61	-0,04

			W = 40deg					
Ws	Vy (kN)	Vz (kN)	M_T kNm	Lever arm (m)	Yaw moment kNm	Yaw fixed floater		Yaw from free floater
5	335		1900	35,218	13698,03		4,94	5,65
10	1050		-159,96	35,218	36818,94		15,7	12,97
15	759		2200	35,218	28930,462		10,83	11,24
20	535		3605	35,218	22446,63		7,6	10,9
25	159,51		900,18	35,218	6517,80		3,26	2,33
30	229,79		703,95	35,218	8796,69422		4,39	3,14
45	517,4		-173,58	35,218	18048,2132		9,02	5,02

			W = 80deg					
Ws	Vy (kN)	Vz (kN)	M_T kNm	Lever arm (m)	Yaw moment kNm	Yaw fixed floater		Yaw from free floater
5	507,81		2358,3	35,218	20242,35258		10,11	8,35
10	1672,6		356,8	35,218	59262,4268		22,55	18,07
15	1073,1		2660,7	35,218	40453,1358		16,95	16,06
20	877,8		3808,5	35,218	34722,8604		14,94	16,25
25	246,9		1540	35,218	10235,3242		5,11	4,71
30	356,48		1320	35,218	13874,51264		6,93	6,82
45	799,16		936,1	35,218	29080,91688		13,09	12,96

		W = 120deg				

Ws	Vy (kN)	Vz (kN)	M_T kNm	Lever arm (m)	Yaw moment kNm	Yaw fixed floater	Yaw from free floater
5	448,35		2064,6	35,218	17854,5903	6,86	7,41
10	1479		67,538	35,218	52154,96	20,55	16,34
15	952,4		2655,8	35,218	36197,4232	13,61	15,22
20	797,25		4046,6	35,218	32124,1505	10,93	15,91
25	217,92		1337,1	35,218	9011,80656	4,50	6,33
30	314,65		1223,6	35,218	12304,9437	6,15	10,58
45	711,76		764,69	35,218	25831,45368	11,64	22,62

		w = 160deg				

Ws	Vy (kN)	Vz (kN)	M_T kNm	Lever arm (m)	Yaw moment kNm	Yaw fixed floater	Yaw from free floater
5	178,96		1032,7	35,218	7335,31328	3,66	3,21
10	593,12		871,73	35,218	21760,23016	10,87	7,61
15	387,35		1875,9	35,218	15517,5923	7,75	7,12
20	349,27		3403	35,218	15703,59086	7,84	9,25
25	83,97		390,41	35,218	3347,66546	1,67	7,83
30	123,78		338	35,218	4697,28404	2,35	10,80
45	289,5		-79,44	35,218	10116,171	5,05	24,62

W = 200deg

Ws	Vy (kN)	Vz (kN)	M_T(kNm)	Lever arm (m)	Yaw moment kNm	Yaw fixed floater	Yaw from free floater
5	-174,6		-266,94	35,218	-6416,0028	-2,99	-2,58
10	-574,78		-2065	35,218	-22307,60204	-9,09	-7,80
15	-357,95		644,41	35,218	-11961,8731	-6,76	-5,56
20	-257,61		2128,8	35,218	-6943,70898	-5,59	-4,39
25	-89,308		886,12	35,218	-2259,129144	-1,13	-5,33
30	-128,63		-1000,1	35,218	-5530,19134	-2,76	-11,73
45	-288,92		-1476,5	35,218	-11651,68456	-5,82	-22,95

W = 240deg

Ws	Vy (kN)	Vz (kN)	M_T kNm	Lever arm (m)	Yaw moment kNm	Yaw fixed floater	Yaw from free floater
5	-445,855		-1169,855	35,218	-16871,97639	-7,26	-6,89
10	-1470,15		-2906,95	35,218	-54682,6927	-19,52	-16,7
15	-922,73		-423,5	35,218	-32920,20514	-13,96	-14,1
20	-748,345		922,3	35,218	-25432,91421	-11,85	-13,82
25	-220,89		-1942	35,218	-9721,30402	-4,86	-6,86
30	-318,44		-2102,4	35,218	-13317,21992	-6,65	-10,94
45	-715,69		-2627,5	35,218	-27832,67042	-12,88	-20,57

W = 280deg

Ws	Vy (kN)	Vz (kN)	M_T kNm	Lever arm (m)	Yaw moment kNm	Yaw fixed floater	Yaw from free floater
5	-508,51		-1354,6	35,218	-19263,30518	-8,26	-7,88
10	-1675,5		-3049,4	35,218	-62057,159	-21,69	-18,41
15	-1078,8		-883,35	35,218	-38876,5284	-15,93	-15,7
20	-891,77		156,68	35,218	-31249,67586	-13,88	-15
25	-246,23		-2216,9	35,218	-10888,62814	-5,21	-4,97
30	-354,39		-2463,9	35,218	-14944,80702	-7,47	-7,23
45	-800,02		-2899,4	35,218	-31074,50436	-11,35	-13,25

W = 320deg

Ws	Vy (kN)	Vz (kN)	M_T kNm	Lever arm (m)	Yaw moment kNm	Yaw fixed floater	Yaw from free floater
5	-332,76		-640,1	35,218	-12359,24168	-5,53	-5,14
10	-1096,8		-2376,6	35,218	-41003,7024	-15,53	-13,22
15	-716,04		-442,56	35,218	-25660,05672	-11,88	-10,43
20	-609,07		402,73	35,218	-21047,49726	-10,92	-9,99
25	-157,62		-1595,1	35,218	-7146,16116	-3,57	-2,51
30	-225,15		-1826,4	35,218	-9755,7327	-4,87	-3,35
45	-510,29		-2641,5	35,218	-20612,89322	-10,30	-5,53

Appendix B. Python code

B.1   Yaw stiffness plot code

```python
# -*- coding: utf-8 -*-
"""
Created on Fri Dec  2 12:59:55 2022

@author: eigil
"""



import numpy as np
from matplotlib import pyplot as plt

#----------- Yaw- data from SIMA simulations -----------#
data_sim = np.array([
[1.23,2498.044],
[3.55,7494.13],
[6.98,1.4988e+04],
[10.4,2.2482e+04],
[13.45,2.9977e+04],
[16.1,3.7471e+04],
[18.8,44964.8],
[21.02,52458.933],
[22.95,59953.0667],
[25.11,67447.2],
[26.71,74941.3333],
[28.26,8.245e+04],
[29.77,8.9926e+04],
[31.54,1.0e+5]
])
```

```python
#----------- Yaw- data from SIMA simulations (positive offset) -----------#
data_sim_1 = np.array([
[0.79,2498.044],
[2.44,7494.13],
[4.88,1.4988e+04],
[7.31,2.2482e+04],
[9.6636,2.9977e+04],
[11.996,3.7471e+04],
[14.261,44964.8],
[16.427,52458.933],
[18.517,59953.0667],
[20.501,67447.2],
[22.392,74941.3333],
[24.144,8.245e+04],
[25.844,8.9926e+04],
[27.978,1.0e+05]
])
#----------- Yaw- data from SIMA simulations (negative offset) -----------#
data_sim_2 = np.array([
[0.944,2498.044],
[2.84,7494.13] ,
[5.57,1.4988e+04],
[8.46,2.2482e+04],
[11.09,2.9977e+04],
[13.627,3.7471e+04],
[16.02,44964.8],
[18.259,52458.933],
[20.352,59953.0667],
[22.351,67447.2],
[24.167,74941.333],
[25.857,8.245e+04],
[27.445,8.9926e+04],
[29.421,1.0e+05]
 ])
```

```
#----------- Stiffness from base case paper -----------#


k = 1.26165*(10**5) # kNm
x_rad = np.linspace(0,0.523598776,100)
x_deg = np.linspace(0,33,100)
y_deg = k*x_rad


plt.plot(x_deg,y_deg,label ='Linear stiffness base case',color = 'blue')
a,b = np.polyfit(x_deg,y_deg,1)
print(a,b)




#----------- Plotting using matplotlib -----------#
x, y = data_sim.T
x1,y1 = data_sim_1.T
x2,y2 = data_sim_2.T
plt.plot(x,y,'ro',linestyle = '--',label = 'Initial stiffness case study',)
plt.plot(x1,y1,'go',linestyle = '-',label = '(+x) Offset stiffness case study')
plt.plot(x2,y2,'yo',linestyle = '-',label = '(-x) Offset stiffness case study')
plt.xlabel('Yaw-angle [degrees]')
plt.ylabel('Applied moment [kNm]')
plt.title('Yaw-stiffness from mooring lines')
plt.legend()
plt.grid()
plt.show()
plt.savefig('yaw-moment.png')
```

B.2 Mooring lines tensile strength plot

```
    # -*- coding: utf-8 -*-
"""
Created on Sun Oct 16 14:32:25 2022


@author: eigil
"""


import numpy as np
from matplotlib import pyplot as plt
```

```python
#----------- Data from SIMA simulations -----------#
data_ML1 = np.array([
[3.333333333333343, 1122.395221027479],
[9.259259259259267, 1111.1913978494624],
[15.18518518518519, 1100.7875746714456],
[20.370370370370367, 1091.184229390681],
[24.07407407407409, 1084.7818399044206],
[27.037037037037052, 1082.7799283154122],
[33.70370370370371, 1080.7756272401434],
[47.777777777777786, 1077.5665471923537],
[64.07407407407406, 1074.3560334528077],
[89.25925925925925, 1069.5397849462365],
[124.8148148148148, 1064.7168458781362],
[175.18518518518522, 1059.8843488649939],
[189.2592592592593, 1056.6752688172041],
[200.37037037037038, 1050.2681003584228],
[204.81481481481484, 1043.8652329749102],
[249.25925925925924, 984.6365591397848],
[281.85185185185185, 950.2155316606929],
[314.44444444444446, 930.1945041816009],
[338.14814814814815, 920.5792114695339],
[359.6296296296296, 917.365352449223],
[362.59259259259255, 917.363440860215],
[367.037037037037, 914.9605734767024],
[373.70370370370375, 910.956272401433],
[395.9259259259259, 910.9419354838709],
[430.00000000000006, 909.3199522102748],
[508.5185185185184, 910.869295101553],
[575.1851851851851, 910.8262843488649],
[644.8148148148148, 910.7813620071684],
[669,911],])


data_ML2 = np.array([
[2.95277943813511, 1194.4680851063831],
[7.770472205618674, 1181.276595744681],
[14.441123729826671, 1169.3617021276596],
```

```
[20.370591751344904, 1160],
[24.076509264793813, 1151.4893617021278],
[28.153018529587555, 1149.7872340425533],
[35.935445307830264, 1148.0851063829787],
[45.57083084279736, 1145.9574468085107],
[58.170950388523636, 1143.8297872340427],
[91.52420800956367, 1137.0212765957447],
[113.01852958756726, 1133.6170212765958],
[135.99521817095038, 1131.9148936170213],
[159.71309025702328, 1129.3617021276596],
[173.0543933054393, 1126.808510638298],
[190.10161386730425, 1125.9574468085107],
[196.03108188882248, 1120],
[200.4781829049611, 1117.0212765957447],
[215.30185295875668, 1096.1702127659576],
[228.27256425582777, 1077.4468085106384],
[267.92588164973097, 1030.6382978723404],
[288.6790197250448, 1011.4893617021278],
[305.72624028690973, 998.2978723404257],
[323.5146443514644, 986.3829787234043],
[348.7148834429169, 978.7234042553193],
[373.9151225343694, 974.4680851063831],
[382.80932456664664, 971.0638297872341],
[385.03287507471606, 970.2127659574469],
[397.6329946204423, 969.3617021276597],
[442.10400478182896, 969.3617021276596],
[485.83383144052596, 969.7872340425533],
[545.869695158398, 970.2127659574469],
[606.6467423789599, 970.2127659574469],
[659.641362821279, 969.7872340425533],])


data_ML3 = np.array([
[3.333333333333357, 1195.304073590063],
[7.037037037037038, 1183.7876668882927],
[9.999999999999986, 1176.962601228369],
[20.370370370370352, 1159.0450206723676],
[25.555555555555543, 1151.3655480915952],
[30, 1148.8038557850787],
[59.629629629629605, 1142.813327117612],
```

```
    [101.1111111111111, 1135.108889755014],
    [112.22222222222221, 1133.3954905452256],
    [152.96296296296293, 1129.9559549920646],
    [167.77777777777771, 1126.534251425922],
    [160.37037037037032, 1129.0979816738122],
    [184.07407407407402, 1125.670164283549],
    [190.37037037037032, 1124.8129551933114],
    [198.14814814814815, 1118.8374563434745],
    [205.55555555555554, 1109.4506983770343],
    [212.96296296296293, 1098.3581834809565],
    [234.4444444444444, 1068.492662137342],
    [253.70370370370364, 1045.4516969683075],
    [275.1851851851851, 1022.4092033432428],
    [297.77777777777777, 1004.0567770466663],
    [324.4444444444444, 986.9808662779292],
    [347.03703703703695, 978.0101030943592],
    [367.7777777777777, 974.5843236454695],
    [375.92592592592587, 972.8729623770548],
    [379.62962962962956, 971.1646580207005],
    [382.5925925925925, 970.3097416145081],
    [385.55555555555554, 968.601946743497],
    [394.44444444444434, 969.5958329193766],
    [438.1481481481481, 969.5657732841171],
    [488.5185185185184, 969.5311282807672],
    [548.5185185185184, 969.4898599679534],
    [629.2592592592591, 969.2872045303436],
    [669.6296296296294, 969.399681062175],])


x, y = data_ML1.T
x1,y1 = data_ML2.T
x2,y2 = data_ML3.T
plt.plot(x,y,label = 'Mooring line 1')
plt.plot(x1,y1,label = 'Mooring line 2')
plt.plot(x2,y2,label = 'Mooring line 3')
plt.xlabel('X-position [m]')
plt.ylabel(' Tensile force [kN]')
plt.title('Static tension forces mooring lines')
plt.legend()
plt.grid()
```

```
plt.show()
plt.savefig('yaw-moment.png')
```

B.3   Wind file generation script

```python
import numpy as np
import pylab as plt


def generate_ramp_wind_file(widir,Vend,tmax,tramp,dt=0.2,plotkey=False):



        ###########################
        ## WRITES SIMO WIND FILE FOR TWO-COMPONENT FLUCTUATING WIND
        ##
        ##########################

        wifilename = widir +'RampWind_%dms.asc' %(Vend*100)


        #####################################

        tstep = tmax-tramp
        time = np.arange(0.,tmax+dt,dt)
        Nt= len(time)

        Vzt = np.zeros(Nt)
        istart = int(np.ceil(tramp/dt))
        istep = int(np.ceil(tstep/dt))

        Vzt[0:istart+1] = (Vend)/tramp*time[0:int(np.ceil(tramp/dt)+1)]
        Vzt[istart+1:istart+istep+1] = Vend


        if plotkey:
                plt.figure()
                ax = plt.subplot(111)
                ax.plot(time,Vzt)
                plt.show()
```

```
        startstr = """{0:d} ' Number of samples
' Comment line
{1:.3f} ' Time step
2    ' Format type
' Text 1
' Text 2\n""".format(Nt,dt)


        wistr = startstr
        for ii in range(Nt):
                wistr += '%5.1f%5.1f\n' %(Vzt[ii],0.)


        f =open(wifilename,'w')
        f.write(wistr)
        f.close()
        return wifilename
## Specify target directory for wind files:
winddir = "C:\Users\eigil\OneDrive\Desktop\NMBU\Master\SIMA\ULS\wind"
windspeed = 25.0
tmax = 700.0
tramp = 200.0
dt = 0.5
filename = generate_ramp_wind_file(winddir,windspeed,tmax,tramp,dt,True)
```

B.4   Script for reading .h5 files

This script has not been the main way to process the .h5 file frm SIMA, for that the QATS GUI has been applied, but this has been used.

```
import pylab as plt
import numpy as np
from qats import TsDB,TimeSeries




def read_resfile
(resfile,analysisname,linename,segmentname,elementname,responsename):

    # locate time series file
    db = TsDB.fromfile(resfile)
    ts = db.get(name='%s/*%s*%s*%s*%s' %(analysisname,linename,segmentname,elementna

    print(ts.name)

    return ts


def read_resfile_simo(resfile,analysisname,bodyname,responsename):

    # locate time series file
    db = TsDB.fromfile(resfile)
    ts = db.get(name='%s/*%s*%s' %(analysisname,bodyname,responsename))

    print(ts.name)

    return ts



####################################################################


## Read results, plot timeseries
in_file = 'Results.h5'
DLCno = 1 # run no.
mno = 1 #mooring line no.
```

```
t_start = 400.

LStyles = ['-','--']
MarkerStyles = ['o','x','d']
prop_cycle = plt.rcParams['axes.prop_cycle']
cmap = prop_cycle.by_key()['color']
MotionNames = ['XGtranslationTotalmotion','YGtranslationTotalmotion','ZGtranslationT
RespUnit = ['m','m','m','deg','deg','deg']
RespNames = ['Surge','Sway','Heave','Roll','Pitch','Yaw']
PlotMotionNo = [1,2,3,4,5,6]

analysis_name = 'RIFLEX_FLS_single_1'
segment_name = 'segment_1'
elementname = 'element_1'
line_name = 'moorLine%s' %mno
bodyname = 'Semi'
##############################################################################
fig,ax = plt.subplots(2)

## Line tensions
# analysis_name = 'run_%s_single_%d' %('FullTurbine',DLCno) ## change this
Tmline = read_resfile(in_file,analysis_name,line_name,segment_name,elementname,'Axia

# Window
t_Tm, Tm_il = Tmline.get(twin=(t_start, 1e12))
Tm_il_ts = TimeSeries('Tmline_win',t=t_Tm,x=Tm_il,kind='force',unit='N')

#Power spectral density function
ff, Sf  = Tm_il_ts.psd()

# Plot timeseries and PSD
ax[0].set_title(line_name)
ax[0].plot(Tm_il_ts.t,Tm_il_ts.x,label='Fairlead tension',ls=LStyles[0])

ax[0].set_ylabel('Tension ($N$)')
ax[0].set_xlabel('Time (s)')

ax[1].set_title(line_name)
```

```
ax[1].plot(ff,Sf,label='Fairlead tension',ls=LStyles[0])


ax[1].set_ylabel('S$(\omega)$ ($N^2s$)')
ax[1].set_xlabel('$\omega$ (rad/s)')
ax[1].set_xlim(0,0.3)
ax[1].set_xticks(np.arange(0,0.35,0.05))


ax[0].grid(True)
ax[1].grid(True)


plt.legend()
plt.tight_layout()


## Plot platform motions
fig2,ax2 = plt.subplots(6,figsize=(6,8))
for ii,motno in enumerate(PlotMotionNo):

    ## Line tensions
    Xm = read_resfile_simo(in_file,analysis_name,bodyname,MotionNames[ii])
    munit = print(Xm.unit)
    # Window
    t_Xm, Xm = Xm.get(twin=(t_start, 1e12))


    Xm_ts = TimeSeries('Tmline_win',t=t_Xm,x=Xm)

    ax2[ii].plot(Xm_ts.t,Xm_ts.x,label=RespNames[ii],ls=LStyles[0])

    ax2[ii].set_ylabel(RespNames[ii]+' (%s)' %munit)
    ax2[ii].grid(True)

    plt.legend()

ax2[ii].set_xlabel('Time (s)')
plt.tight_layout()

plt.show()
```

Appendix C. SIMA simulations

This chapter will counting a selection of the time-series simulation for the rotating floater

C.1 Rotating floater

This section will contain a selection time series for the rotating floater where the platform yaw will be shown.

Wind from 0 °
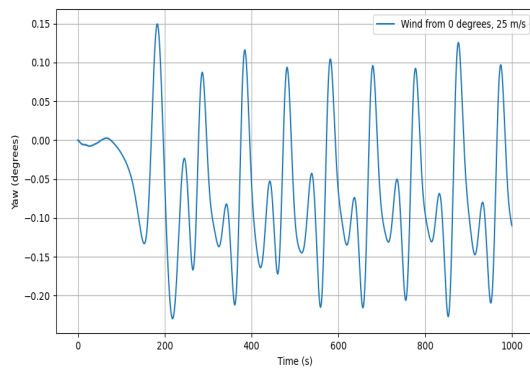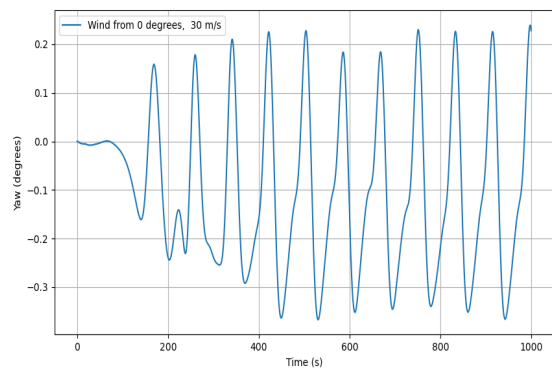
(a)   (b)

Figure C.1: Wind from 0 °. 25 m/s & 30 m/s

Wind from 40°

(a)   (b)
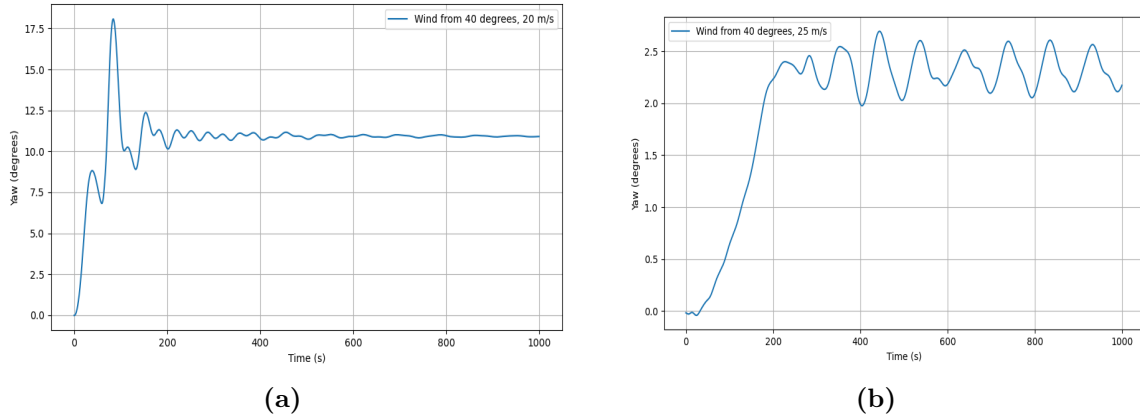
Figure C.2: Wind from 40°. 20 m/s & 25 m/s

(a)   (b)
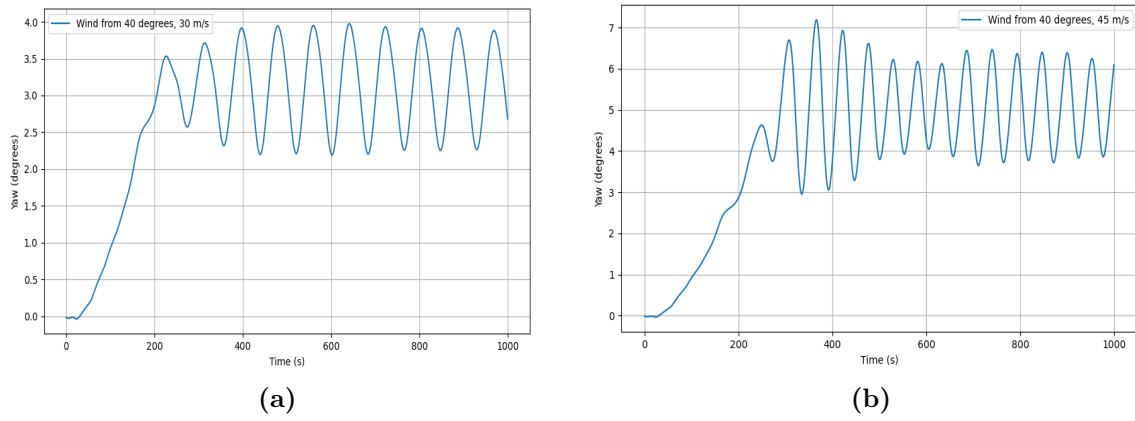
Figure C.3: Wind from 40°. 30 m/s & 45 m/s

Wind from 80°
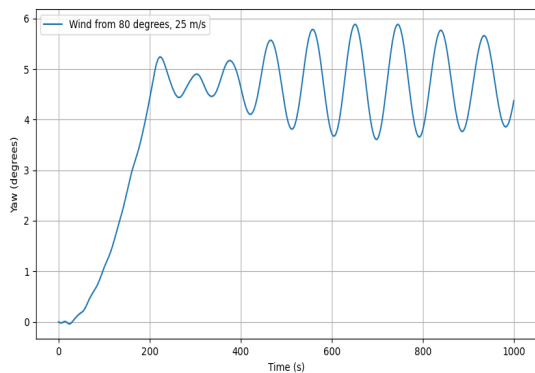
(a)
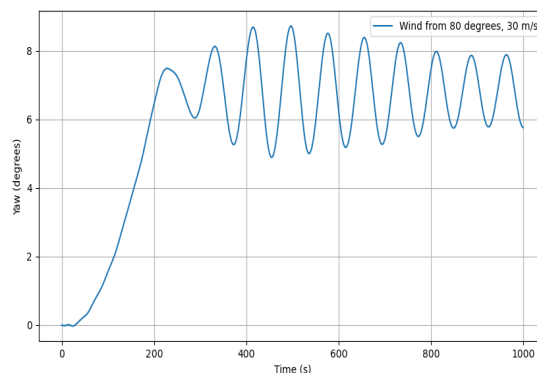
(b)

Figure C.4: Wind from 80°. 25 m/s & 30 m/s
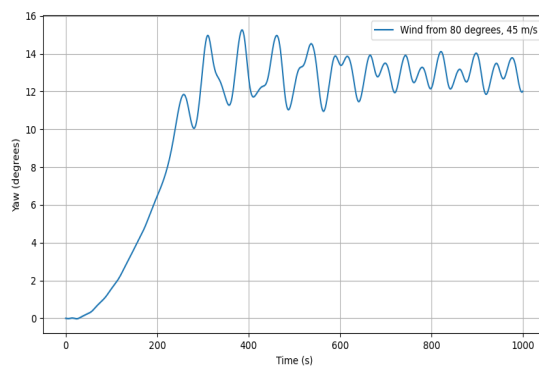
Figure C.5: 45 m/s

Wind from 120°

(a)   **(b)**
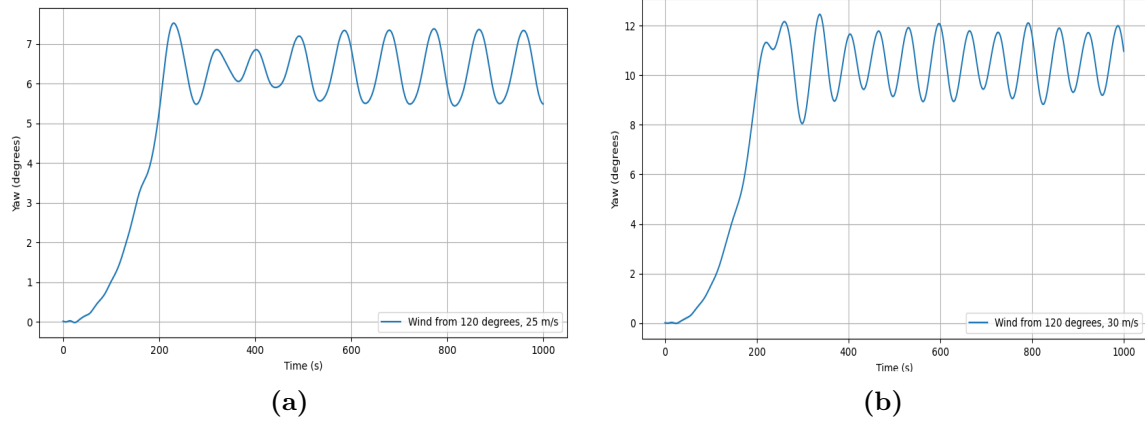
Figure C.6: Wind from 120°. 25 m/s & 30 m/s
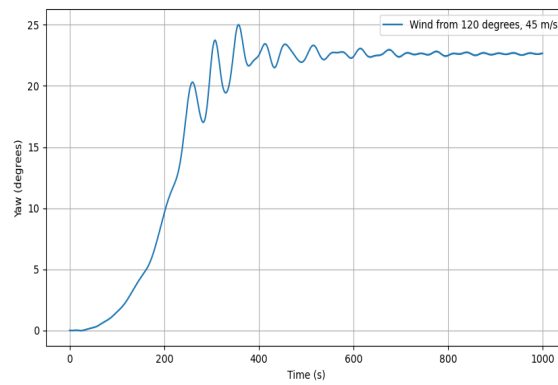
Figure C.7: Wind from 120°. 45 m/s

Wind from 160°
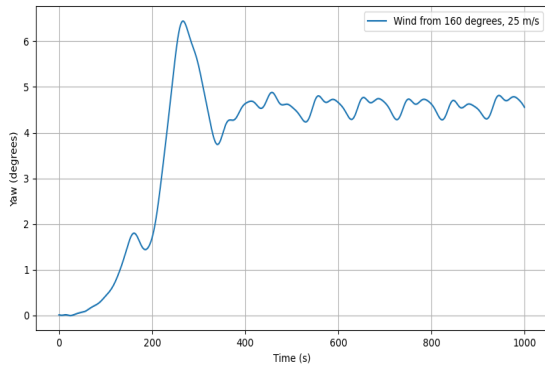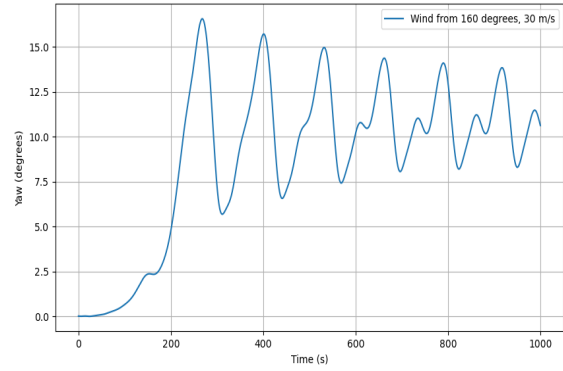
(a)   (b)

Figure C.8: Wind from 160°. 25 m/s & 30 m/s
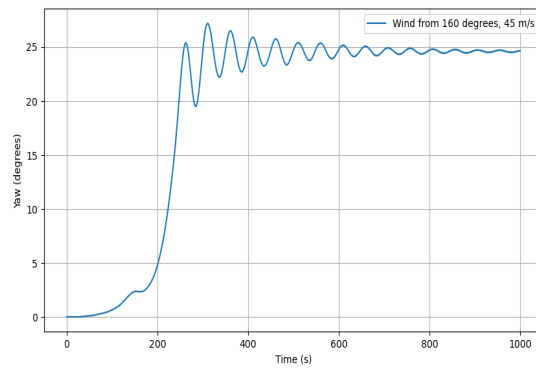
Figure C.9: Wind from 160°. 45 m/s

Wind from 200°
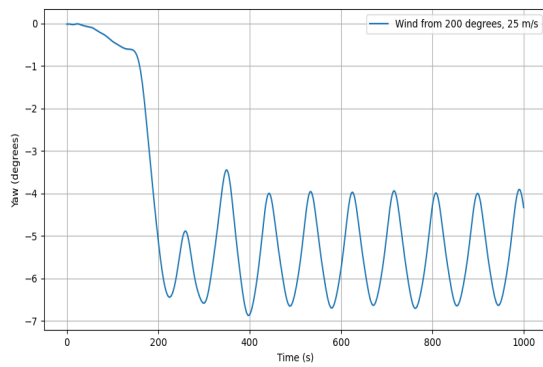
(a)
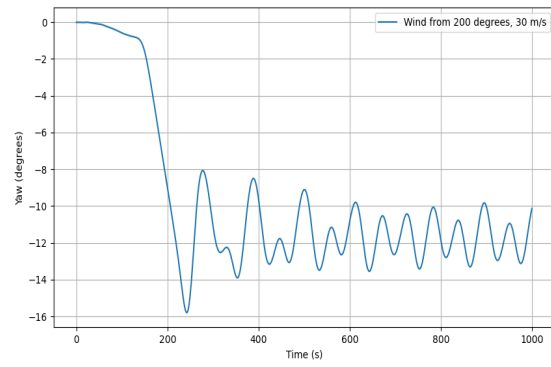
(b)

Figure C.10: Wind from 200°. 25 m/s & 30 m/s
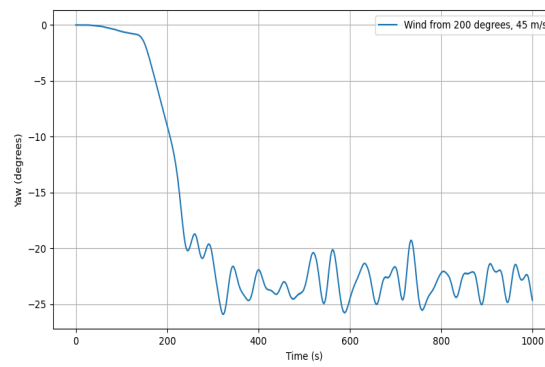
Figure C.11: Wind from 200°. 45 m/s

Wind from 240°

(a)   (b)
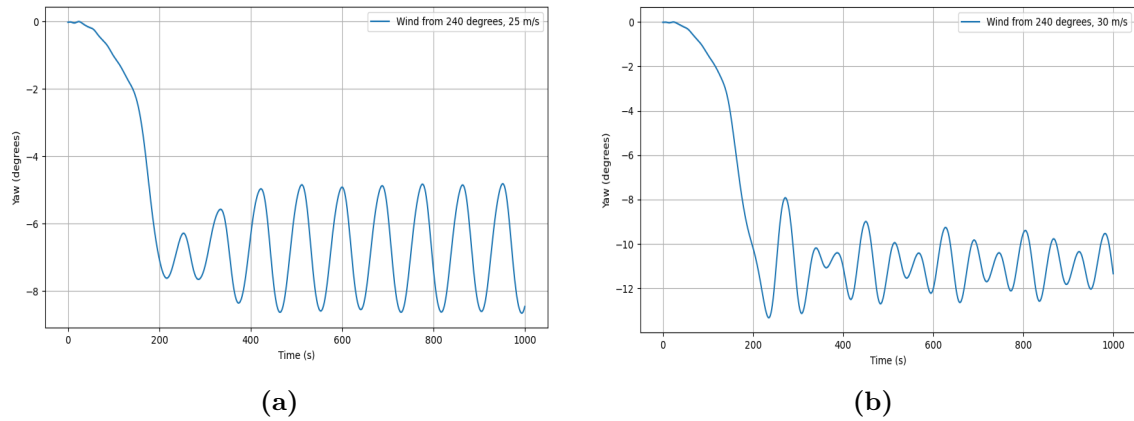
Figure C.12: Wind from 240°. 25 m/s & 30 m/s
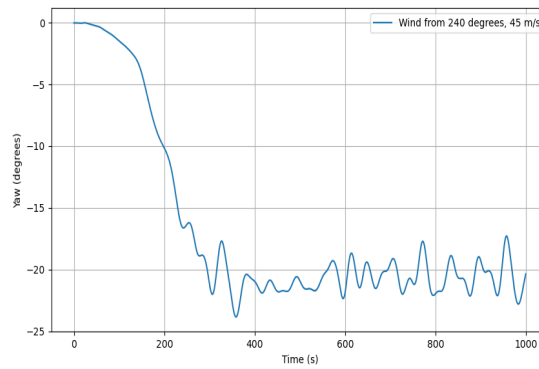
Figure C.13: Wind from 240°. 45 m/s

Wind from 280°
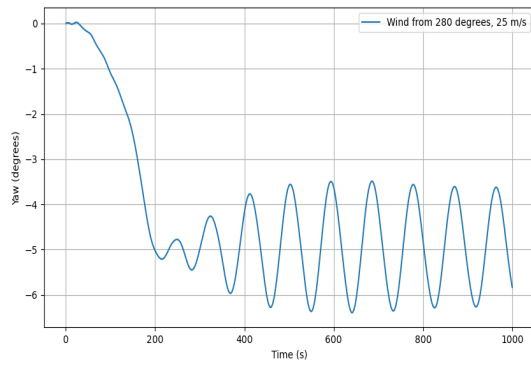
(a)
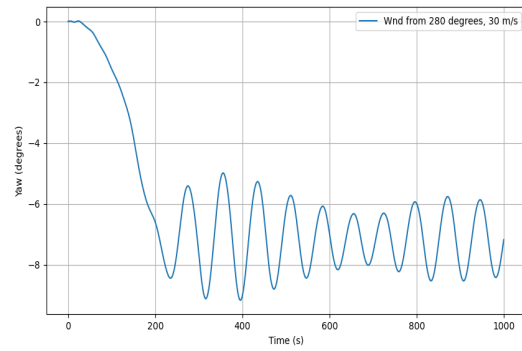
(b)

Figure C.14: Wind from 280°. 25 m/s & 30 m/s
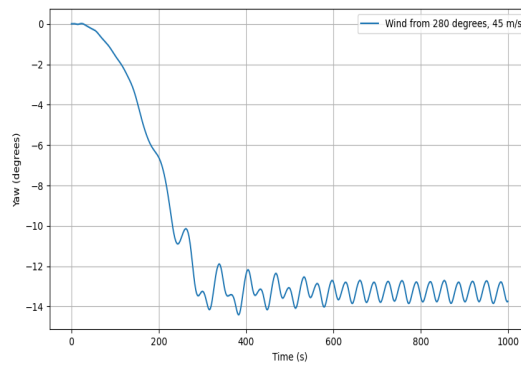
Figure C.15: Wind from 280°. 45 m/s

Wind from 320°
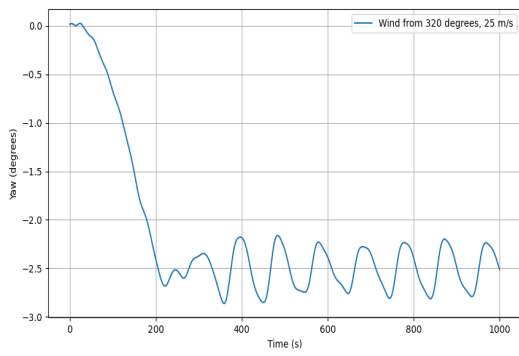
(a)
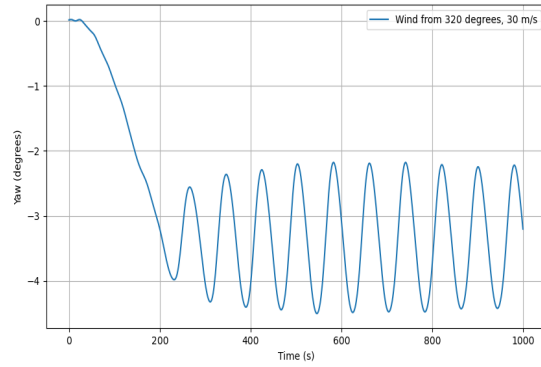
(b)

Figure C.16: Wind from 320°. 25 m/s & 30 m/s
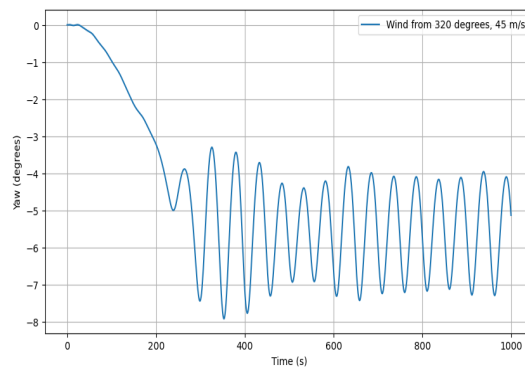
Figure C.17: Wind from 320°. 45 m/s

C.2 Stiffness simulations

In this section I have added the platform yaw for the positive offset. All the stiffness simulations have been done in a similar manor, with the same moment, but opposite or no offset force.
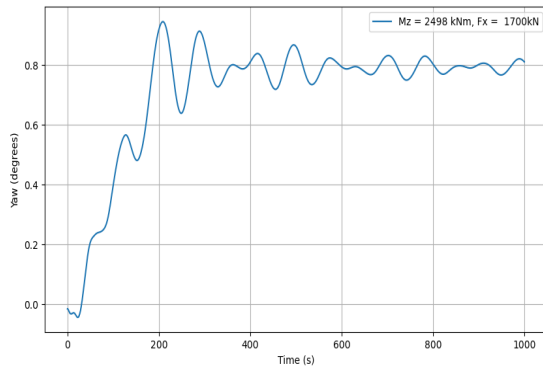
(a) Mz = 2498 kNm, Fx = 1700 kN
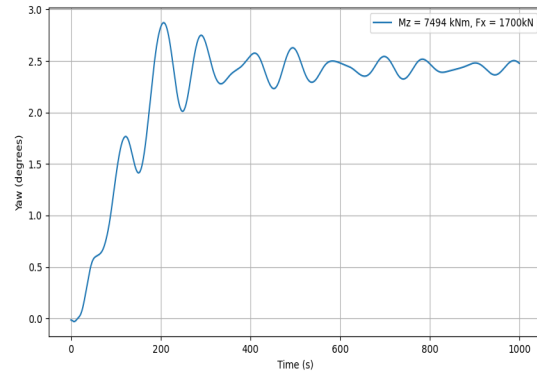
(b) Mz = 7494 kNm, Fx = 1700 kN

Figure C.18: Run 1 & 2
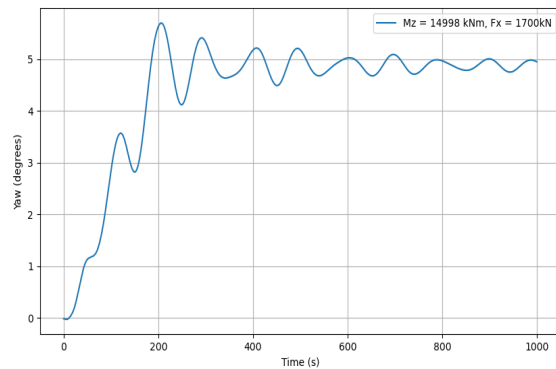
(a) Mz = 14988 kNm, Fx = 1700 kN
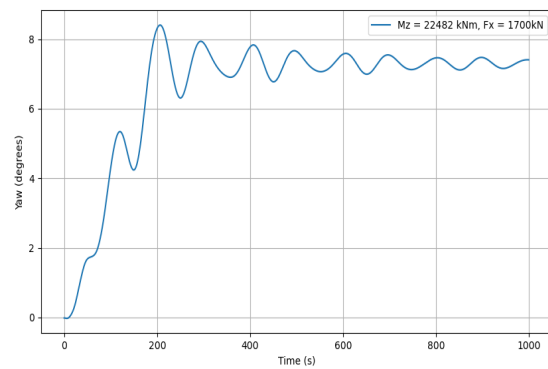
(b) Mz = 22482 kNm, Fx = 1700 kN

Figure C.19: Run 3 & 4
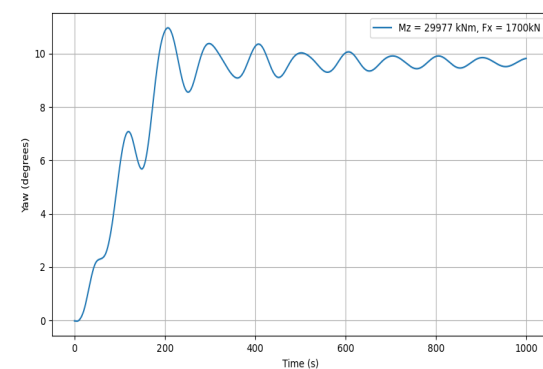
(a) Mz = 29977 kNm, Fx = 1700 kN
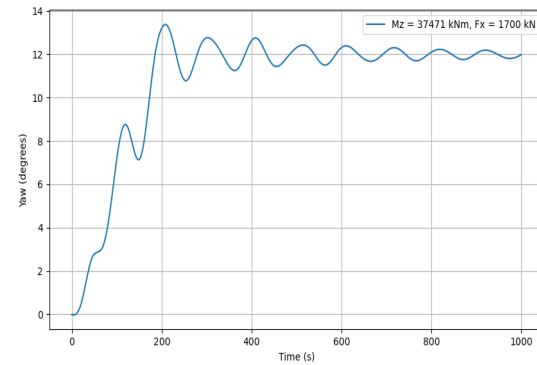
(b) Mz = 37471 kNm, Fx = 1700 kN

Figure C.20: Run 5 & 6
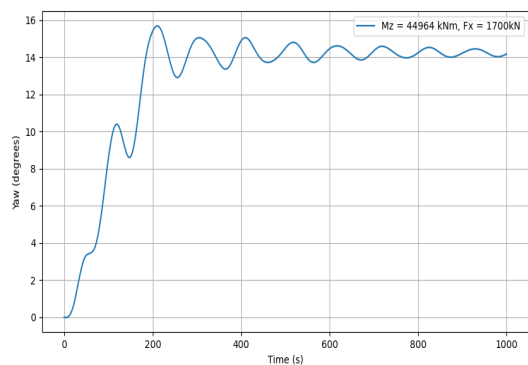
(a) Mz = 44964 kNm, Fx = 1700 kN
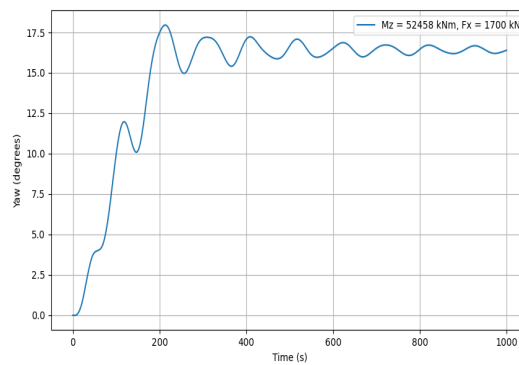
(b) Mz = 52458 kNm, Fx = 1700 kN

Figure C.21: Run 7 & 8
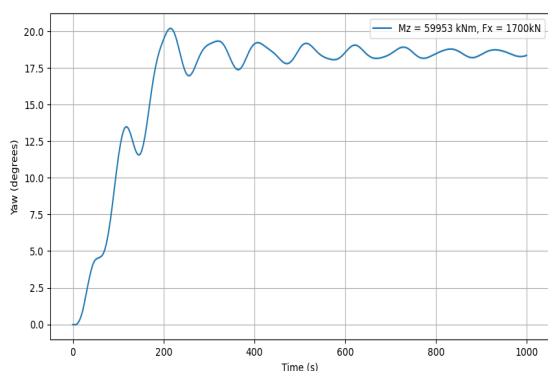
(a) Mz = 59953 kNm, Fx = 1700 kN
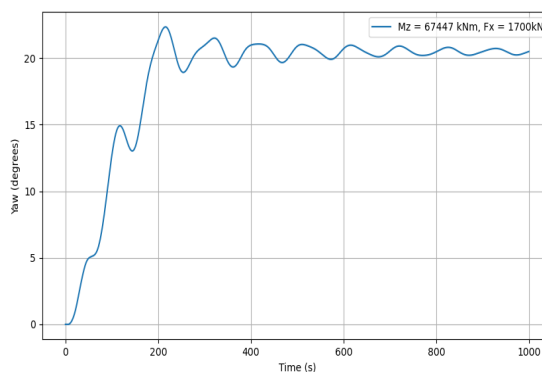
(b) Mz = 67447 kNm, Fx = 1700 kN

Figure C.22: Run 9 & 10
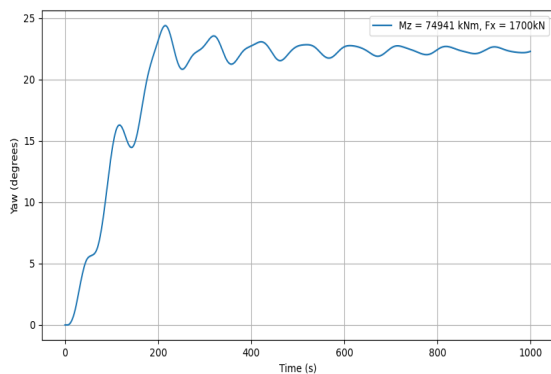
(a) Mz = 74941 kNm, Fx = 1700 kN
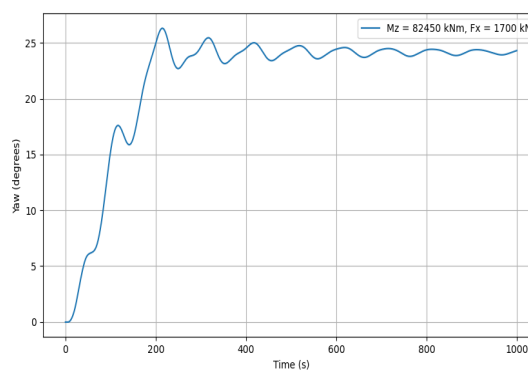
(b) Mz = 82450 kNm, Fx = 1700 kN

Figure C.23: Run 11 & 12
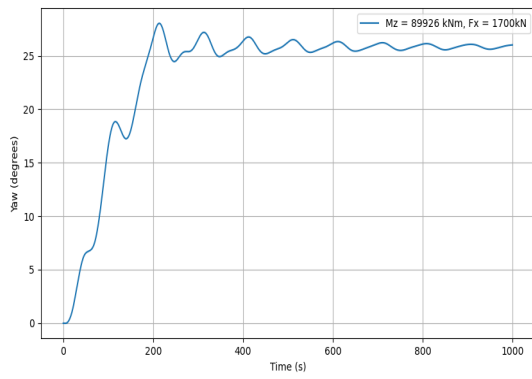
(a) Mz = 89926 kNm, Fx = 1700 kN

(b) Mz = 100 000 kNm, Fx = 1700 kN

Figure C.24: Run 13 & 14